Neue Biosensoren aus Mehrwandigen Kohlenstoffnanoröhren für die Elektrochemische Analyse von Biomolekülen

Dissertation zur Erlangung des

akademischen Grades Doctor rerum naturalium (Dr. rer. nat.)

Vorgelegt der Fakultät für Mathematik und Naturwissenschaften

der Technischen Universität Ilmenau

von M. Sc. Shereen Haj Othman

1. Gutachter: ap. Prof. Dr. rer. nat. habil. U. Ritter

2. Gutachter: Prof. Dr. rer. nat. habil. Dr. h.c. A. Bund

3. Gutachter: Prof. Dr. P. Athanassios

Tag der Einreichung: 26.09.2017

Tag der wissenschaftlichen Aussprache: 19.06.2019

urn:nbn:de:gbv:ilm1-2019000279

Acknowledgment

Firstly, I would like to express my sincere gratitude to my supervisor Prof. Dr. Uwe Ritter for the continuous support of my Ph.D. study and research, for his patience, motivation, and immense knowledge. My sincere thanks also go to PD Dr. habil. Nikos Tsierkezos for his help, discussion, and enthusiasm throughout the project.

Thanks as well to the coworkers of research working team, Prof. Dr. Michael Köhler, Dr. A. Knauer, L. Hafermann, and to the lab members Dr. E.Täuscher, M.Sc. Y. Thaha, S. Günther, K. Risch, C. Siegmund for their dedicated work.
I would like to express my gratitude to D. Schneider, and S. Heusing who helped me with all the lab issues and SEM measurements.

I would like to thank Dr. Paweł Szroeder (Institute of physics, Torun, Poland) for Raman measurements. Prof. Dr. Antonios Kelarakis and Dr. Diogo Fernandes (University of Central Lancashire, Preston, UK) are also knowledge for Raman measurements. My thanks also go to Dr. Eoin K. McCarthy (Trinity College Dublin, Ireland) for SEM and TEM analysis.

Furthermore, highly acknowledgment to financial support from Thüringer Graduiertenförderung (project number: 4555625).

Warmly thanks to Faculty of Science, University of Aleppo, Syria for their support during my Bachelor and Master study.

I am very grateful to my entire family, my parents, my sisters, and brothers for all their love and support. Of course I will never forget my husband Nader and my sons, Muhammad and Shaker for their encouragement, patience and support all these years.

Table of Contents

List of Abbreviations

AA	Ascorbic acid
AC	Acetaminophen
AgNPs	silver nanoparticles
AuNPs	gold nanoparticles
CNT	Carbon nanotube
CV	Cyclic Voltammetry
CVD	Chemical vapor deposition
DA	Dopamine
DPV	Differential pulse voltammetry
DV	Direct voltammetry
DL	Detection limit
EIS	Electrochemical Impedance Spectroscopy
GC	Glassy carbon electrode
MNPs	Metallic nanoparticles
MWCNT	Multi-walled carbon nanotube
NAC	*N*-acetylcysteine
N-MWCNTs	Nitrogen-doped multi-walled carbon nanotubes
N-P-MWCNTs	Nitrogen-Phosphorus-doped multi-walled carbon nanotubes
PBS	Phosphate Buffer Solution
PdNPs	Palladium nanoparticles
Pt	Platinum electrode
PtNPs	Platinum nanoparticles
RE	Reference electrode
RhNPs	Rhodium nanoparticles
SCE	Saturated Calomel electrode
SWCNT	Single-walled carbon nanotubes

SEM	Scanning electron microscopy
TEM	Transmission electron microscopy
UA	Uric acid
WE	working electrode
XPS	X-ray photoelectron spectroscopy

Abstract

The synthesis of nitrogen-doped multi-walled carbon nanotubes (N-MWCNTs) and nitrogen-phosphorus-doped multi-walled carbon nanotubes (N-P-MWCNTs) was performed by means of chemical vapor deposition technique (CVD).

The synthesized films were grown on silicon/silicon oxide wafer with decomposition of either acetonitrile (ACN) for N-MWCNTs or both acetonitrile (ACN) and triphenylphosphine (TPP) for N-P-MWCNTs in the presence of ferrocene ($FeCp_2$) as catalyst. The morphology of films was studied by means of scanning electron microscopy (SEM) in combination with energy dispersive X-ray spectroscopy (EDX), and transmission electron microscopy (TEM), as well as by Raman spectroscopy.

Cyclic Voltammetry (CV) and electrochemical impedance spectroscopy (EIS) techniques were applied for the electrochemical characterization of synthesized N-MWCNTs and N-P-MWCNTs by using the standard redox system, ferrocyanide/ferricyanide, $[Fe(CN)_6]^{3-/4-}$. The results demonstrate that N-MWCNTs exhibit higher sensitivity, lower detection limit, and faster kinetics of electron transfer compared to N-P-MWCNTs. Namely, it was observed that the electrochemical response and the sensitivity of composite films decrease with phosphorus doping.

The modification of fabricated N-MWCNTs with metal nanoparticles MNPs was also investigated. For this purpose, rhodium (RhNPs), palladium (PdNPs), iridium (IrNPs), platinum (PtNPs), silver (AgNPs), and gold (AuNPs) nanoparticles were used for the decoration of fabricated films. The N-MWCNTs/MNPs (M: Rh, Pd, Pt, Ag) films were electrochemically characterized by using the standard redox system $[Fe(CN)_6]^{3-/4-}$. The extracted results indicate that the modified N-MWCNTs/MNPs (M: Rh, Pd, Pt, Ag) films exhibit powerful response, since the nanoparticles play a role as catalyst that improves significantly the electrocatalytic activity of electrode. Namely, the response of the films towards $[Fe(CN)_6]^{3-/4-}$ tends to increase with the following order: N-MWCNTs < N-MWCNTs/RhNPs < NMWCNTs/PdNPs < N-MWCNTs/PtNPs < N-MWCNTs/AgNPs.

Furthermore, the modified composite films N-MWCNTs/MNPs (M: Rh, Pd, Ir, Pt, Au) were applied as a working electrode for the simultaneous analysis of some interesting biomolecules such as acetaminophen, *N*-acetyl-cysteine, ascorbic acid, dopamine, and uric acid in phosphate buffer solution PBS (pH 7.0). The findings demonstrate that the detection capability of composite films towards oxidation of AA, DA, and UA enhances with the following order: N-MWCNTs < N-MWCNTs/RhNPs < NMWCNTs/PdNPs < N-MWCNTs/IrNPs < N-MWCNTs/PtNPs < N-MWCNTs/AuNPs.

From the results it can be concluded that N-MWCNTs/AuNPs is the best composite film for the simultaneous determination of the studied molecules.

Electrochemical studies reveal that N-P-MWCNTs film is quite suitable for individual analysis of AA, DA, and UA. However, the simultaneous analysis of AA, DA, and UA on this particular film was not possible due to the overlapping of oxidation peaks of AA and DA. Generally, the N-P-MWCNTs films appear to be less sensitive compared to N-MWCNTs films.

Zusammenfassung

Stickstoff-dotierte (N-MWCNT) und Stickstoff-Phosphor-dotierte (N-P-MWCNT) mehrwandige Kohlenstoffnanoröhren wurden mittels chemischer Gasphasenabscheidungstechnik (CVD) erfolgreich hergestellt. Die synthetisierten MWCNTs sind auf Silizium/Siliziumoxid Wafer durch die Zersetzung von Acetonitril und Triphenylphosphin in Gegenwart vom Ferrocen als Katalysator gewachsen. Die Morphologie wurde mittels Rasterelektronenmikroskopie (REM) in Kombination mit Energiedispersiver Röntgenspektroskopie (EDXS), Transmissionselektronenmikroskopie (TEM), und Raman Spektroskopie untersucht.

Die REM Aufnahmen zeigen, dass die N-MWCNTs einen Teppich aus vertikal ausgerichteten Kohlenstoffnanoröhrchen bilden und die Oberfläche des Films weitgehend homogen ist. TEM Aufnahmen einzelner Röhren zeigen, dass die N-MWCNTs eine sogenannte Bambus-Struktur besitzen. REM-Aufnahmen der N-P-MWCNT Filme zeigen ebenfalls eine homogene Struktur der Filme, die ähnlich der der N-MWCNT ist, mit zusätzlichen Knoten in der Röhrenstruktur. Dabei ändert sich die Morphologie der hergestellten Filme mit zunehmendem TPP Gehalt (zwischen 0.7 und 1 Gew %) in der Kohlenstoffquelle (Acetonitril). Eine Schicht aus amorphem Kohlenstoff bedeckt die Kohlenstoffnanoröhrchen teilweise, sodass keine ausgerichteten Kohlenstoffnanoröhrchen in den REM-Bildern erkannt werden können. Durch die Erhöhung des TPP Gehalts bis auf 1 Gew % im Lösungsmittel entstehen sehr dünne Filme aus N-P-MWCNTs. Die TEM-Bilder bestätigen, dass die N-P-MWCNTs noch eine Bambus-Struktur besitzen (erkennbar bis zu einem Zusatz von 0.6 Gew %. TPP). Darüber hinaus (mehr als 0.6 Gew %. TPP) konnten durch den abgeschiedenen amorphen Kohlenstoff keine TEM-Bilder mehr aufgenommen werden.

Die quantitative Auswertung der Raman-Spektren zeigt, dass das Verhältnis der Intensitäten der Raman Banden D und G für N-MWCNT-Filme kleiner ist als das Verhältnis für N-P-MWCNT-Filme ist. Es wurde festgestellt, dass das Intensitätsverhältnis bei der Dotierung mit Phosphor zunimmt und folglich der Grad der Defekte abnimmt.

Die elektrochemische Charakterisierung der gewachsenen Schichten mittels Zyklischer Voltammetrie und Elektrochemischer Impedanz Spektroskopie wurde gegenüber dem Redoxsystem $[Fe(CN)_6]^{3-/4-}$ durchgeführt. Die Ergebnisse zeigen, dass die hergestellten N-MWCNTs die höchste Sensitivität, die kleinste Nachweisgrenze, und die schnellere Kinetik der Elektronübertragung im Vergleich zu den N-P-MWCNTs zeigen. Die Dotierung von Kohlenstoffnanoröhren mit Stickstoff verbessert die elektrokatalytischen Eigenschaften, während die zusätzliche Dotierung der N-MWCNTs mit Phosphor die Sensitivität und die Kinetik der elektrochemische Prozess auf diesen Filmen deutlich verringert.

Die nachträgliche Modifizierung von N-MWCNTs mit Metall-Nanopartikeln (MNP) wurde ebenfalls untersucht. Dabei wurden Rhodium- (RhNP), Palladium- (PdNP), Platin- (PtNP) und Silber- (AgNP) Nanopartikel für die Modifizierung der Oberflächen verwendet. Die hergestellten Filme aus N-MWCNTs/MNP wurden ebenfalls elektrochemisch mit dem Redoxsystem $[Fe(CN)_6]^{3-/4-}$ als Modellsystem charakterisiert. Die Ergebnisse zeigen, dass die modifizierten N-MWCNTs/MNP stärkere Signale (response) zeigen, da die Nanopartikels als Katalysator wirken. Die elektrokatalytische Aktivität der Elektroden verbessert sich in der folgenden Reihenfolge: N-MWCNTs < N-MWCNTs/RhNP < N-MWCNTs/PdNP < N-MWCNTs /PtNP < N-MWCNTs/AgNP.

Die Anwendung von N-MWCNTs/MNP (M: Rh, Pd, Ir, Pt, und Au) Filmen als Arbeitselektroden für die gleichzeitige quantitative Analyse von einigen medizinisch relevanten Biomolekülen, wie zum Bespiel Ascorbinsäure, Dopamin, und Harnsäure in Phosphat-Puffer-Lösung PBS (pH 7.0) wurde ebenfalls erfolgreich demonstriert. Die Ergebnisse zeigen, dass die Nachweisgrenze von N-MWCNTs/MNP in der folgenden Rheinfolge abnimmt: N-MWCNTs > N-MWCNTs/RhNP > N-MWCNTs/PdNP > N-MWCNTs/IrNP > N-MWCNTs /PtNP > N-MWCNTs/AuNP. Die AuNP zeigen den größten Effekt auf die Empfindlichkeit und die elektrokatalytische Aktivität bei der gleichzeitigen Bestimmung der untersuchten Moleküle. Die hergestellten nanostrukturierten Schichten aus N-MWCNTs und AuNP konnten auch für die Analyse von Acetaminophen (AC) und *N*-Acetyl-Cystein (NAC) erfolgreich eingesetzt werden.

Die Stabilität der synthetisierten Kohlenstoffnanofilme über längere Zeiträume und die Reproduzierbarkeit der Synthese der Filme wurden untersucht und zeigen, dass die hergestellten Elektrodenfilme eine sehr gute Stabilität und Reproduzierbarkeit in den elektrochemischen Messungen aufweisen.

1 Introduction

1.1 Background

Nanotechnology is considered to be the technology of future, and its applications are very wide in various fields. With the advancement of science and analysis tools, a lot of attractive researches that interested in nanomaterial and its application in electronics, optics, energy storage, and sensors were investigated.

Carbon nanotubes CNTs are undoubtedly one of the most attractive material and still an interesting research topic until now. Due to their novel properties such as hardness, electrical and thermal conductivity, CNTs appear to be the most interesting material until now. Many efforts have been made to improve their properties through the doping with different dopant such nitrogen, phosphorus, boron, and silicon. Through the doping, not just the morphology of the CNTs will be changed, but also their physical and chemical properties. The growing interest in nitrogen-doped multi-walled carbon nanotubes (N-MWCNTs) and nitrogen-phosphorus carbon nanotubes (N-P-MWCNTs) was a topic for researcher in the last years. The fabrication of (N-MWCNTs) and (N-P-MWCNTs) are explained more in paragraph below (see 2.1.4).

The CNTs were widely used as sensor material in electrochemical applications was widely applied, since they reduce the overpotential and enhance the current response, as well as the increase the selectivity and chemical stability. In addition, CNTs improve the reaction rate, the sensitivity, and the detection limit of redox system. Therefore, they have been used as sensor to analyze different biomolecules successfully. The modification of CNTs with metal nanoparticles (MNPs) has become of increased importance. Various approaches were developed to immobilize metal nanoparticles on the surface, since the MNPs enhance the sensitivity and also can play important role as catalyst (see 2.1.6). Various electrodes (glassy carbon-ceramic and more) were modified with CNTs to detect interesting biomolecules such ascorbic acid, dopamine, uric acid, paracetamol, and *N*-acetylcysteine (see 2.1.8). These electrodes required a lot of steps for preparation with difficulty in order to be used for the measurement. Therefore, it stills a challenge to develop a simple, rapid, inexpensive, selective, and sensitive method for simultaneous determination of biomolecules.

In the present work, nitrogen-doped multi-walled carbon nanotubes were fabricated directly on the substrate, modified with metal nanoparticles (MNPs), and further used as working electrode for analyzing interesting biomolecules in simple method.

Many challenges still remain in synthesis of CNTs, growth mechanisms, and the effect of nitrogen and phosphorus doping on their structure, properties, modification, and its application.

1.2 Motivation (objectives)

The research aims to the following goals:

I. Synthesis of nitrogen (N-MWCNTs) and nitrogen-phosphorus (N-P-MWCNTs) doped multi-walled carbon nanotubes using chemical vapor Deposition (CVD) method.

II. Characterization of fabricated films with SEM, TEM, EDX, and Raman spectroscopy.

III. Modification of the fabricated films with various metallic nanoparticles (MNPs) such as, rhodium (RhNPs), palladium (PdNPs), iridium (IrNPs), platinum (PtNPs), silver (AgNPs), and gold (AuNPs) nanoparticles.

IV. Electrochemical characterization of composited film using the standard redox system $[Fe(CN)_6]^{3-/4-}$ by means of cyclic voltammetry and impedance spectroscopy techniques.

V. The fabricated composite films were used for simultaneous electrochemical analyzing of interesting biomolecules such as, ascorbic acid, dopamine, uric acid, paracetamol, and *N*-acetylcysteine.

2 Theoretical Background

2.1 Carbon nanotubes

2.1.1 Structure and properties

Carbon is a remarkable chemical element that was described as a basic of all living system on the Earth [1]. The well-known allotropes of carbon are diamond (sp^3 hybridized carbon), graphite (sp^2 hybridized carbon), amorphous carbon, and fullerenes [2]. A new form of pure carbon that is perfectly straight tubules with diameter in nanometers, length in micrometer is carbon nanotubes CNTs.

In 1991, MWCNTs were identified by S. Iijima who examined carbon soot as obtained from arc discharge of graphite electrodes via transmission electron microscopy (TEM) [3]. After that single walled carbon nanotubes (SWCNTs) were investigated in 1993 [4].

There are two main types of CNTs, single-walled carbon nanotubes (SWCNTs) possess a cylindrical nanostructure formed by rolling up a graphite sheet into a tube, and multi-walled carbon nanotubes (MWCNTs), which formed by several concentric layers of rolled graphite.

(a) (b)

Fig. 1 Schematic diagram of partially rolled-up graphene layer **(a)**, and a fully rolled-up graphene layer **(b)** [5].

Since their discovery, CNTs have become one of the most interesting and valuable material in nanotechnology due to their excellent electrical, chemical, and mechanical properties [6].

The SWCNT can be characterized by its chirality, which can be defined by the chiral vector C_h, $C_h = na_1 + ma_2$ [7]

Where $\mathbf{a}_1$ and $\mathbf{a}_2$ are the unit cell base vectors of the graphene sheet, n and m are integers.

When a graphite sheet will be twisted into a cylinder, namely by joining the beginning and the end of an (n,m) lattice vector, different electronic structure can be obtained depending on the value of (n,m).

(1) Zigzag tubes have n or m=0 , (2) Armchair tubes are defined by $n = m$ and are metallic, (3) Chiral

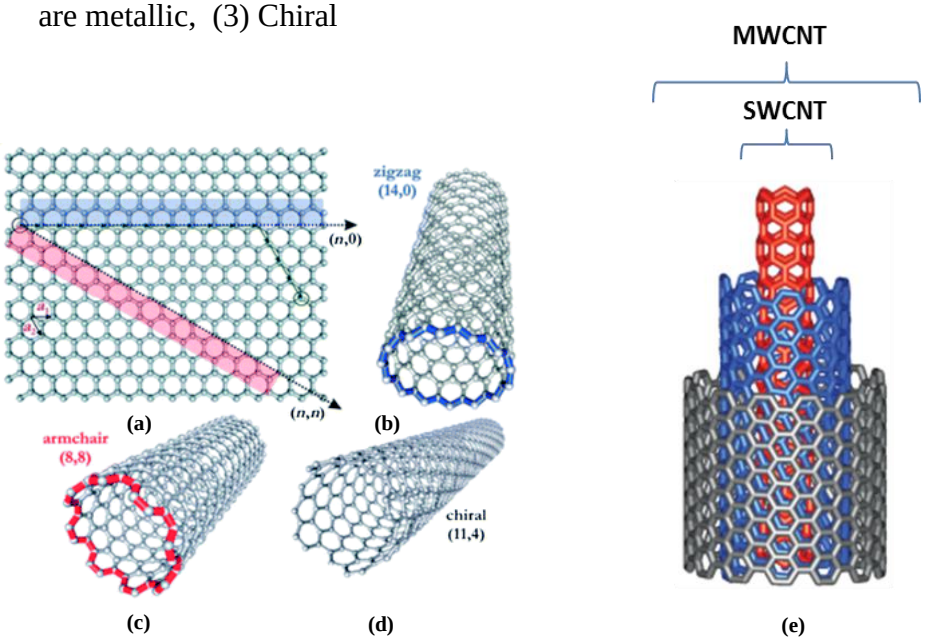

Fig. 2 (a) An infinite graphite layer with *(n,m)* nanotube naming scheme describing how a nanotube is rolled up, (b) SWCNT of zigzag structure, (c) SWCNT of armchair structure, (d) SWCNT of chiral structure [8], and (e) explain the distinction between SWCNT and MWCNT [9].

SWCNTs can be metallic or semiconducting depending on the diameter and chirality [10]. An overview of some of the electronic, mechanical, and thermal properties compared to conventional materials are presented in Table 1.

Table 1 Physical properties of CNTs compared to traditional materials of the respective category [11].

Properties	CNTs	Compare material
E-Module [TPa]	≈1	Diamond ≈ 1
tensile strength [GPa]	≈30	Steel ≈ 0.7
Density [Kg/m^3]	≈1300	Steel ≈ 8000
Thermal conductivity [W/mk]	≈2000	Copper ≈ 400
critical current density [A/cm^2]	1×10^9	Copper ≈ 500

These properties depend on the perfection of the CNTs structure and its bulk-and surface structure. The properties are also influenced by the expression of existing defects, as well as inter interactions. Since the degree of defect is affected by the

synthesis conditions, various structures can be observed for different types of produced CNTs.

These excellent properties of the CNTs make them an important material for the development of emerging technologies and to be used in numerous applications such composite materials, coatings and films, microelectronics, energy storage (batteries and solar cell), environment, and biotechnology [12].

2.1.2 CNTs Market

Carbon nanotubes (CNTs) have been attracted huge attention of researchers over the past 25 years. According to Markets and Markets (M&M), the global market for carbon nanotubes in 2015 was worth about $2.26 billion [13]; an increase of 45% from 2009 (i.e. ~ $ 1.24 billion). This was due to the growing potential of CNTs in electronics, plastics and energy storage applications and the projected market of CNTs is expected to be around $ 5.64 billion in 2020. It was obvious in the last five years a rising in the production of multi wall carbon nanotubes in the global market see (Fig. 3b). The main method for large scale production of CNTs is the chemical vapor deposition (CVD) method [14]. As we see from (Fig. 3a), the most popular application of CNT was in polymers, and it is expected to increase the demand of CNT in the coming years. Its application in electronics is also in demand, since they exhibit a good conductivity and optoelectronic properties. Growing the need for alternative energy Sources such solar cells and wind turbines is anticipated to promote the growth of carbon nanotubes market.

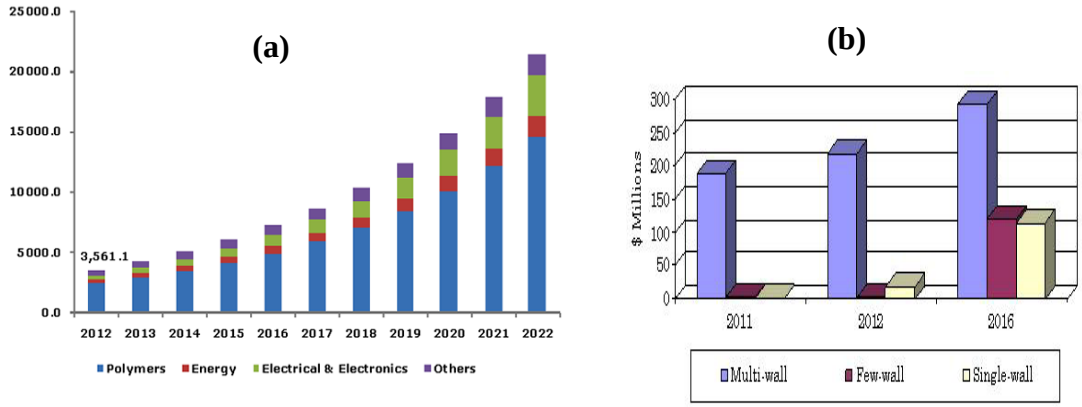

Fig. 3 Global Carbon Nanotubes Market Estimates and Forecast, by Application, 2012 - 2022 (Tons) [15] **(a)**, global market for CNTs grades based on committed production, 2011-2016 ($ millions) Source: BCC Research **(b)**.

2.1.3 Synthesis methods

Carbon nanotubes can be produced by three different methods: namely be means of chemical vapor deposition, laser ablation or arc discharge.

2.1.3.1 Chemical vapor deposition technique

The growth mechanism involves the decay of hydrocarbon molecules catalyzed by the transition metal, and the saturation of carbon atoms in the metal nanoparticles [16]. The growth of CNTs is affected with several parameters such as the concentration of carbon source material and catalyst, the temperature, the pressure, the reaction time, and the volume of spray solution. The method is also controllable compared to other synthesis methods [17, 18].

The most common supported transition metal catalysts are Fe, Co, Ni from sources such as ferrocene, cobaltocene, and nickelocene, nitrates and others [19, 20]. The catalyst nanoparticles can be deposited on substrates. The ideal substrate material is silicon due to its porous, that is suitable for growing the nanotubes on large surface [21].

Both SWCNTs, MWCNTs can be produced with this process depending on the temperature; that production of SWCNTs occurs at high temperature (900-1200°C), whereas the MWCNTs growths takes place at lower temperature (600-900°C) [22-27].

In 1993, chemical vapor deposition (CVD) technique was first reported to produce MWCNTs [28]. Three years later, SWCNTs was also successfully produced [22].

Generally, substrates are placed in the quartz tube and heated to the growth temperature. Afterwards, the reaction mixture containing carbon source, catalyst, dopant source (in case of fabrication of doped-CNTs) and an inert gas (N_2, Ar) are introduced into the reaction chamber by applying an appropriate system conditions (temperature, pressure, etc.), these precursors lead to formation of CNTs. The growth process is carried out for a certain period of time. As soon as the supply process is terminated, the heating will be switched off and the system will be cooled down to ambient temperature at which the substrate can be safely removed.

The main advantages of CVD are: simple reactor design, economic technique, easy to control the structure (length and diameter), high purity of the obtained material, ability to use various substrates, allows CNT growth in different forms, such as powder, thin or thick films, aligned or entangled, straight or coiled nanotubes, as well as low synthesis temperature [29, 30].

2.1.3.2 Laser ablation

It is one of the methods for synthesis of SWCNTs that it was first discovered in 1995 [31]. In laser ablation technique, laser beam is used as energy source, a pulse laser irradiates on a graphite pellet containing catalyst materials (usually nickel or cobalt) in the presence of inert gas such as helium which vaporizes a graphite target. The soot produced by the laser vaporization will deposited onto a water-cooled copper collector. The process occurs in furnace at (1200 °C) [32].

The advantage of this method is a high quality produced SWCNTs. On the other hand, high energy and more purification step are required to produce SWCNTs by this method that limits their use as large scale industrial processes [21].

2.1.3.3 Arc discharge

The arc discharge technique generally involves the use of two high-purity graphite electrodes in an evacuated chamber which is filled with inert gas (Argon or helium). The distance between the electrodes is about 1 mm. Direct current passes through the two electrodes and creates a high temperature discharge between them. Carbon is vaporized from a graphite rod (anode) and condenses on another rod (cathode) [33].

Multi-walled carbon nanotubes can be obtained without catalyst, while for the synthesis of SWCNT the presence of metallic catalyst (Fe, Co, Ni) is required. The growth temperature is considerable higher than by other methods (2000-3500°C) [3, 34].

Several factors influencing the arc discharge process, such as the carbon vapor concentration, the carbon vapor dispersion in inert gas, the temperature, the composition of catalyst, and the presence of hydrogen. These factors affect the growth of the nanotubes, their inner and outer diameters, and the type of nanotubes (SWCNTs, MWCNTs) [35].

2.1.4 Doped carbon nanotubes

The doping of carbon nanotubes with foreign atoms has recently attracted considerable interest, since it changes their electronic structure and consequently affects their electronic and chemical properties that enhance their application in different fields. Doping is the introduction of atoms into the backbone of material.

It can be achieved by intercalating electron donors or acceptors, substitutional doping, encapsulating atoms, molecules or clusters gas adsorption, non-covalent functionalization with organic molecules or wrapping of polymers or covalent functionalization [36]. Substitutional doping of carbon nanotubes was first reported by Stéphan *et al.* in 1994 [37] using the arc discharge method.

The most common dopants are the neighbors of carbon in the periodic table nitrogen, phosphorus, and boron because of their similarity in physical and chemical properties to the carbon atom. The presence of these elements can significantly improve the electronic structure and enhance the electro-catalytic properties of carbon nanotubes [38-43].

2.1.4.1 Nitrogen-doped multi-walled carbon nanotubes

Nitrogen can be easily incorporated into carbon nanotubes. The incorporation of N into CNTs leads to nitrogen doped carbon nanotubes N-CNTs. Since nitrogen has five valence electrons compared to four of carbon, which can lead to doping effect. Namely nitrogen acts as an electron donor by creating an electron donor states near the conduction band [44].

Nitrogen doping also leads to n-type semiconductor behavior. Resulting to improvement in conductivity [45], significant changes in the structure, hardness, and chemical reactivity [46-51].

Different sources of nitrogen were used in the synthesis of N-CNTs such as ammonia gas [52-55] or liquid contained nitrogen (N-liquid) including ethylenediamine [56], acetonitrile [57,58], pyridine, methylpyrimidine [59], benzylamine [60-63] , toluene/benzylamine [52], and pyrazine [64].

The heteroatom can be introduced into the CNT during the synthesis reaction by using NH_3, or by adding N atoms to the carbon source or the catalyst ligand (floating catalyst). The advantage of organonitrogen sources is that it can be nitrogen and carbon source at the same time.

The possible bonding configurations for nitrogen in graphitic networks are presented in Fig.4

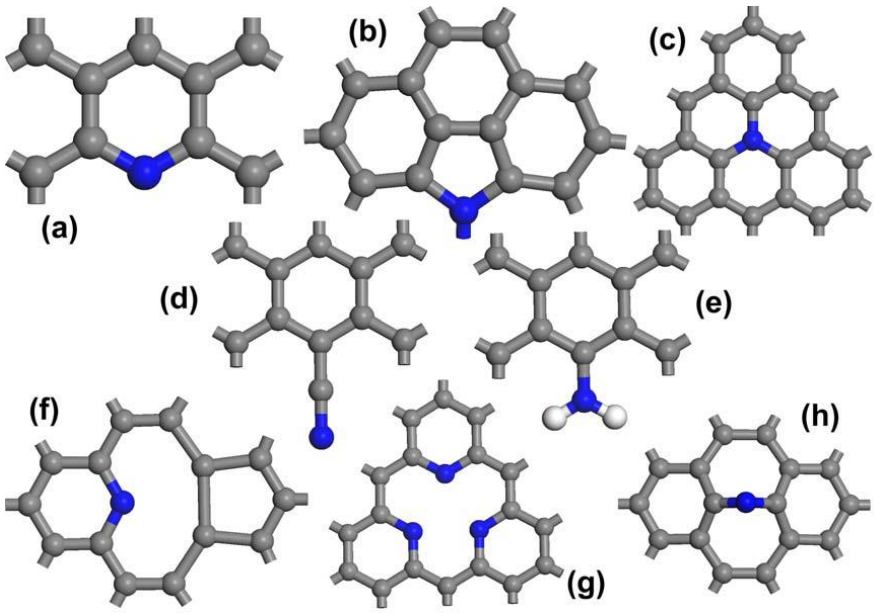

Fig. 4 Possible bonding configurations for N in graphitic networks: **(a)** pyridine-like N, **(b)** pyrrole-like N, **(c)** substitutional N, **(d)** nitrile –C≡N, **(e)** amine - NH_2, **(f)** single N pyridinic vacancy, **(g)** triple N pyridinic vacancy, and **(h)** interstitial N [65].

The three most common bonding configurations are:

Pyridine-like sp^2 - hybridized 6-fold ring arrangement (a).

Pyrrole-like sp^2 - hybridized 5-fold ring arrangement (b).

Substitutional sp^3 - hybridized 6-fold ring arrangement (c).

Nitrogen doped MWCNTs exhibit very distinct morphologies. The structure has been studied by transmission electron microscopy (TEM) and the results revealed that the N-MWCNTs have a so-called 'bamboo' structure, due to the presence of nitrogen, which produce a unique corrugated hollow nanotube structure. The bamboo structures were more distinctly observed by lateral force microscopy (LFM) [66]. The effect of growth temperature on bamboo-shaped C-N nanotubes synthesis was investigated and reported in literature [67]. It was found that the atomic percentage of nitrogen content in the nanotubes depends on the growth temperature. Three different temperatures were studied 850, 900, and 950 °C. It was observed that the bamboo compartment distance and the diameter of nanotubes increase with increasing the temperature. Furthermore, the ratio I_D/I_G decreases with increasing the growth temperature. This can be explained with the increase the size of crystal planar domain in graphite sheets, resulting to a lowering of the degree of disorder and defects.

Many researches have been involved in synthesis of N-CNTs due to their interesting improved electrical properties [68-71].

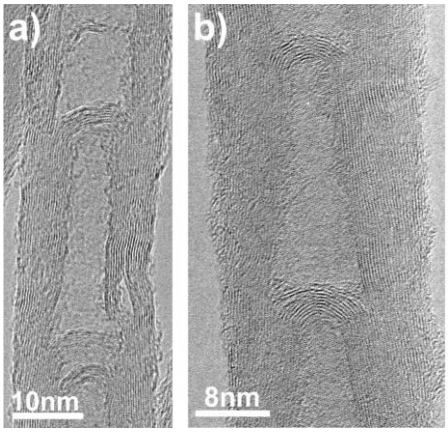

Fig. 5 TEM images of multi-walled carbon nanotubes doped with N atoms, produced by the thermolysis of ferrocene-benzylamine solutions at 850 °C: **(a)** low-resolution image showing the compartmentalized structure of N-doped MWCNTs; **(b)** high-resolution image of an individual compartment showing the continuous closure of tubes [72].

2.1.4.2 Nitrogen-Phosphorus-doped multi-walled carbon nanotubes

Phosphorus is another doping element that can be effectively incorporated in the structure of CNTs leading to modification of the morphology and the properties of CNTs. The doping with phosphorus can be achieved either as single dopant (P-CNTs) [64,73,74] or as co-dopant along with nitrogen (N-P-CNTs) [75, 76]. It has been found that both substitutional P and P-N doping creates highly localized electronic state near to the Fermi level modifying their electronic structure and enhancing the ability of the doped material to be used in electrochemical sensing [77].

The P incorporation mechanism is still an open question. However, the understanding of this process is important for the understanding the N and P co-doping of MWNTs. Triphenylphosphine as phosphorus source with concentration in the rage of 0.15 -0.65 wt. %, ferrocene 2.0 wt. % as catalyst were applied to fabrication the P-MWCNTs [74]. It was reported that the nanotubes in P-MWCNTs exhibit a carbon necklace-like structure. SEM images taken for P-MWCNTs exhibit that the sample consist of corrugated tubes with special structure independently of the content of TPP and they are shorter compared to undoped tubes grown under the same condition. TEM images demonstrate presence of catalytic nanoparticles at the tips as well as inside the tubes (see Fig.6).

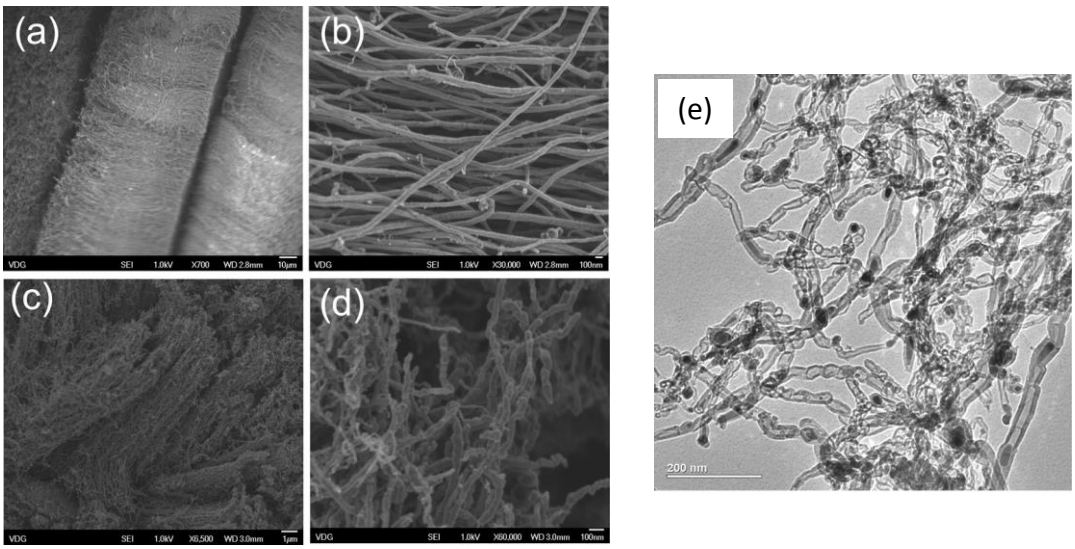

Fig. 6 SEM images of the as-grown MWCNTs: **(a)** and **(b)** undoped tubes having length of about 100 µm. **(c)** And **(d)** corrugated and shorter phosphorus doped MWCNTs prepared with 0.2 wt. % of triphenylphosphine, **(e)** TEM image of P-MWCNTs obtained by pyrolysis of ferrocene and triphenylphosphine in toluene showing carbon necklace morphology [74].

From X-ray diffraction measurement, iron, iron oxide, and iron phosphorus compounds were recognized. These nanoparticles are placed at the walls, at the tips, and inside the tubes. It was found that they play a catalyst role in the growth process. Also XPS spectra confirm the presence of phosphorus doping by recognizing three different peaks refer to P-O, C-P and P-P bonds.

It must to be mentioned that a limited number of articles were reported in co-doping N-P-MWCNTs. According to our knowledge only two studies concerning N-P-CNTs are reported in literature. Triphenylphosphine, benzylamine, and ferrocene were used as phosphorus source, nitrogen source, and catalyst, respectively for the synthesis of N-P-MWCNTs by means of catalytic vapor deposition method (CVD) [75]. The morphology of samples was characterized by means of SEM analysis. The SEM images indicate the high order array of MWCNTs. The results explain also that the length of MWCNTs decrease from 12 µm to 2 -3 µm with increasing the phosphorus content in the spray solution from 2.5 to 3.3 wt %.

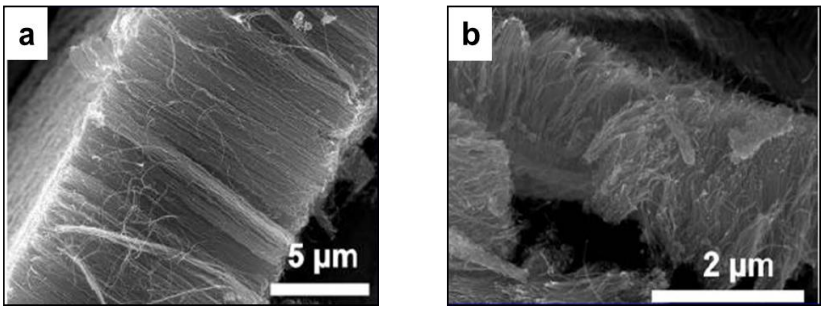

Fig. 7 SEM of N-P-MWCNTs arrays, synthesized at the optimum temperature and carrier gas flow rate, and different TPP concentrations: (a) 2.5 wt %. TPP (b) 3.3 wt %. TPP [75].

TEM micrographs indicate that carbon nanotubes have bamboo-like structure and the catalytic particles are placed in the nanotubes.

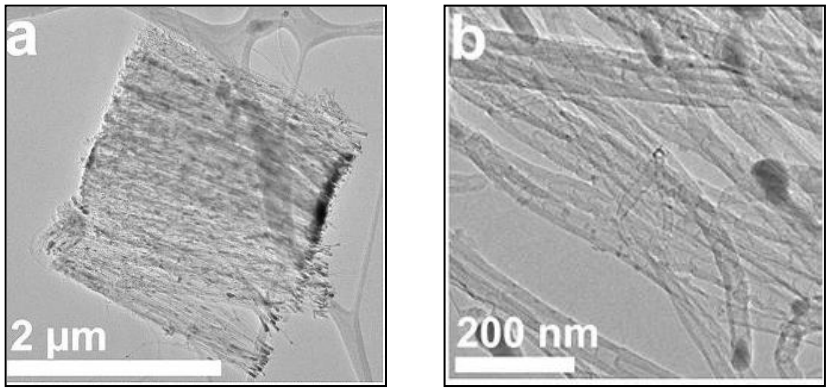

Fig. 8 Low-resolution TEM (a,b) shows the position of metal particles inside CNTs, and their overall morphology [75].

The X-ray diffraction pattern of N-P-MWCNTs show a combination of two phases of iron phosphide Fe_2P and Fe_3P in addition to iron carbide Fe_3C, but EDX spectra confirmed that the iron phosphide particles were the most. Similarly, a reduction of the yield of CNTs was observed with increasing the content of TPP. This is a result of the reduction of nanotubes length, which is attributed to increasing in the ratio Fe_2P to Fe_3P in the catalyst (reduced catalytic activity for Fe_3P).

The production of N-P-MWCNTs was also achieved by using a floating catalyst chemical vapor deposition (**FCCVD)** [76]. In that work imidazole, triphenylphosphine, and ferrocene were used as nitrogen, phosphorus, and catalyst sources, respectively. SEM analysis indicates that the yield and length of carbon nanotubes decreased by increasing the amount of TPP. The length decreased from 29 to 12 µm with increasing TPP from 10 to 50 mg. The results were in agreement with the previous published research work [75].

TEM image confirmed that the N-P-MWCNTs have a similar structure to N-MWCNTs (bamboo-like structure) but different ratio (D_I/D_O), where D_I and D_O are the inner and outer diameters of N-P-MWCNTs, respectively. This ratio is greatly decreased from 0.48 to 0.22 by increasing the TPP content from 10 to 50 mg. The presence of elongated catalyst particles inside the tubes was also observed (Fig.9).

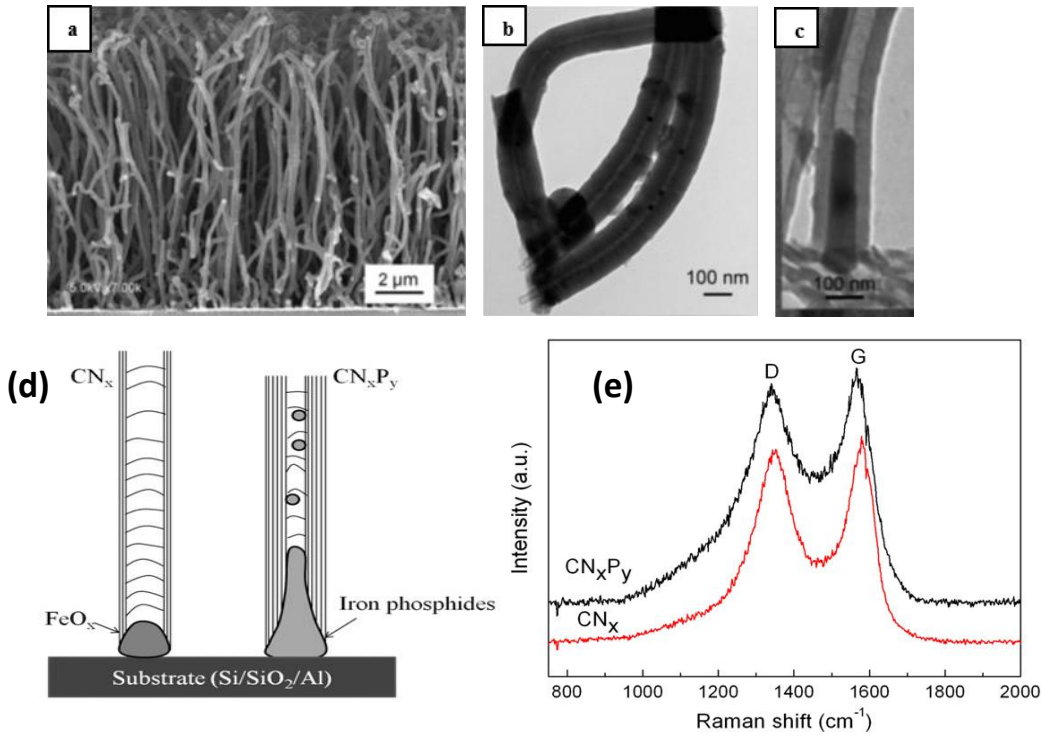

Fig. 9 (a, b) SEM and TEM images of N-P-MWCNTs synthesized with 50 mg of TPP, **(c)** TEM image of an individual N-P-MWCNT synthesized with 30 mg of TPP, **(d)** Schematic diagram of growth mechanisms for CNx and CNxPy, **(e)** Raman spectra of CNx and CNxPy synthesized with 50 mg of TPP [76].

Raman spectroscopy study demonstrates that the addition of TPP increases the disorder and defects in the structure CNxPy. The downshift of G-band was also noticed, which can be attributed to the P doping. In this work we have discussed and studied the effect of addition of TPP to the N-MWCNTs by means of cyclic voltammetry, impedance spectroscopy, SEM, TEM, and Raman spectroscopy (see 4.3.1 and 4.3.2).

2.1.5 Growth mechanisms of carbon nanotubes

2.1.5.1 Undoped carbon nanotubes

Many different models of carbon nanotube growth have been proposed [78-82]. Generally, there are two major mechanisms used to explain the catalytic growth of CNTs which depend on the position of the catalyst particle (sides) with respect to

the substrate. (a) The tip-growth mechanism, where the catalyst particle is located at the tip of the growing tube and (b) the root-growth mechanism, where the catalytic particle is found at the bottom of the tube [83]. The location of the catalyst during formation depends on the strength of the interatomic forces between the metal atoms (catalyst) and the substrate. Thus, if the catalyst-substrate interaction is strong the base growth mechanism will be established. Namely, the hydrocarbon will be decomposed to hydrogen which flies away and carbon that precipitate out on the hot catalyst particle in the form of CNT. The CNTs precipitation cannot push the metal sides up and therefore it is compelled to emerge out from the particles tip. The second growth process result when the interaction between the catalyst and the substrate is weak. The hydrocarbon will be decomposed on the surface of the metal particle, and the carbon will be diffused down. CNTs precipitate out across the particle bottom, pushing the whole metal particle off the substrate and at the end the tip growth mechanism will be formed [84, 85].

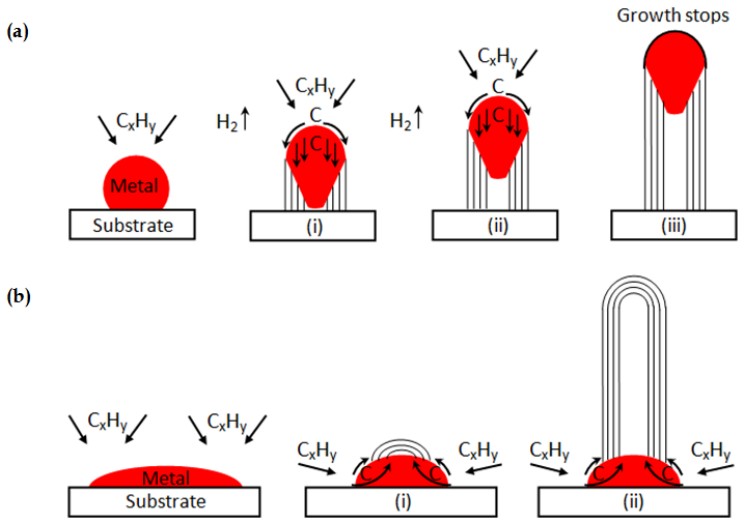

Fig. 10 Widely-suggested growth mechanisms for CNTs: **(a)** tip-growth model, **(b)** base-growth model [86].

2.1.5.2 Nitrogen-doped multi-walled carbon nanotubes

N-MWCNTs have the so-called bamboo structure which consists of regular internal bamboo cavities. This bamboo structure is due to the presence of nitrogen. It was suggested that the role of nitrogen in bamboo compartment formation is because of the generation of pentagons in addition to hexagons [87, 88]. Considerable effort has been made to study the growth mechanism of carbon nanostructures with nitrogen as dopant and several types of models have been proposed [89- 92].

Both illustrated mechanisms (tip and base growth mechanism) (Fig.10) which relate to a deposited catalyst on the substrate have been reported to explain the formation of N-CNTs. The base growth mechanism is commonly proposed

method to the formation of bamboo shaped N-CNTs. In this model, the catalyst particles dissociate reactant molecules giving C and N atoms which incorporated in and on the catalyst particle to form a tubular structure and they will be ejected from the metal particle due to accumulated stress on its surface [93].

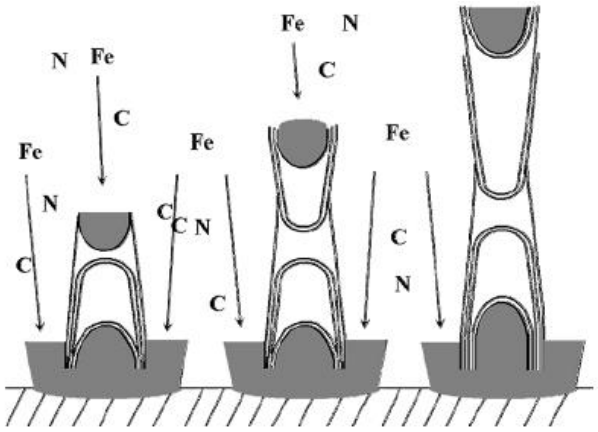

Fig. 11 Model of mixed (base and tip) growth mechanism of N-CNTs [94].

2.1.6 Modification of carbon nanotubes with metal nanoparticles

In recent years, many efforts have led to the development of methods to modify CNTs to obtain derivatives with more attractive properties. Composite nanomaterials that consist of nanocarbon in combination with nanometals are of considerable interest due to their novel optical, electronic, and catalytic properties [95-97]. Metal nanoparticles (MNPs) have a high effective surface area and their optical, electronic, magnetic properties differ from those of bulk material [98-100], and depend on the size and shape of the MNPs [101], therefore they have been used to facilitate the electron transfer and to increase the sensitivity for simultaneous determination of biomolecules [102, 103]. The supported substrates used for the immobilization of metal nanoparticles play a significant role. MWCNTs can be considered as a good substrate for the deposition of metal nanoparticles since they have great electrical conductivity, which improve the kinetic of electron transfer of redox system. Consequently, to enhance their sensitivity and their detection ability, the MWCNTs based-electrodes were modified with the MNPs [104].

The first attempts of decorating CNTs with metal clusters were carried out in 1994. Ajayan and coworkers [105] have spread ruthenium 2,5-pentanedionate onto SWCNTs and reduced it with a hydrogen. The obtained RuNPs were well dispersed on the nanotube surface.

The modification of CNTs with MNPs can be achieved through two main pathways. MNPs either can be grown onto CNTs directly (reduction-deposition) or can be pre-formed and then connected to CNTs.

The reduction of noble metal salts is commonly used to produce MNPs. In this process reducing agent are required such as light, heat or chemicals to reduce the metal cation. The interaction bonds between the MNPs and CNTs are van der Waals bonds, While the commonly used metals are Pt, Au, Pd, Ag, Rh, and Ru [106 -110].

CNTs can also be treated with acids (nitric acid or sulfuric acid) to create functions groups that play a role as anchors in the deposition of MNPs in the presence of reducing agent [111]. Microwave irradiation is another method that was applied to generate function groups (carboxyl, carbonyl, and hydroxyl) without any acid treatment or ultra-sonication [112]. Other methods for the deposition of MNPs are a galvanic cell [113] and electro-deposition [114].

MNPs can be also introduced on the surface of CNTs with indirect methods. Covalent or noncovalent bonds may exist between the MNPs and the surface of CNTs. The MNPs are prepared and connected to the CNTs. The linkers can be classified into two types, functional groups may form covalent bonds with functional groups present on the CNTs [115, 116] and linkers that bind to the CNTs surface through weak interactions such as π-π stacking [117-119] hydrophobic and hydrogen bonds [120] , or electrostatic interactions [121, 122].

Zhu and coworkers [123] have proposed that bamboo-like carbon nanotubes which contain nitrogen can be used as a substrate for the immobilization of AuNPs rather better than undoped carbon nanotubes. They have observed that the AuNPs were finely dispersed, and an increase in the density of MNPs was also remarkable comparing to classic CNTs. These authors explained that by the presence of specific Au–N interactions which make the functionalization with nitrogen benefit for a uniform assembly of metal nanoparticles on CNTs surface.

Many efforts have been devised in this field to improve the modification methods. The direct method is simple and efficient but the size, shape and other properties of MNPs cannot be controlled. The second method is more complicated and requires many chemical reactions, including processes such as the preparation of MNPs and making some surface modification. On the other hand, the advantage of this procedure is the ability to synthesize a desired size and shape of MNPs which is important in many applications.

2.1.7 Carbon nanotubes in sensing

Carbon nanotubes (CNTs) is a very attractive electrode material for the development of sensors, due to their unique properties such as high surface area, great electrical conductivity, excellent mechanical properties, biocompatibility, as well as a great chemical stability [124-126].

Recently, many investigators have demonstrated that CNTs possess good electro-catalytic activities, since they reduce the overpotential and improve the current response of the redox system [127]. Furthermore, CNTs are capable to promote electron-transfer reactions when used as electrode materials in electrochemical reactions providing fast electron transfer kinetic [128].

These properties have attracted much attention and raised interest in CNTs applications making them ideal candidates for sensor to investigate different interesting molecules such as paracetamol, dopamine, ascorbic acid, uric acid, aspirin, and epinephrine [129-133].

2.1.8 Analysis of Biomolecules

Paracetamol is also known as acetaminophen **(AC)** (*N*-acetyl-p-aminophenol or 4-acetamidophenol) is a widely used analgesic and antipyretic drug, especially for the patients that are sensitive to aspirin [134].

It is used worldwide to treat pains such as headache, toothache, arthritis, migraine, neuralgia, muscular aches, and postoperative pain [135]. Generally, AC does not exhibit any harmful side effects, but the overdose in few cases leads to the liver and kidney damage [136]. Therefore, its determination and quality control are of vital importance [137]. AC is an electroactive molecule and its electrochemical behavior has been investigated using various electrochemical methods [138-141]. It was also electrochemically studied in the presence of other molecules such aspirin [142], ascorbic acid [143], and epinephrine [144].

***N*-acetylcysteine (NAC)** is a pharmaceutical drug that can be used because of its hepato-protective activity as antidote for treating acetaminophen poisoning [145]. It is also effective and act as antioxidant and some researcher have suggested his role in preventing some types of cancer [146]. Its electrochemical behavior was also investigated [147- 152]. Since NAC is effective as an antidote in AC overdoses, it would be quite interesting to determine these molecules simultaneously.

Recently, several electrode materials were used for simultaneous determination of Acetaminophen (AC) and *N*-acetylcysteine (NAC), but however the most popular was a modified carbon paste electrode [153, 154].
In this work, AC and NAC were simultaneously investigated on N-MWCNTs modified with AuNPs and PtNPs. To our knowledge, no report about the simultaneous analysis of AC and NAC on N-MWCNTs modified electrode was recorded.

Ascorbic acid (AA) is an important water-soluble substance that is present in many biological fluids, pharmaceuticals, fruits and vegetables. AA is also added to foodstuffs as an antioxidant for stabilizations of color and aroma. It is well known that AA takes part in several biological processes, furthermore AA prevents and treats the scurvy, common cold, mental illness, and cancer [155, 156].

Dopamine (DA) is one of the most important neurotransmitters in the mammalian central nervous system [157]. Low levels of DA may cause neurological disorders such as schizophrenia and Parkinson's disease [158]. DA plays an important and essential role in brain and regulates functions such mood, attention, learning, controlled movement, sleep, motivation and memory [159].

Another physiologically important molecule is **uric acid (UA)** which is the primary end-product of purine metabolism. Abnormal concentrations of UA dissolved in human urine and/or blood are symptoms of several diseases such as gout, hyperuricemia, Lesch-Nyan syndrome, cardiovascular, and kidney diseases [160, 161].

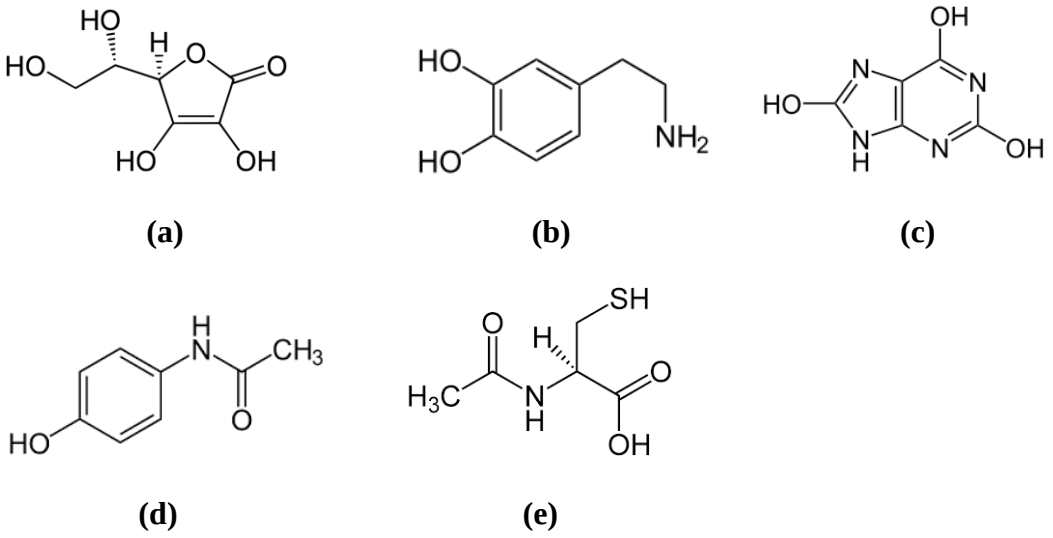

(a) **(b)** **(c)**

(d) **(e)**

Fig. 12 Chemical structure of **(a)** ascorbic acid, **(b)** dopamine, **(c)** uric acid, **(d)** paracetamol, and **(e)** *N*-acetylcysteine.

Since AA, DA, and UA are electrochemically active compounds and coexist in biological fluids, such as in human blood plasma and urine, considerable efforts have been devoted for the detection of these molecules. Various analytical methods were used for this purpose. Among these, electrochemical techniques have more advantages over other methods in sensing due to their relatively low

cost, simple instrumentation, high selectivity, and sensitivity and less time consuming.

Many studies in the literature for individual analysis of these compounds have been reported [162- 164]. The oxidation potentials of AA, DA, and UA at standard electrodes are in the same regions, and thus the peaks are overlapped making their simultaneous determination difficult [165]. To overcome this problem various modified electrode materials, include polymers modified electrodes [166], carbon-ceramic modified electrodes were used [167]. Many modified electrodes have been constructed for the simultaneous detection of AA, DA, and UA [168-174].

In recent years, metal nanoparticles have attracted much more attention in electro analysis because of their unusual physical and chemical properties [175, 176]. Composite materials modified with nanoparticles were applied for simultaneous analysis of AA, DA, and UA [177-181].

In the present work nitrogen-doped multi-walled carbon nanotubes (N-MWCNTs) were decorated with rhodium (RhNPs), palladium (PdNPs), iridium (IrNPs) platinum (PtNPs), and gold (AuNPs) nanoparticles possessing diameters of 2.7, 2.6, 2.7, 2.7, and 14 nm, respectively and were used for the detection of AA, DA, and UA. Furthermore N-MWCNTs composite films were successfully used to simultaneous determination of AA, DA, and UA in a single measurement.

3 Experimental

3.1 Synthesis of doped-MWCNTs

3.1.1 Substrate preparation

The MWCNTs were grown on silicon/silicon oxide substrate Si/SiO_2 (Siegert Consulting e.K., Germany) with geometric surface area was 1.0 cm^2. The used wafer has a thickness of about 525±25 μm /1.7 μm, respectively. Four wafers were sonicated in ethanol for about 5 min and then cleaned with a cotton swab. Afterwards they were placed on the holder (quartz glass), which was placed in a quartz tube (100 cm long). The position of the holder was about 15 cm from the beginning of the tube.

3.1.2 Fabrication of N-MWCNTs

In the present work the (N-MWCNTs) were produced by means of the chemical vapor deposition (CVD) using ferrocene ($FeCp_2$) as catalyst and acetonitrile (ACN) as carbon and nitrogen source for synthesis of (N-MWCNTs).

The spray solution was prepared with following method: 0.1 gr ferrocene was dissolved in 12.8 ml ACN ($d=0.78 g/cm^3$, equivalent to 10 gr) to obtain a solution contain 1% $FeCp_2$ in 10 gr ACN. After that the solution was sonicated about 5 min. The synthesis process was performed in cylindrical furnace at temperature of 850 ^oC using Argon as carrier gas under pressure of 20 KPa. The heating rate was 15 ^oC /min. After the temperature was stabilized at 850 ^oC the solution mixture was introduced in the furnace through a syringe using syringe pump with a flow rate of 10 ml/h. The nebulizer was attached to the quartz tube reactor (internal diameter: 3 cm; length: 100 cm). The decomposition of the carbon-nitrogen containing compounds occurrs on the surface of iron nanoparticles, which play a role as catalyst for the decomposition of carbon source material. Namely, these catalyst nanoparticles are sides for the growing of N-MWCNTs. The growth process lasts for about 20 min for 3 ml spray solution. After that the furnace was switched off and the tube reactor was cooled to ambient temperature under Argon flow. As soon as the oven is cold, the holder can be taken from the tube and the black fabricated wafers can be stored in a small box. The used parameters and conditions such as sprayed volume, flow rate, and the position of the substrate in the quartz tube were the optimum parameters for fabrication of N-MWCNTs in this work.

3.1.3 Fabrication of N-P-MWCNTs

A mixture consists of acetonitrile (ACN) as nitrogen and carbon source, triphenylphosphine (TPP) as phosphor and carbon source, and ferrocene ($FeCp_2$)

as catalyst was used for fabrication of nitrogen-phosphorus doped multi-walled carbon nanotubes (N-P-MWCNTs). 0.2 gr $FeCp_2$ and various amount of TPP (between 0.02 and 0.1 gr) were dissolved in 12.8 ml acetonitrile ACN and sonicated for 5 min. Namely, the last ternary mixture contained 2% $FeCp_2$, TPP (0.2-1 wt %.) in 10 gr acetonitrile. 3ml of the spray solution was sprayed in the oven. The conditions for the production of N-P-MWCNTs were the same with those used for the production of N-MWCNTs.

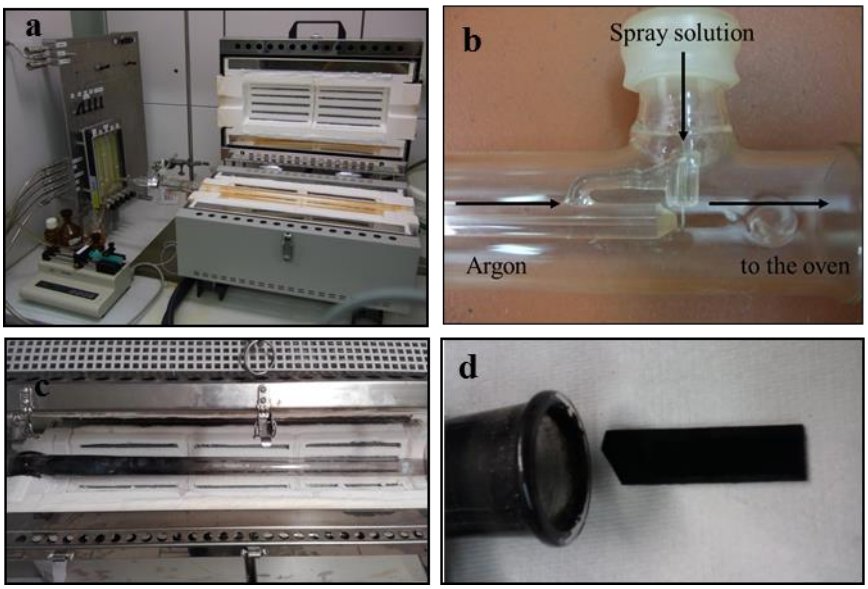

Fig. 13 The scheme of pyrolysis apparatus CVD **(a)**, the spray unit **(b)**, the tube after spraying **(c)**, the produced films on the holder **(d)**.

3.2 Physical characterization of doped-MWCNT films

3.2.1 Scanning electron microscopy (SEM)

To characterize the structures in the micro- and nanometer range an appropriate resolution is require which goes far beyond the conventional light-optical microscopes. The SEM is a microscope that uses electrons instead of light to produce a largely magnified image. It is a most popular technique which is available to give information about the overall morphology of fabricated samples. The process begins at the top of the microscope, where a beam of energetic electrons is produced by an electron gun. This focused beam of high energy electron follows a vertical path in the microscope, which is held within a vacuum. The beam transmitted through electromagnetic fields and lenses until it reaches the sample. The electrons enter the surface of the sample with an energy range from 50 to 30.000 volts leading to eject electrons (secondary SE and backscattered BSE electrons) as well as X-rays from the sample producing

various signals which give information about the sample's surface topography and composition. Detectors collect these electrons and convert them into a signal that produces the SEM image. SEM produces black and white, three-dimensional images.

In conventional SEM the magnification ranging from 20X to approximately 30.000X. In this work a FEI/Philips (model XL30 SEM) equipped with an energy dispersive X-ray spectrometer (SEM/EDS) was used to investigate the arrangement and the alignment of the grown CNTs as well as elemental analysis.

3.2.2 Transmission electron microscopy (TEM)

The transmission electron microscope (TEM) based on the same basic principles as the light microscope but uses electrons instead of light. It uses electrons as "light source" and their much lower wavelength makes it possible to get a resolution a thousand times better compared to a light microscope. The possibility for high magnifications has made the TEM a valuable tool in both medical, biological and materials research.

TEM consist of an electron source which can be tungsten, lanthanum hexaboride (LaB_6 - often called “lab six”), and field emission gun (FEG) which is placed usually at the top of the microscope. Tungsten sources are least expensive but offer lower brightness and have limited lifetimes. The electron gun emits the electrons that travel through vacuum in the column of the microscope and is condensed into a very thin beam at the specimen by the condenser lenses. The specimen must be thin enough to transmit the electrons, typically 0.5 μm or less. After the electron beam passed through the sample, the unscattered (transmitted) electrons are collected and focused by the objective lens and a magnified real image of the specimen is projected by the projection lenses onto the viewing device at the bottom of the column [182].

TEM analysis for various produced and modified films was performed by means of TEM (FEI Titan) operating at 300 KV, images acquired using TEM and elemental analysis acquired using STEM.

3.2.3 X-ray photoelectron spectroscopy (XPS)

X-ray photoelectron spectroscopy (XPS) is a surface characterization technique that can analyze a sample to a depth of 2 to 5 nanometers (nm). XPS reveals the chemical elements that are present at the surface as well as the nature of the chemical bond that exists between these elements. It provides valuable quantitative and chemical state information. In XPS the sample is illuminated with a beam of x-radiation (1.5 kV) in an ultrahigh vacuum causing photoelectrons to be emitted from the sample surface. These give rise to small shifts in the peak

positions in the spectrum, the so-called chemical shifts. An electron energy analyzer is used to measure the energy of the emitted photoelectrons. From the binding energy and intensity of a photoelectron peak, the elemental identity, chemical state, and quantity of detected element can be determined.

3.2.4 Raman Spectroscopy

Raman spectroscopy is a spectroscopic technique based on Raman Effect. In this technique, the sample is illuminated with a monochromatic laser beam which interacts with the molecules of sample. It may be reflected, absorbed or scattered in some manner. Most of the radiation is elastically scattered (called the Rayleigh scatter), a small portion is inelastically scattered (Raman scatter, consist of Stokes and anti-Stokes portions). The inelastic scattering is used to construct a Raman spectrum. The scattered light has a different frequency from that of incident light because of the change in the vibrational energies associated with the bonds of molecules in the sample which provide information about the molecular structure. It is presented as an intensity-versus-wavelength shift. Raman spectroscopy is a powerful tool that is useful in the study of the vibrational properties and electronic structures of CNT [183].The most prominent Raman features in CNTs are the radial breathing modes (RBMs) appears at about 120-250 cm^{-1} and indicate the diameter of CNTs, the so-called G-line is a characteristic feature of the graphitic layers and corresponds to the tangential vibration of the carbon atoms in all sp^2 carbon materials occurs at 1580 cm^{-1}, the characteristic mode is D-line (disordered) which is a typical sign for defective graphitic structures. It occurs around 1350 cm^{-1}; the defects can be porous, impurities or other breaking defects, and G' (second-order Raman scattering from D-band variation) at 2700 cm^{-1}. The intensity ratio of these two peaks (I_D/I_G) gives information and characterizes the relative disorder (degree of defects) of CNTs, the higher the I_D/I_G ratio, the lower the graphitic structural quality of the material [184].

This work reports some investigations carried out by Raman spectroscopy on (MWCNTs) and (doped-MWCNTs). The N-MWCNT films were found to exhibit smaller value of intensity ratio (I_G/I_D) compared to N-P-MWCNTs film, indicating greater degree of structural defects in N-MWCNTs.

3.3 Fabrication of metal Nanoparticles

3.3.1 Photochemical segmented flow technique

Colloidal noble metal nanoparticles were prepared using the photochemical segmented flow technique [185]. A representative scheme of apparatus used for the fabrication of metal nanoparticles is shown in Fig. 14. The apparatus consists of three PC-controlled syringe pumps, PTFE-tubing with an inner diameter of 0.5 mm, standard fluid connectors and one 4-port manifold (both made of polyether ether ketone).

The segmented flow technique is well suited for micro continuous-flow synthesis of plasmonic nanoparticles with high size homogeneity [186, 187] and for tuning of nanoparticle properties [188]. It causes a narrow residence time distribution for all volume elements of the reactant mixture under the UV ray and a high reproducibility of the fluid motion in this range. All noble metal nanoparticles were prepared using the corresponding metal salt solutions (1.0 mM). The salt solution was mixed with the polyvinylpyrrolidone/photoinitiator solution (PVP/PI) in a 4-port-manifold and segmented with perfluoromethyldecalin (PP9). The PVP/PI solution was previously prepared from PVP solution (2 wt %) and 2-hydroxy-40-(2-hydroxyethoxy)-2-methylpropiophenone solution (1.0 mM). The nucleation starts with the irradiation of the segments in the photo initiation element (2 mm length of the focus, irradiation time: 135 ms). The properties of the synthesized metal nanoparticles, such as the particles diameter, the full width at half maximum and the particles number are reported in Table 2.

Table 2 Properties of the fabricated metal nanoparticles.

Parameter	**RhNPs**	**PdNPs**	**IrNPs**	**PtNPs**	**AuNPs**
Particles diameter/nm	2.7	2.6	2.7	2.7	14.4
Full width at half maximun/nm	1.7	1.4	1.5	1.5	5.03
Particles number/ml^{-1}	3.40×10^{13}	2.40×10^{13}	1.66×10^{13}	$3.10x10^{13}$	2.33×10^{12}

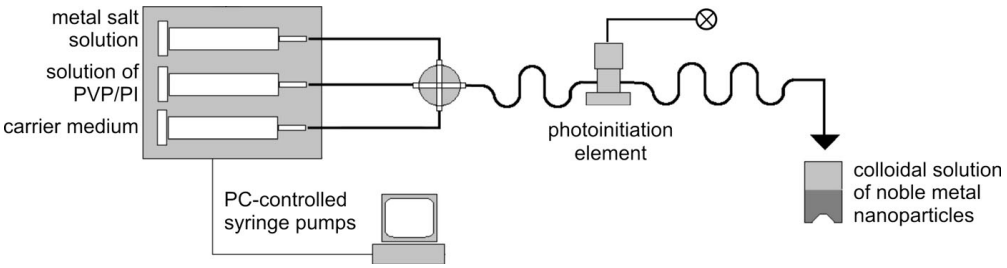

Fig. 14 Scheme of apparatus used for the fabrication of metal nanoparticles (MNPs). *The fabrication of nanoparticles was achieved in cooperation with group of prof. Dr. Köhler, department of Physical Chemistry / Microreaction Technology.*

3.3.2 Chemical fabrication of AuNPs

Another method was applied for synthesis of AuNPs (simple immersion method). The decoration of N-MWCNTs with AuNPs was carried out according to the following procedure: the films were immersed in aqueous solution of $HAuCl_4$ (1.0 mM) and left in solution for about 15 min. Afterwards, the reduction to AuNPs was done with treatment with ascorbic acid (1.0 mM). At the end of treatment, the modified films were washed with doubly distilled water and dried at the room temperature. It must be mentioned that the size of fabricated gold particles was in the range of 200-500 nm.

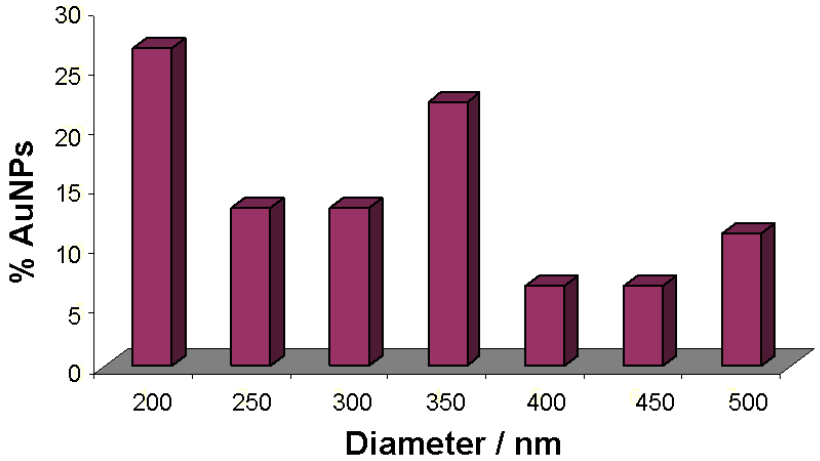

Fig. 15 Histogram showing the diameter of AuNPs and their % content on surface of N-MWCNTs.

3.4 Modification with metal nanoparticles

The doped-MWCNTs were decorated with different metal nanoparticles by immersing the films in aqueous solution of sodium citrate (2.5 mM) for about 10 min. Afterwards the films were dried in the air for about 120 min at room temperature. By using a micropipette, 50 µL MNPs solution was dropped on the surface of films and left for drying. Finally, the films washed carefully with doubly distilled water and let again for drying.

3.5 Electrochemical application

The electrochemical reactions take place at the interface between an electrode and an electrolyte. The relatively low cost, simple instrumentation, high selectivity and sensitivity, and less time consuming make the electrochemical techniques a preferred method that can be applied in wide field. Cyclic voltammetry, impedance spectroscopy, and differential pulse voltammetry are widely accepted methods to solve electrochemical systems problems.

3.5.1 Chemicals and solutions

Polyvinylpyrrolidone (Mw=10000 $g \cdot mol^{-1}$) (>99%), 2-hydroxy-4'-(2-hydroxyethoxy)-2-methyl-propiophenone (>98%), dihydrogenhexachloro-platinate (>99.95%), potassium hexacyanoferrate (III), potassium hexacyanoferrate (II) trihydrate, silver nitrate, potassium chloride, *L*-ascorbic acid (>99%)(Merck), uric acid (>99%) (Fluka), dopamine hydrochloride (>99%), paracetamol or acetaminophen AC (>99.0 %) and *N*-acetylcysteine NAC (>99.0 %), Triphenylphosphine (TPP) (>99 %), ferrocene $FeCp_2$ (>98 %) were purchased from Sigma-Aldrich Chemie GmbH, Germany, Acetonitrile ACN (Merck) was stored over 0.4 nm molecular sieves.

Tetrachloroauric(III) acid trihydrate (>99.5%) and palladium(II) nitrate dehydrate (>99%) were obtained from Carl Roth GmbH, Germany (www.carlroth.com), while perfluoromethyldecalin (>99%), iridium(III) chloride hydrate (>99.9%), and rhodium(III) chloride hydrate (>99.5%) were obtained from F2 Chemicals Ltd., England (http://f2chemicals.com) and Alfa Aesar GmbH & Co KG, Germany (www.alfa.com), respectively.

The solutions for the electrochemistry measurements were prepared by dilution of stock solution of $K_3 Fe(CN)_6/K_4 Fe(CN)_6$ (0.01 M) in 1.0 M aqueous KCl solution. The stock solution was prepared immediately prior to the electrochemical experiments using high-quality deionized water.

Phosphate buffer solution PBS (pH 7.0) was used as electrolyte for the analysis of biomolecules such as paracetamol, *N*-acetylcysteine, ascorbic acid, dopamine and uric acid, since this pH value is very close to the physiological pH (pH 7.36). All solutions were deoxygenated by purging with high-purity nitrogen before the measurement. The measured solutions of biomolecules were prepared prior to measurements directly in electrochemical cell with progressive addition of an appropriate volume of stock solution of each analyst into PBS (pH 7.0).

3.5.2 Preparation of working electrode

The fabricated doped-MWCNTs and modified doped-MWCNTs/MNPs films were connected to copper wire by using silver conducting coating. After about 24 h (when the silver coating was dried), the silver part and the copper wire were carefully covered with a protective coating (nail enamel). Once the varnish layer was dried (after about 15 min), the electrode was ready to be used as working electrode for electrochemical measurements (Fig.16).

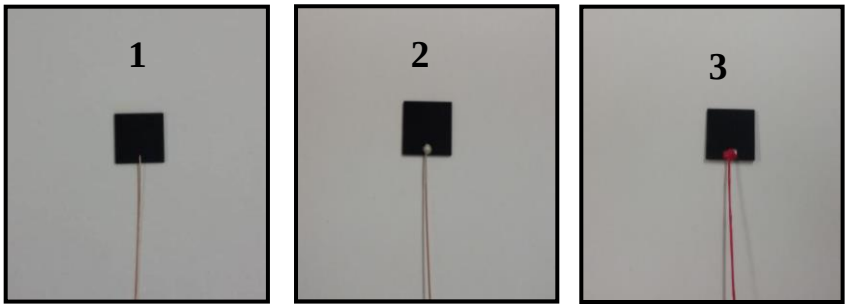

Fig. 16 Images illustrating the steps for the preparation of working electrode.

3.5.3 Electrochemical Cell

A three-electrode system consisting of the working electrode, the auxiliary (counter) electrode, and the reference electrode was used in electrochemical experiment. The electrodes were placed in cell containing the sample solution.

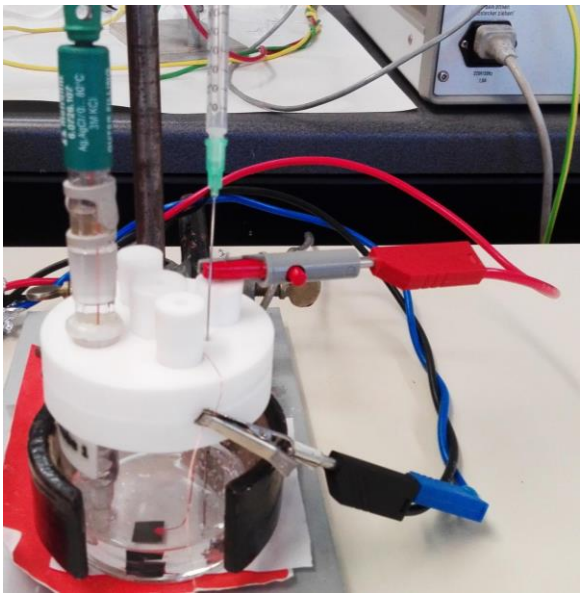

Fig. 17 The electrochemical cell used in this work.

The working electrode, on which the studied process takes place, was either N-MWCNTs, modified N-MWCNTs/MNPs or N-P-MWCNTs films. In some studies, we have also used conventional electrodes such Pt and GC. Silver-silver chloride Ag/AgCl (saturated KCL) was used as reference electrode. It acts as a reference against which the potential of the working electrode is compared. To complete the circuit, counter electrode is required. An inert conducting material, like platinum wire or graphite rod is commonly used [189, 190]. In the present work, platinum plate (3.75 cm^2) was used as counter electrode

3.5.4 Cyclic Voltammetry (CV)

Cyclic voltammetry is the most popular used technique for studying the electrochemical reactions. Its relative simplicity and ability to give information about the redox processes and kinetic, make it widely applied in electroanalytical study. It is a powerful method for characterizing the electrochemical behavior of analyst which can oxidized or reduced [191].

In a cyclic voltammetry the applied potential at a working electrode is ramped linearly versus time. This ramping is known as a scan rate (V/s). The voltage is swept between two values V_1, V_2 at a fixed rate, however when the voltage reaches V_2 the scan is reversed, and the voltage is swept back to V_1. In cyclic voltammetry measurement the potential is applied between the reference and working electrode and the current will be measured between the working and auxiliary electrode [192]. The response of the current is recorded as a function of the applied potential I=f (E), the resulted curve of this measurement is called voltammogram.

All electrochemical measurements were carried out on electrochemical working station Zahner (IM6/6EX, Germany) and the obtained data were analyzed by means of Thales software (version 4.15). All measurements were performed at the room temperature.

3.5.5 Electrochemical Impedance Spectroscopy (EIS)

Impedance spectroscopy is a powerful method which became very popular in applied electrochemistry and materials science. It is used for characterizing the electrical behavior of systems and to obtain information about the reaction mechanism of an electrochemical process. This technique is significant important and widely used in thin-film technology, materials fabrication, corrosion or even in basic electrochemical research.

The concept of EIS is to study the system response with the application of a periodic small amplitude AC signal over a range of frequencies. Impedance is the ratio between voltage and current, demonstrating the ability of a circuit to resist the flow of electrical current, represented by the real impedance term Z_{real}, but it also reflects the ability of a circuit to store electrical energy represented by imaginary impedance term Z_{imag} [193]. The obtained data can be plotted either in a Bode plot or a Nyquist plot. The electrochemical process on an electrode can be simulated to an equivalent circuit consisting of resistors R, capacitors C and inductors W.

In this Study, the electrochemical impedance spectra were recorded with a computer-controlled system Zahner (IM6/6EX, Germany) in the frequency range of 0.10 Hz-100 KHz at the half-wave potential of studied redox system. The EIS spectra were analyzed and simulated using the software Thales (version 4.15).

4 Results and Discussion

4.1 Characterization of N-MWCNTs

4.1.1 Physical characterization of N-MWCNTs

4.1.1.1 Scanning electron microscopy analysis

The N-MWCNTs films were characterized by means of scanning electron microscopy (SEM). The low magnification SEM images reveal that the film's surface is quite homogeneous, and the high magnification SEM images show a carpet of vertically oriented aligned carbon nanotubes. The thickness of the film varies from 20 to 30 µm (Fig.18). To study the chemical composition of film the X-ray photoelectron spectroscopy analysis (XPS) was performed. The extracted data are presented in Table 3. The Results confirmed that the N atoms are incorporated into the structure of the tubules and the overall nitrogen amount was about (~7 wt %).

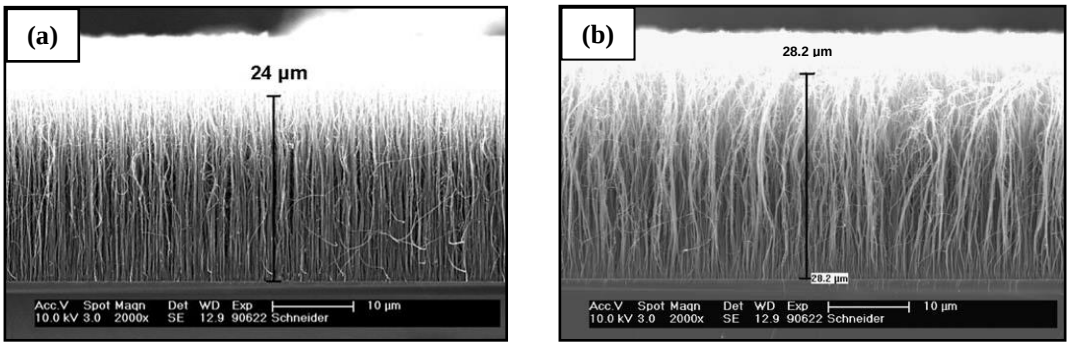

Fig.18 SEM images of vertically aligned N-MWCNTs.

Table 3 The chemical composition of nitrogen doped multi wall carbon nanotubes (N-MWCNTs) estimated by means of XPS [194].

Element	C	N	Fe
Element content %	92.6	7.0	0.4

4.1.1.2 Transmission electron microscopy analysis

TEM images obtained from synthesized wafers are shown in Fig.19. The N-MWCNTs possess bamboo-like morphology, which is common and result from

nitrogen doping. The central channel of the tube contains encapsulated iron nanoparticles. The inner diameter was found to be between 5 and 20 nm whereas the outer diameter lies in the range of 50-100 nm.

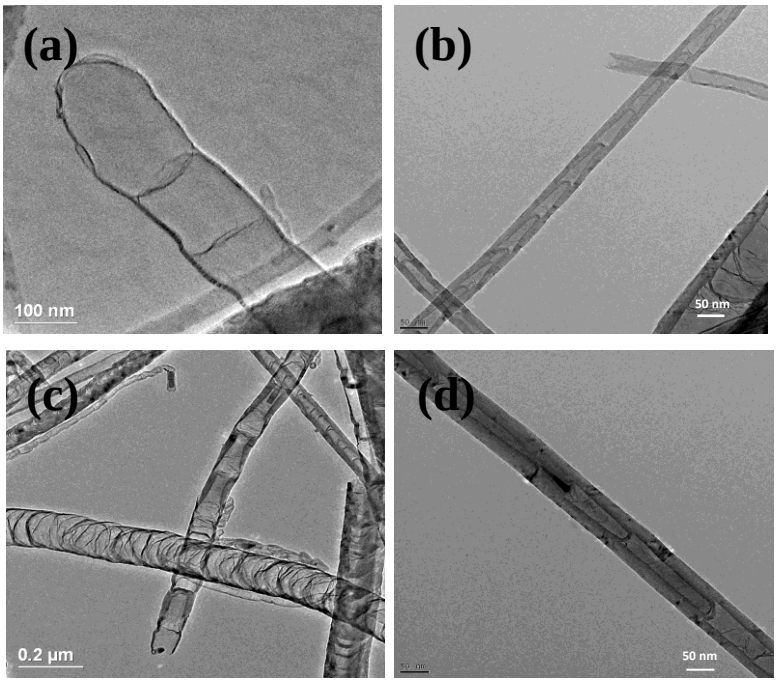

Fig.19 TEM images showing the bamboo-like Structure of N-MWCNTs films.

4.1.2 Electrochemical characterization of N-MWCNTs

4.1.2.1 Cyclic voltammetry

Representative CVs recorded for the standard redox system $[Fe(CN)_6]^{3-/4-}$ (1.0 M KCl) on N-MWCNTs composite films showing the effect of change of concentration of redox system on anodic current density are shown in Fig. 20a.
Quite symmetrical CVs consist of an oxidation wave in the range of 0.31–0.32 V (vs. Ag/AgCl), corresponding to one electron oxidation of $[Fe(CN)_6]^{4-}$ to $[Fe(CN)_6]^{3-}$, and reduction wave in the range of 0.24–0.25 V (vs. Ag/AgCl), representing the reduction of $[Fe(CN)_6]^{3-}$ to $[Fe(CN)_6]^{4-}$ were obtained.

A slight shift of oxidation and reduction peaks to more positive and less positive potentials, respectively, were observed with the increase of concentration of studied redox system $[Fe(CN)_6]^{3-/4-}$. Consequently, the anodic and cathodic peak potential separation $\Delta E_p = E_p^{ox} - E_p^{red}$ tends to increase with the rise in concentration of redox system.

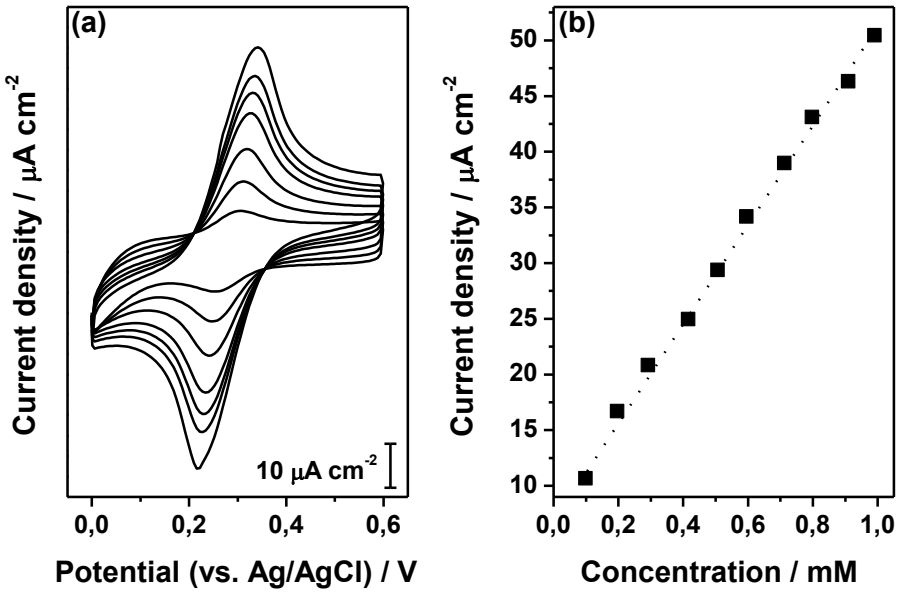

Fig. 20 (a) CVs recorded for various concentrations of $[Fe(CN)_6]^{3-/4-}$ (1.0 M KCl) (from inner to outer: 0.099, 0.196, 0.415, 0.595, 0.712, 0.797, and 0.990 mM) on N-MWCNTs composite film at the scan rate of 0.02 $V.s^{-1}$; **(b)** Variation of oxidation peak current of $[Fe(CN)_6]^{3-/4-}$ with its concentration in the range of 0.099-0.990 mM.

Since the slow electron-transfer kinetic is independent of concentration of redox system, while the effect of uncompensated resistance of electrochemical cell dependents on concentration, the findings reveal that the shift of oxidation and reduction potentials, and thus, the variation of peak potential separation with the change of concentration of redox system is due to cell resistance that remains uncompensated.

The peak current ratio of reverse and forward scans is equal to unity (within experimental error) and independent of the scan rate applied for recording the CVs indicating that there are no parallel chemical reactions coupled to electrochemical process. Furthermore, the oxidative and reductive peak currents are essentially constant for large number of cycles, demonstrating that there are no chemical reactions coupled with the electron transfer and confirming that the studied electro-active species are stable in the time frame of the experiment and that the charge-transfer process occurring on studied composite films is reversible.

The half-wave potential ($E_{1/2}$) of $[Fe(CN)_6]^{3-/4-}$ estimated as the average value of oxidation and reduction peak potential ($E_{1/2}$ = 0.280 V vs. Ag/AgCl), something that is expectable for reversible redox systems. The anodic and cathodic peak potential separation (ΔE_p) obtained on N-MWCNTs film ($\Delta E_p \approx 0.083$ V) appears to be greater compared to the theoretical ΔE_p that is suggested for one-electron-

transfer process ($\Delta E_p \approx 0.059$ V) [195], demonstrating slight deviation of $[Fe(CN)_6]^{3-/4-}$ from reversibility on this particular electrode.

The heterogeneous electron-transfer rate constant k_s was estimated by means of electrochemical absolute rate relation [196] that is based on degree of peak potential separation between the forward and reverse scans. k_s was also determined by means of EIS. It must be mentioned the small amount of cell resistance that remains uncompensated affects slightly the peak-to-peak potential separation and therefore the rate of charge transfer. For the determination of k_s, the diffusion coefficient value of $D = 7.26\times10^{-6}$ $cm^2.\ s^{-1}$ was considered for $[Fe(CN)_6]^{3-/4-}$ [197].

The oxidation peak current density for N-MWCNTs films towards $[Fe(CN)_6]^{3-/4-}$ investigated in concentration range of 0.099–0.990 mM by means of CV technique was found to be linear against the concentration permitting, thus, the determination of lower limit of detection and sensitivity (Fig.20b). The electrochemical parameters extracted from recorded CVs and the estimated values of detection limit and sensitivity are reported in Table 4.

Table 4 Parameters extracted from CVs measurements

parameter	E_p^{ox} (V) [a]	E_p^{red} (V) [a]	ΔE_p (V)	A (cm^2)	i_p^{ox}/i_p^{red}	$K_s(10^{-2}$ cm $s^{-1})$ [b]	$K_s(10^{-2}$ cm $s^{-1})$ [c]	R_{ct} (Ω) [d]	LOD (μM) [e]	S (A M^{-1} cm^{-2})
N-MWCNTs	0.321	0.238	0.083	3.93	1.01	0.51	0.62	58	0.341	0.464

[a] All potentials are reported with respect the Ag/AgCl (KCl sat.) reference electrode.

[b] The k_s values were determined from electrochemical absolute rate relation: $\Psi = (D_o/D_R)^{a/2}k_s(n\pi FvD_o/RT)^{-1/2}$, where Ψ is kinetic parameter, a the charge-transfer coefficient ($a \approx 0.5$), D_o, D_R the diffusion coefficients of oxidized and reduced species, respectively ($D_o \approx D_R$), and n the number of electrons involved in the redox reaction (n = 1) [196]

[c] The k_s values were determined from EIS parameters according to relation: $R_{ct} = RT/n^2F^2Ak_sc$, where R_{ct} is the charge-transfer resistance, A the active surface area, and c the concentration of redox system [198].

[d] The EIS parameters were determined using the equivalent electrical circuit ($R_s + (C_{dl}/(R_{ct} + Z_w))$) (software Thales, version 4.15)

[e] The detection limits were estimated on the basis of signal-to-noise (S/N) ratio of 3 by means of CV technique.

4.1.2.2 Impedance spectroscopy

The electrochemical impedance spectroscopy (EIS) technique is an analytical toll for the investigation of electrical properties of composite films. Consequently, EIS experiments were applied and the electrochemical impedance spectra were recorded in the whole investigated concentration range of 0.099–0.990 mM.

The recorded EIS spectra (presented as Nyquist plots) have the shape of characteristic impedance spectrum, namely they include a part of depressed semicircle followed by a straight line. The depressed semicircle, observed at higher frequencies (it is almost not observable), corresponds to the electron-transfer limited process (very slow electron-transfer procedure), whereas the linear part that can be seen in lower frequencies represents the diffusion limited electron-transfer process (very fast electron-transfer Process).

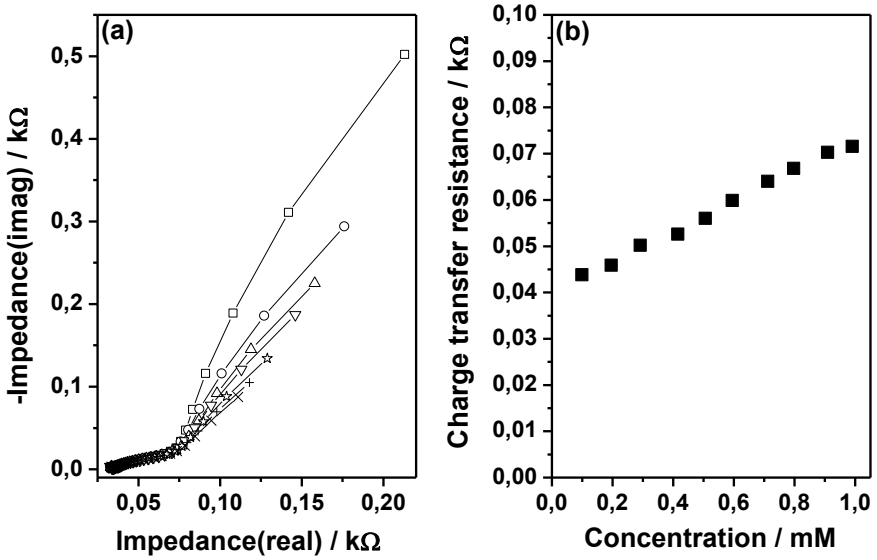

Fig. 21 (a) EIS spectra recorded for various concentrations of $[Fe(CN)_6]^{3-/4-}$ (1.0 M KCl) on N-MWCNTs composite film at the frequency range from 0.1 Hz to 100 kHz. The EIS spectra were recorded at the half-wave potential of $[Fe(CN)_6]^{3-/4-}$ (+0.280 V vs. Ag/AgCl). The symbols are denoted as follows: 0.099 mM (open square); 0.196 mM (open circle); 0.291 mM (open upward triangle); 0.415 mM (open downward triangle); 0.595 mM (star); 0.797 mM (plus symbol); 0.990 mM (X symbol); **(b)** Variation of charge transfer resistance of $[Fe(CN)_6]^{3-/4-}$ with its concentration in the range of 0.099-0.990 mM.

As it can be seen in EIS spectra shown in Fig.21a, an obvious semicircle on N-MWCNTs film can be recognized in high-frequency region of the spectrum indicating that a limited electron-transfer process takes place onto this particular electrode. The equivalent electrical circuit of (R_s + (C_{dl}/ (R_{ct} + Z_w))) was used for

the simulation of the spectra. The circuits' elements can be explained as follows: R_s is the solution resistance, C_{dl} the double layer capacitance (constant phase element was used instead of capacitor), R_{ct} the charge-transfer resistance and Z_w the Warburg diffusion impedance [199].

To study the interfacial properties of N-MWCNTs films, the charge-transfer resistance (R_{ct}) element is chosen, since it controls the electron-transfer kinetics of redox system at electrode interface and represents the barrier for the electron-transfer process.

It was observed that the charge-transfer resistance increases slightly with the rise of the concentration of electro-active substance (Fig.21b). This observation can be connected to the interruption of the electron-transfer process caused by the uncompensated resistance effect, which becomes more significant with increase of concentration of the electro-active substance. From the impedance parameters, the k_s values of $[Fe(CN)_6]^{3-/4-}$ redox system on N-MWCNTs composite films were once more estimated and are included in Table 4.

It was found that the k_s values estimated by means of EIS Technique differ somewhat 21 % from those approximated by means of electrochemical absolute rate relation. This disagreement can be attributed to the greater inaccuracy of calculating k_s by means of electrochemical absolute rate relation (because of the hardness and roughness of the films and also the effect of uncompensated resistance).

4.1.3 Application of N-MWCNTs for analysis of biomolecules

4.1.3.1 Electrochemical detection of acetaminophene on N-MWCNTs and MWCNTs

Paracetamol (AC) is an active electrochemically compound because of the presence of hydroxyl Group in its molecular structure. It is very interesting to study its oxidation behavior on synthesized N-MWCNTs films and get some more information about the kinetic. AC is oxidized to *N*-acetyl-p-quinone imine (NAPQI) and this electrochemical oxidation that involves two electrons and two protons transfer is quite common for other aminophenol (Fig.22).

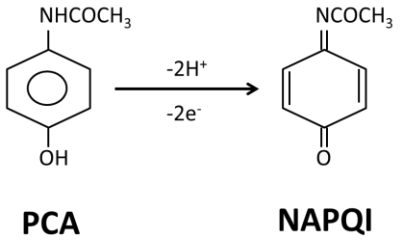

Fig. 22 Electrochemical oxidation of paracetamol PCA [200].

CVs for various concentrations of AC in the range of 0.118-0.907 mM in (PBS, pH 7.0) were recorded on N-MWCNTs films. Some represented CVs at scan rate 0.05 V.s^{-1} are shown in Fig.23.

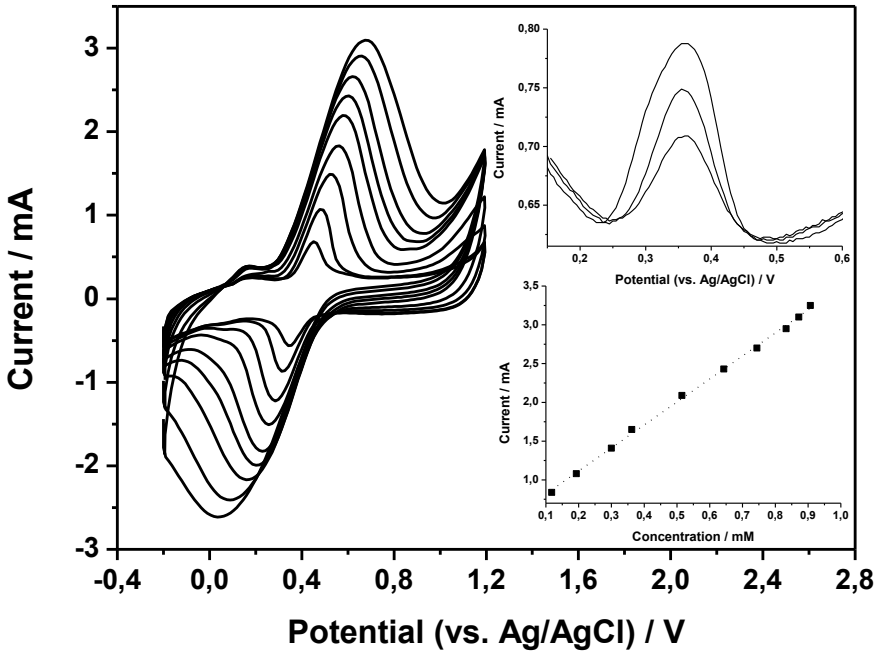

Fig. 23 Representative CVs recorded for various concentrations of AC (PBS, pH 7.0) on N-MWCNT film at the scan rate of 0.05 V.s^{-1} (from inner to outer: 0.118, 0.193, 0.300, 0.362, 0.515, 0.643, 0.744, 0.833, and 0.872 mM); Insets: Representative DPVs recorded for AC (PBS, pH 7.0) on N-MWCNT film (from inner to outer: 0.118, 0.193, and 0.300 mM), and the effect of concentration of AC on anodic peak current in the concentration range of 0.118–0.907 mM.

As it can be seen in Fig.23, the CVs seem to be symmetric in the studied range (0.118-0.907 mM), which indicate that the amount of oxidized and reduced current is almost equal. The N-MWCNT film exhibits a reproducible quasi-reversible redox response towards oxidation of AC, confirming that no parallel chemical reaction takes place, and that the charge–transfer process occurring on N-MWCNT film is quasi-reversible.

The effect of concentration of AC on anodic peak current is graphically presented (inset Fig.23). The current increases linearly with increasing the concentration in the range 0.118–0.907 mM. The oxidation potential of AC lies at about 0.440 V (vs. Ag/AgCl) and appears to be less positive potential comparing to that measured on other electrode material (see Table.5), and the reduction potential was about 0.350V (vs. Ag/AgCl). From the recorded CVs the oxidation and reduction peak separation $\Delta E_p = E_p^{ox} - E_p^{red}$ was estimated. The obtained ΔE_p value exhibit that is greater than what was theoretical expected for Nernstian, two-electron transfer process $\Delta E_p = 0.059/n$ V, n is the number of transferred electron (in this case $n = 2$, $\Delta E_p = 0.0295$ V) [201]. The ΔE_p values of this redox system on N-MWCNTs vary from 0.113 to 0.655 V in the studied range of concentration and increases almost linearly with increasing the concentration of AC (Fig.24).

As it was expected, the anodic and cathodic peak currents increase with increasing scan rate, and the dependence of current on square root of scan rate is linear, showing that the charge–transfer process occurring on N-MWCNT film is diffusion controlled [202, 203].

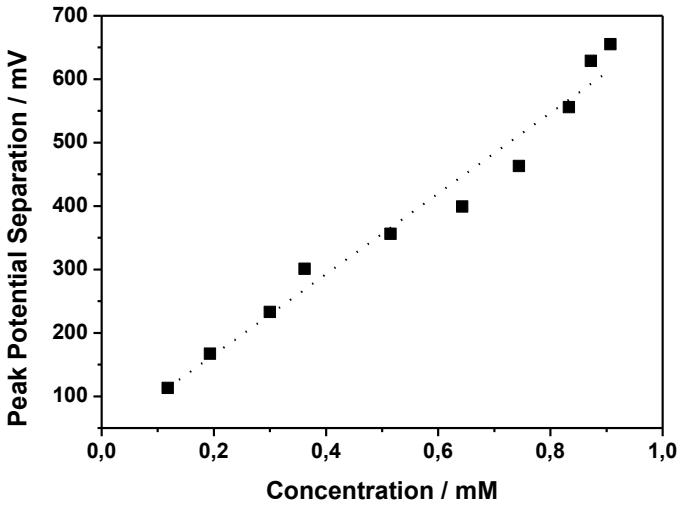

Fig. 24 Plot of variation of peak potential separation with the concentration of AC on N-MWCNTs film (PBS, pH 7.0).

The great ΔE_p value (ΔE_p>600 mV) for the oxidation of AC on conventional glassy carbon electrode was also observed by other scientists [204]. If one considers that ΔE_p is inversely related to heterogeneous electron transfer rate constant (k_s) and therefore to kinetics of redox reaction, it can be concluded that the large ΔE_p values demonstrate the significant deviation of AC/NAPQI redox couple from reversibility. However, considering that the slow electron transfer kinetic does not depend on concentration of electroactive species, while the effect

of uncompensated resistance depends on their concentration, the observed concentration dependence of peak potential separation clearly reveals that the residual uncompensated solution resistance is probably responsible for the great ΔE_p values. In addition, the great peak potential separation can be also result from coupled chemical reactions, something which is not the case that the cathodic and anodic peak current ratio reaches unity.

Anyhow, the peak potential separation value is not realistic, and thus, the value of rate constants of studied redox system cannot be determined from the electrochemical absolute rate relation, which is based on the degree of peak potential separation between the forward and the reverse scans.

In other words, for redox systems displaying ΔE_p values less than 390 mV [205] (the ΔE_p values of AC/NAPQI on N-MWCNT vary from 113 to 655 mV in studied concentration range of 0.118– 0.907 mM). Nevertheless, the "real" peak potential separation (ΔE_p^{kin}) can be approached graphically from the plot of peak potential separation versus peak current for different concentrations of electroactive species at a given potential scan rate according to the relationship: $\Delta E_p = \Delta E_p^{kin} + 2 i_p R$ (where R is the uncompensated resistance) [206]. Thus, from the linear plot ΔE_p versus i_p (correlation coefficient 0.9766) (Fig.25), the ΔE_p^{kin} value of 0.074 V was estimated, which is more than two times greater from the expected ΔE_p for a reversible two-electron transfer (ΔE_p=0.0295V), confirming that the redox process involving AC/NAPQI is quasi-reversible. From the ΔE_p^{kin} value of 0.074 V, the heterogeneous electron transfer rate constant of $k_s = 3.6\times10^{-3}$ cm s^{-1} was estimated for AC/NAPQI on N-MWCNT film using the absolute rate relation.

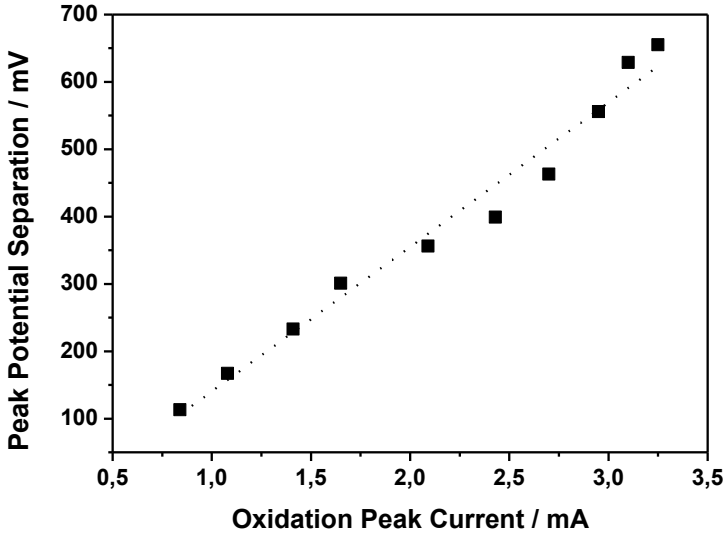

Fig.25 Plots of variation of peak potential separation with the oxidation peak current on N-MWCNT film (PBS, pH 7.0).

In order to estimate the detection limit and the sensitivity of N-MWCNT towards AC/NAPQI, the relationship between the oxidation peak current and concentration of AC in the range of (0.118–0.907 mM) was investigated (inset Fig.23). It can be seen that the relation is linear in the whole investigated range with correlation coefficient of 0.9939. The value of detection limit and sensitivity were estimated graphically to be 0.485 μM and 0.8406 A M^{-1} cm^{-2}, respectively. The detection limit was also calculated using DPV technique in the concentration range of (0.118–0.515 mM) (inset Fig.23). The relationship between peak current for oxidation of AC versus its concentration was linear (correlation coefficient 0.9980), and the estimated detection limit of 0.475 μM seems to be in a very good agreement within experimental error (∼3 %), with that determined by means of CV method.

The same study was carried out on the pristine MWCNTs. Namely, CVs were recorded for different concentration of AC in PBS pH 7.0 at the same conditions (Fig.26). A quasi-reversible behavior for AC/NAPQI redox system was identified, and the CVs seem to be somewhat unsymmetrical with slight current differences between forward and reverse scans. It muss to mention that an additional peak which lies at about 0.2 V can be seen, that is probably attributed to the presence of iron nanoparticles incorporated in the structure of pristine MWCNTs. A poorer detection limit (0.950 μM) and sensitivity (0.601 A M^{-1} cm^{-2}) were determined graphically from the calibration curve current versus AC concentration in same concentration range (inset Fig.26). The findings clearly indicate that the doping of MWCNTs with nitrogen affects strongly their electrochemical quality. In this work, it was verified that the N-MWCNTs possess a rapid response with enhanced detection ability and sensitivity comparing to the pristine MWCNT-based films.

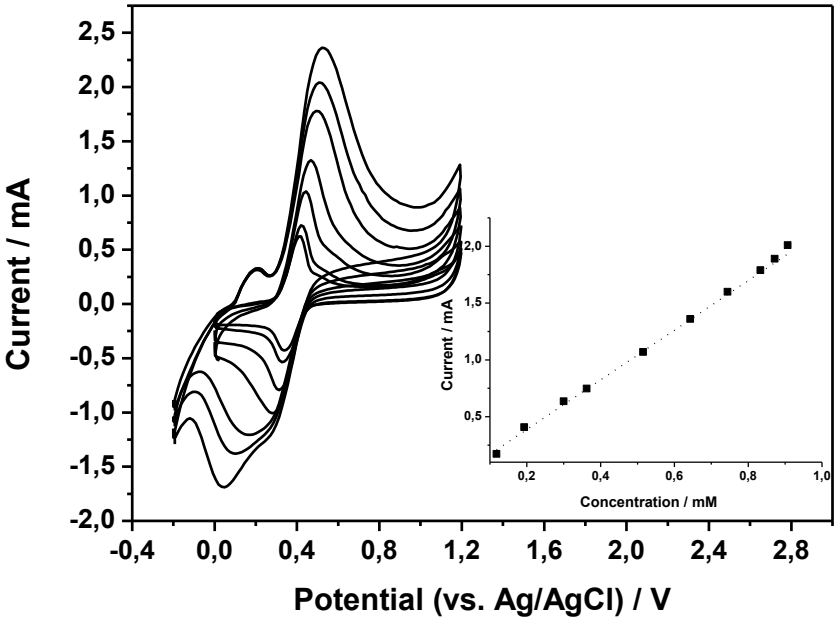

Fig.26 Representative CVs recorded for various concentrations of AC (PBS, pH 7.0) on film consisting of pristine MWCNTs at the scan rate of 0.05 V s^{-1} (from inner to outer: 0.300, 0.362, 0.515, 0.643, 0.744, 0.833, and 0.907 mM); Inset: Effect of concentration of AC on anodic peak current in the concentration range of 0.118–0.907 mM.

The impedance spectroscopy technique was also applied to study the response of the fabricated N-MWCNTs towards the oxidation of AC/NAPQI. EIS spectra were recorded on the N-MWCNTs films in the presence of AC with different concentrations (Fig.27). The obtained Nyquist plots were simulated by means of equivalent electrical circuit: (R_s+(C_{dl}/R_{ct})+C_f+Z_w) (software Thales, version 4.15) (inset Fig.27). The circuit's elements can be explained as follows: R_s is resistor representing the cell's uncompensated resistance, R_{ct} is resistor representing the charge–transfer resistance, C_{dl} and C_f are capacitors corresponding to double-layer capacitance and film's surface capacitance, respectively, and Z_w represents the Warburg diffusion impedance. The microscopic roughness of N-MWCNT film causes an inhomogeneous distribution in solution resistance and double-layer capacitance, and for this reason, the capacitor was replaced by constant phase element (CPE).

From EIS spectra it can be seen that in high-frequency range of the spectrum the impedance is controlled by the interfacial electron transfer, while at low-frequencies, the Warburg impedance is generated. The extracted values of R_{ct} were presented versus the concentration of AC in inset of Fig.27. It was observed that the value of charge transfer resistance decreases with increasing the concentration of AC, clarify that the barrier for electron transfer slightly decreases, and thus, the charge–transfer rate increases. It is interesting that the

obtained R_{ct} values for the oxidation of AC on N-MWCNT are significantly smaller compared to those obtained on bare glassy carbon electrode under the same conditions [207].

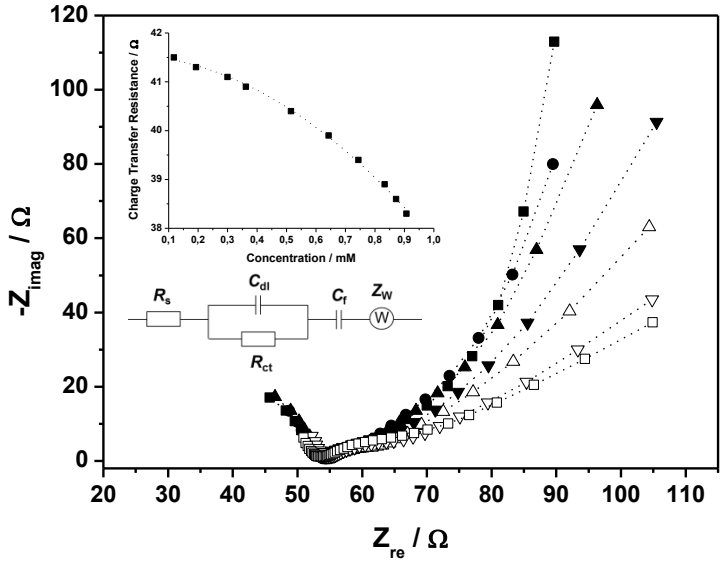

Fig. 27 Representative Nyquist plots for various concentrations of AC (PBS, pH 7.0) on N-MWCNT film. The symbols are denoted as follows: (filled square) 0.118 mM, (filled circle) 193 mM, (filled upward triangle) 0.300 mM, (filled downward triangle) 0.362 mM, (open upward triangle) 0.515 mM, (open downward triangle) 0.643 mM, and (open square) 0.744 mM. Insets: The effect of concentration of AC on charge transfer resistance in the concentration range of 0.118–0.907 mM; the electrical circuit used for the simulation of recorded EIS spectra (software Thales, version 4.15).

As a result, smaller values were obtained on N-MWCNTs. These findings demonstrate clearly the importance of carbon nanotube material in enhancing the electrocatalytic activity. Also interesting is that the R_{ct} values for AC/NAPQI on N-MWCNT film are somewhat smaller (around 9 %) compared to those obtained on film consisting of pristine MWCNTs. The last finding confirms once more the important effect of nitrogen doping on electrocatalytic activity of carbon nanotubes. The heterogeneous rate constant k_s was also estimated from the impedance parameters, its value was in the range from 3.9×10^{-3} to 5.47×10^{-4} cm s^{-1} (in concentration range of 0.118– 0.907 mM) and seems to be agree well to k_s values calculated using the electrochemical absolute rate relation (3.6×10^{-3} cm s^{-1}). A comparison of detection limits and sensitivities of N-MWCNT with those of other novel electrode materials reported in literature towards AC/NAPQI is shown in Table 5. From this comparison, it is remarkable that the detection ability of N-MWCNT film is quite enhanced.

Table 5 Comparison of electrochemical parameters of AC obtained in the present work on N-MWCNT film with those reported in literature for other novel electrode materials.

Electrode	Conditions	E_p^{ox}/V[a]	DL/μM	S/A M^{-1} CM^{-2}
N-MWCNT[b]	PBS/pH 7.0	0.440	0.485	0.8406
MWCNT[b]	PBS/pH 7.0	0.437	0.950	0.6010
GCE/C60 [c]	PBS/pH 7.2		50	13.04
PGE/MIP[d]	PBS/pH 7.0		0.79	
PVC/TTF–TCNQ[e]	PBS/pH 7.4	0.425	0.66	53
CPE/Cu/Z[f]	BRBS/pH 10	0.300	0.10	
GCE/MWCNT[g]	PBS/pH 7.0		0.19	
CPE/G[h]	AMBS/pH 8.5	0.344	0.60	0.282
GCE/G/Nd[i]	PBS/pH 3.0	0.650	14.22	0.531
CCE/Co[j]	KOH/pH 13	0.450	0.37	0.0296

[a] Potential versus Ag/AgCl reference electrode.
[b] N-MWCNT and pristine MWCNT films fabricated in present work.
[c] Glassy carbon electrode modified with C_{60}. The sensitivity is reported in μA mM^{-1} [208]
[d] Pencil graphite electrode modified with molecularly imprinted polypyrrole [209]
[e] Composite electrode consisting of poly(vinyl chloride), tetrathiafulvalene 7,7,8,8 tetracyanoquinodimethane salt modified with gold nanoparticles. The sensitivity is given in mA M^{-1} [210]
[f] Carbon paste electrode modified with copper(II)-doped zeolite [211]
[g] Glassy carbon electrode modified with multi-walled carbon nanotubes [212]
[h] Carbon paste electrode modified with graphene. The potential is reported versus saturated calomel reference electrode. The sensitivity is reported in μA $μM^{-1}$; AMBS ammonia/ammonium buffer solution [213]
[i] Glassy carbon electrode modified with graphene oxide and neodymium hexacyanoferrate [214]
[j] Carbon ceramic electrode modified cobalt oxide nanoparticles. The potential is reported versus saturated calomel reference electrode. The sensitivity is given in μA $μM^{-1}$ [215]

4.2 Characterization of N-MWCNTs/MNPs

4.2.1 Characterization of N-MWCNTs modified with AuNPs (chemical reduction)

4.2.1.1 Scanning electron microscopy SEM/EDX

As it can be seen in SEM micrographs (Fig.28), the bright particles AuNPs having various diameters are dispersed homogeneously onto the surface of N-MWCNTs films and no agglomeration of nanoparticles takes place. By using ascorbic acid as reducing agent to reduce the Au^{3+} ions from its aqueous solution (Chloroauric acid, $HAuCl_4$) to AuNPs, relative large particles are obtained, their diameter in the range of (200-500 nm), (see Fig.15 in 3.3.2). From SEM images we can see that the AuNPs with diameter 200 nm appear to be formed in the greater amount on

the surface of N-MWCNTs (about 27 %). The SEM/EDX analysis of selected AuNPs confirms that these nanoparticles consist of gold (94.4 %). As it is already known, the size of deposited nanoparticles depends on the type of the reducing agent, and faster reaction with strong reducing agents results to smaller nanoparticles [216].

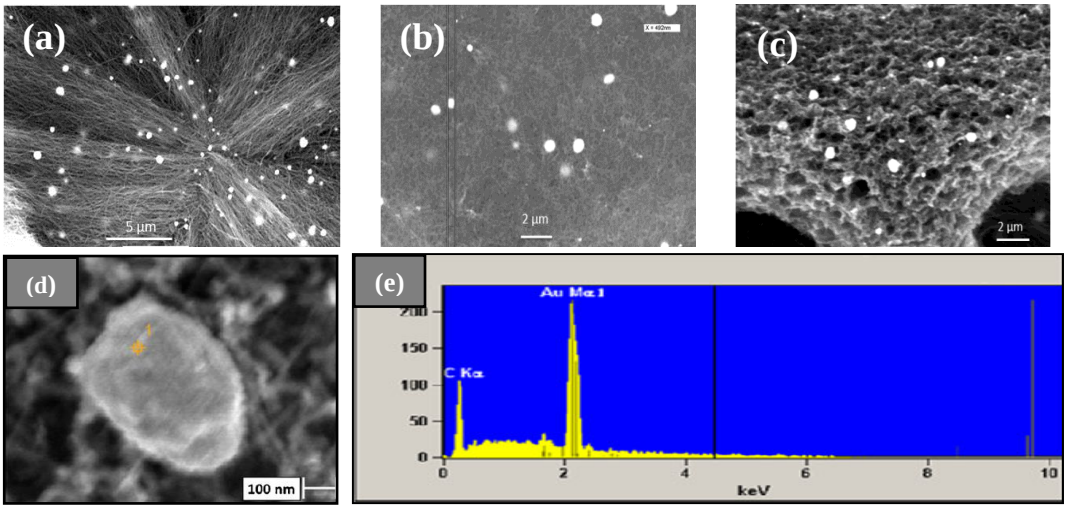

Fig. 28 SEM images of N-MWCNTs/AuNPs using ascorbic acid as reducing agent **(a,b,c)**, SEM micrograph showing the selected AuNPs and its recorded corresponding EDX spectrum **(d,e)**.

Hydrogen gas (H_2) was also used as another reducing element. Firstly, Argon gas was introduced to a small Pre-heated oven (100°C) containing wafers which were already immersed in $HAuCl_4$. Afterwards H_2 gas was introduced for about 10 min to reduce the Au^{3+} ion to AuNPs. At the end the oven was turned off and let to cool until 40°C under the flowing of Ar gas. SEM images recorded for N-MWCNTs/AuNPs films reveal that the deposited AuNPs (recognized as bright cyclic dots) dispersed also homogeneously on the fabricated films without agglomeration and significantly have smaller size comparing to those deposited using ascorbic acid (Fig.29).

The size of AuNPs obtained using Hydrogen as reducing agent was not unified, but the prevailing size was about 100 nm (about 70% from the total number of AuNPs).

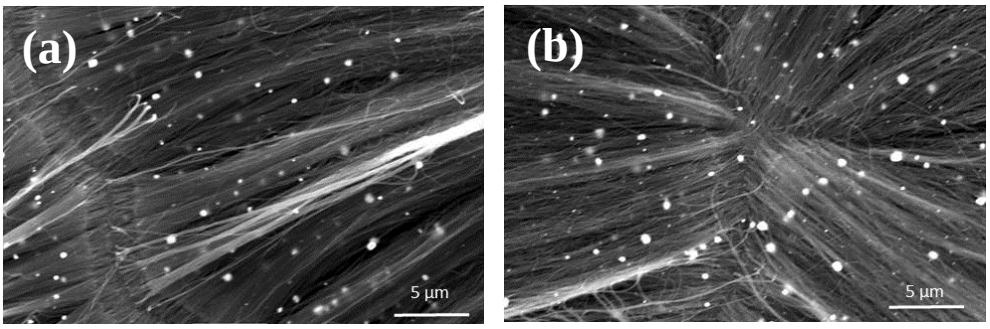

Fig.29 SEM images of N-MWCNTs/AuNPs films using H_2 gas as reducing agent (a,b).

4.2.2 Elechtrochemical Characterization of N-MWCNTs/AuNPs

4.2.2.1 Cyclic voltammetry

The electrochemical response of the synthesized films was investigated toward the standard redox system ferro/ferricyanide, $[Fe(CN)_6]^{3-/4-}$ (1.0 mM) in aqueous 0.1 M KCl solution. CVs recorded for $[Fe(CN)_6]^{3-/4-}$ on N-MWCNTs/AuNPs exhibit a pair of quite reversible anodic and cathodic peaks (Fig.30a). The peak potential separation of $\Delta E_p \approx 0.070$ V (v = 0.02 V s^{-1}) was observed, which is very close to that expected for one-electron reversible redox process (ΔE_p=0.064 V), and smaller compared to that obtained on unmodified N-MWCNTs film ($\Delta E_p \approx 0.083$ V; v = 0.02 V s^{-1}).

CVs show also that the peak current ratio of reverse and forward scans is equal to unity and is independent of scan rate indicating that there are no parallel chemical reactions coupled to the studied electrochemical process (it is well known that parallel reactions change significantly the ratio of peak currents). Furthermore, the oxidative and reductive peak currents are constant for numerous cycles, indicating that there are no chemical reactions coupled to electron transfer process, and confirming that the studied couple $[Fe(CN)_6]^{3-/4-}$ is stable in time frame of experiment and that the charge transfer process occurring on N-MWCNTs/AuNPs film is reversible. The half wave potential of $E_{1/2}$=+0.228 V (vs. Ag/AgCl) was estimated for $[Fe(CN)_6]^{3-/4-}$ on N-MWCNTs/AuNPs. The anodic peak current was found to vary linearly with the square root of the scan rate (in the range of 0.02–0.30 V s^{-1}) demonstrating that the redox system $[Fe(CN)_6]^{3-/4-}$ is diffusion controlled on N-MWCNTs/AuNPs film (Fig.30b).

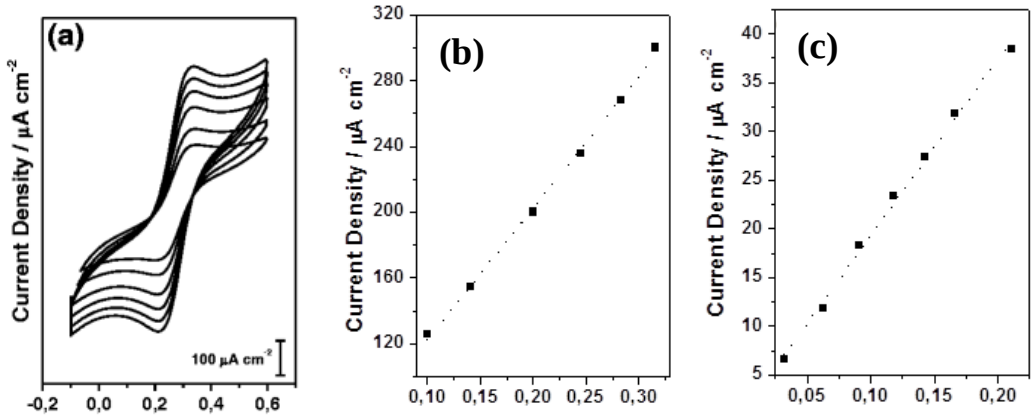

Fig.30 (a) CVs recorded for 1.0 mM $[Fe(CN)_6]^{3-/4-}$ (1.0 M KCl) on N-MWCNTs/ AuNPs in scan rate range of 0.01–0.10 V s^{-1} (from inner to outer: 0.01, 0.02, 0.04, 0,06, 0.08, and 0.10 V s^{-1}). **(b)** Variation of anodic peak current density with the square root of scan rate in the range of 0.01-0.10 V s^{-1} for 1.0 mM $[Fe(CN)_6]^{3-/4-}$ (1.0 M KCl) on N-MWCNTs/AuNPs. **(c)** Variation of anodic peak current density with the concentration of $[Fe(CN)_6]^{3-/4-}$ in the range of 0.032-0.211 mM for $[Fe(CN)_6]^{3-/4-}$ (1.0 M KCl) on N-MWCNTs/AuNPs.

It was verified that an improvement of film's current response occurs upon modification with AuNPs. Namely, an obvious increase of film's current response towards $[Fe(CN)_6]^{3-/4-}$ of about ~50 % can be observed upon modification with AuNPs compared to the current response of unmodified N-MWCNTs (Fig.31).

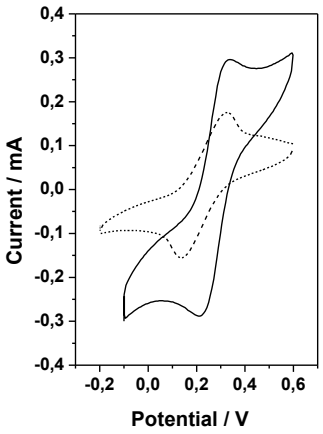

Fig.31 CVs recorded for $[Fe(CN)_6]^{3-/4-}$ (1.0 mM) on either N-MWCNTs (dotted-dashed lines) or N-MWCNTs/AuNPs (solid lines) (0.1 M KCl).

The findings demonstrate that the presence of AuNPs onto N-MWCNTs surface enhances their electrocatalytic properties and improves significantly their electrochemical response.

4.2.2.2 Impedance spectroscopy

The electrochemical impedance spectroscopy technique was also applied to study the kinetic of $[Fe(CN)_6]^{3-/4-}$ redox system on N-MWCNTs/AuNPs. Representative EIS spectra recorded for various concentrations in the range of 0.063–0.211 mM are shown in Fig.32a. As it can be seen, the impedance is controlled by the interfacial electron transfer at high frequencies, while at low frequencies the Warburg impedance is generated. Furthermore, the variation of concentration of electroactive compound affects slightly the film's impedance behavior. The extracted impedance data were fitted by using the software Thales (version 4.15) in order to study the interfacial properties of modified films. It was found that the charge transfer resistance R_{ct} tends to decrease upon modification of films with AuNPs demonstrating the barrier for electron transfer decreases and the electron transfer rate increases.

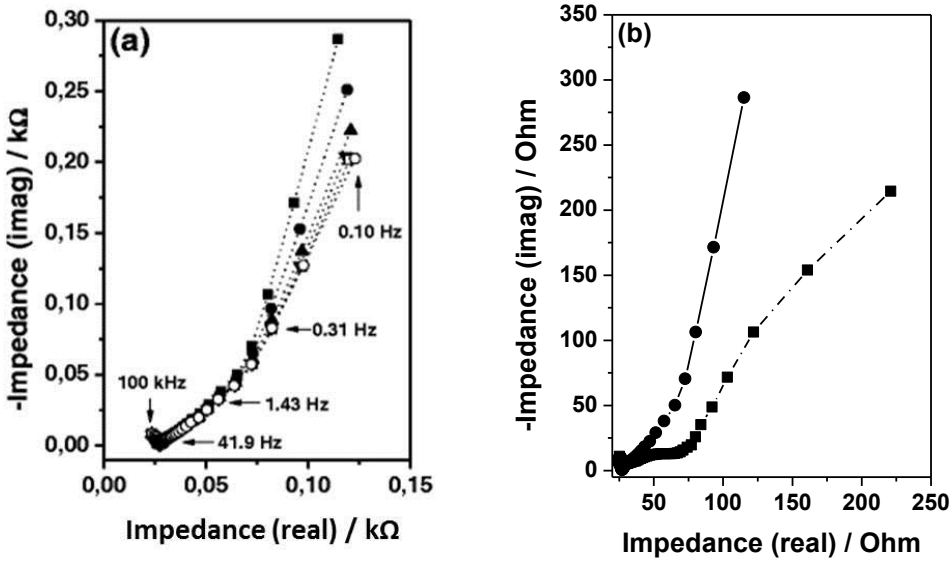

Fig.32 (a) EIS recorded for various concentrations of $[Fe(CN)_6]^{3-/4-}$ (1.0 M KCl) in the range of 0.063–0.211 mM on N-MWCNTs/ AuNPs in the frequency range of 0.1 Hz to 100 kHz. The symbols are denoted as follows: 0.063 mM (■); 0.091 mM (●); 0.118 mM (▲); 0.143 mM (▼); 0.167 mM (□); 0.211 mM(○), **(b)** EIS spectra recorded for $[Fe(CN)_6]^{3-/4-}$ (1.0 mM) on either N-MWCNTs (dotted-dashed lines) or N-MWCNTs/AuNPs (solid lines) (0.1 M KCl).

The heterogeneous electron transfer rate constant k_s value was determined by using the obtained impedance parameters (R_{ct}) and it found to be about $\approx 9.5\times10^{-3}$ cm s^{-1}. The findings demonstrate that the quality and thus the electrochemical response of films are enhanced upon modification with AuNPs. This result confirms the important role of AuNPs for the improvement of electrochemical quality of electrode. Namely, with the modification with AuNPs lower charge transfer resistance and less significant barrier for electron transfer can be observed, resulting thus to faster kinetics of redox process occurring on the modified films compared to unmodified N-MWCNTs (6.2×10^{-3} cm s^{-1}). It is remarkable that the kinetic of redox system on the modified N-MWCNTs/ AuNPs is about 53% faster compared to that on unmodified N-MWCNTs for the same concentration (Fig.32b).

4.2.3 Application of N-MWCNTs/AuNPs in Bioanalysis

4.2.3.1 Electrochemical detection of NAC and AC on N-MWCNTs/AuNPs

In the present work, both (NAC) and (AC) are determined on the N-MWCNTs/AuNPs films. The most important application was their simultaneous determination in single experiment. It's already known that the problem in the simultaneous analysis is the overlap of the oxidation peak potential resulting, consequently, to the interference current responses of the substances, and thus, making the distinguish of the voltammetric peak very difficult. For example, at the unmodified N-MWCNTs film the oxidation potential of AC appears at about +0.445 V (vs. Ag/AgCl), and the oxidation potential of NAC lies in the same potential region +0.250 V (vs. Ag/AgCl). The peak potential separation seems to be less than 200 mV (~195 mV) and therefore overlapped oxidation waves can be obtained for NAC and AC substances on unmodified N-MWCNTs (Fig.33).

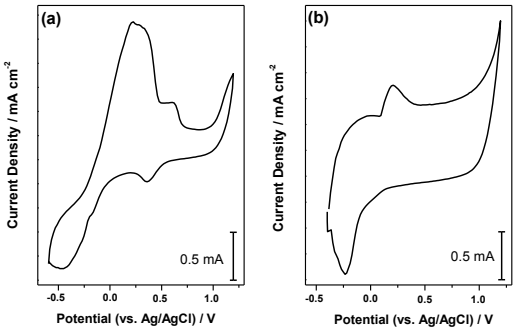

Fig. 33 Representative CVs recorded for NAC (1.78 mM) / AC (0.137 mM) mixture **(a)** and NAC (1.78 mM) **(b)** on unmodified N-MWCNTs at 0.02 $V{\cdot}s^{-1}$ (PBS, pH 7.0).

However, this problem can be solved with modification the N-MWCNTs films with AuNPs. As it can be seen in Figs.34-37 the modified N-MWCNTs/AuNPs film shows an excellent catalytic activity towards electrochemical oxidation of NAC and AC compared to unmodified N-MWCNTs film. It's very interesting that the oxidation peak potential of AC on modified film is the same on the unmodified N-MWCNTs (+0.445 V vs. Ag/AgCl), while that of NAC is shifted to more anodic potential on the modified film (+0.884 V vs. Ag/AgCl). Namely, the oxidation of NAC occurs at about 634 mV more positive compared to that on unmodified N-MWCNTs film (+0.250 V vs. Ag/AgCl). These results demonstrate that the potential peak separation AC-NAC is about ~440 mV, while the separation between the redox waves of NAC and AC on unmodified N-MWCNTs film is significantly less than the half (~195 mV).

Firstly, the response of N-MWCNTs/AuNPs film towards NAC was investigated in the absence of AC. For this purpose, CVs for various concentrations of NAC in range of 0.100–0.909 mM (PBS, pH 7.0) were recorded on N-MWCNTs/AuNPs. As it can be seen in Fig.34, the oxidation potential of NAC on N-MWCNTs/AuNPs film is lying at about +0.884 V (vs. Ag/AgCl) and the current response increases with rising the NAC concentration. In order to estimate the detection limit and the sensitivity of the fabricated electrode towards NAC, the variation of oxidation current with the concentration of NAC was considered (Fig.36b). A linear relation of current versus concentration in investigated concentration range of 0.100–0.909 mM was observed. The detection limit and the sensitivity were estimated to be 3.00 μM and 0.069 A M^{-1} cm^{-2}, respectively.

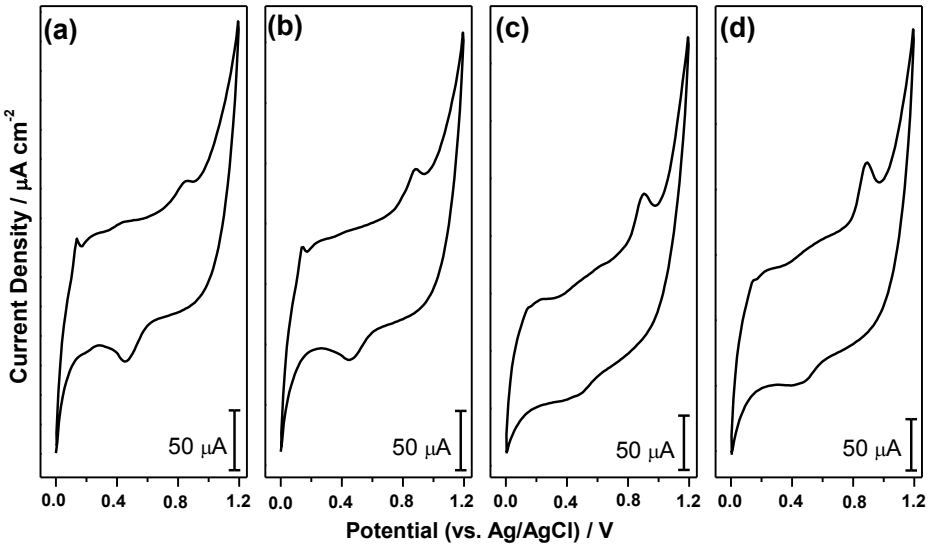

Fig. 34 Representative CVs recorded for various concentrations of NAC (a) 0.100 mM, (b) 0.163 mM, (c) 0.384 mM, (d) 0.625 mM) on N-MWCNTs/AuNPs at 0.02 V. s^{-1} (PBS, pH 7.0).

Furthermore, NAC was analysed in the presence of AC. For this purpose, different concentrations of NAC in the range of 0.100-1.510 mM were investigated in the presence of constant concentration of AC (0.495 mM) in order to test the sensitivity and the detection ability of synthesized film toward simultaneous oxidation of AC and NAC. The CVs shown in Fig.35 demonstrate that the oxidation peaks of binary compound are well separated from each other. The potential peak separation for oxidation of NAC+AC was about ~392 mV. The variation of oxidation current with NAC concentration was linear in the investigated range (R^2 =0.9983). The lower limit of detection and sensitivity of N-MWCNTs towards NAC in the presence of AC were estimated to be 3.00 μM and 0.070 A M^{-1} cm^{-2}, respectively.

The oxidation current density responses of N-MWCNTs/AuNPs towards AC versus its concentration in the presence of NAC are shown in Fig.36a. For comparison reasons, the oxidation current density responses of N-MWCNTs/AuNPs towards NAC versus its concentration in the presence and absence of AC are shown in Fig.36b. It can be seen that the values are very similar to those determined for NAC in the absence of AC. It can be, consequently, concluded that the analysis of NAC is not influenced by the presence of AC and thus the simultaneous determination of NAC and AC can be successfully done on the N-MWCNTs/AuNPs.

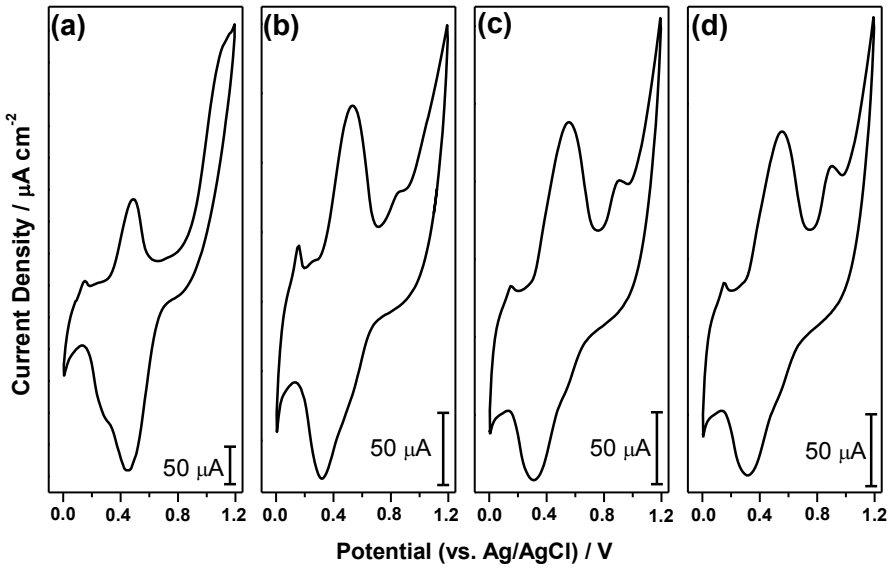

Fig. 35 Representative CVs recorded for various concentrations of NAC (a) 0 mM, (b) 0.194 mM, (c) 0.380 mM, (d) 0.560 mM) containing AC (0.495 mM) on N-MWCNTs/AuNPs at 0.02 V. s^{-1} (PBS, pH 7.0)

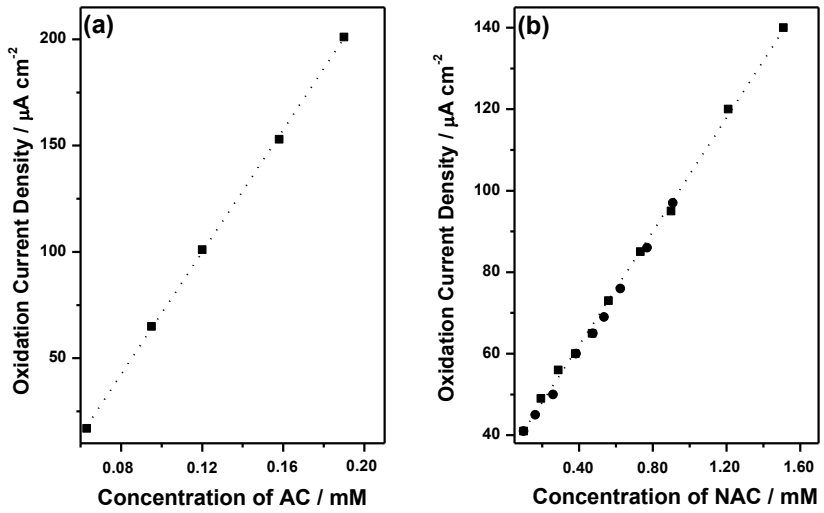

Fig. 36 (**a)** Variation of oxidation current density of AC with its concentration in the range 0.063–0.190 mM in the presence of NAC (0.476 mM); (**b)** variation of oxidation current density of NAC with its concentration in the ranges 0.100–0.909 mM and 0.100–1.510 mM in the absence (*filled circle*) and the presence (*filled square*) of AC (0.500 mM), respectively.

In addition, the binary system was investigated by varying the concentrations of AC in the presence of constant concentration of NAC. Representative CVs recorded for various concentrations of AC (in range of 0.063–0.190 mM) in presence of NAC (0.476 mM) on N-MWCNTs/AuNPs are displayed in Fig.37.

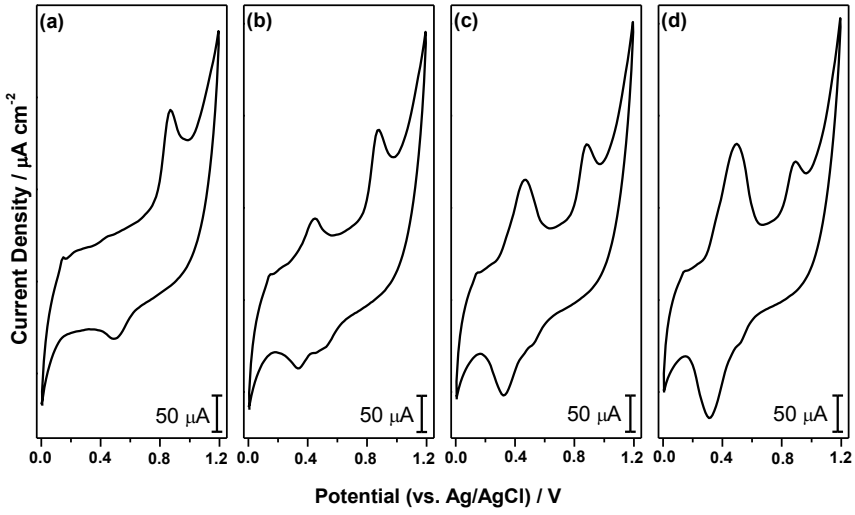

Fig. 37 Representative CVs recorded for various concentrations of AC (a) 0 mM, (b) 0.063 mM, (c) 0.120 mM, (d) 0.190 mM in presence of NAC (0.476 mM) on N-MWCNTs/AuNPs at 0.02 V. s^{-1} (PBS, pH 7.0).

It is remarkable that the oxidation peaks of AC and NAC are well separated from each other (potential peak separation is ~440 mV) and the peak separation is independent of variation of concentration of AC. Furthermore, the current response of AC enhances with increasing its concentration. Namely, it was observed that the oxidation peak current increases linearly upon increasing AC concentration in the range of 0.063–0.190 mM (R^2 = 0.9997).

The detection limit (S/N=3) and the sensitivity of N-MWCNTs/AuNPs towards AC (in the presence of NAC) were determined to be 0.35 μM and 0.866 A M^{-1} cm^{-2}, respectively. It must be mentioned that the detection limit and the sensitivity of N-MWCNTs/AuNPs towards AC seem to be slightly better compared to those obtained on unmodified N-MWCNTs film (0.485 μM; 0.8406 A M^{-1} cm^{-2}) (see 4.1.3.1), demonstrating the important role that plays the modification with AuNPs for improvement and enhancement of the electrocatalytic properties of N-MWCNTs. The obtained results show that the detection ability of modified film N-MWCNTs/AuNPs towards AC (0.35 μM) seems to be smaller compared to that for NAC (3.00 μM) indicating, thus, the film's sensitivity towards AC is greater than that for NAC.

It would be very interesting to compare the detection limits of N-MWCNTs/AuNPs film towards NAC and AC with those of other electrodes reported in literature. This comparison is shown in Table 6.

The comparison of results obtained for the pure substances demonstrates that in general the N-MWCNTs/AuNPs film exhibits greater detection ability towards NAC and AC compared to other novel films reported in literature. Thus, the N-MWCNTs/AuNPs film can be successfully applied as voltammetric sensor for simultaneous determination of NAC and AC with good sensitivity and detection ability.

Table 6 Comparison of detection limits (S/N=3) of N-MWCNTs/AuNPs with those of other novel electrodes reported in literature towards oxidation of NAC and AC.

Electrode	Detection limit/μM		References
	NAC	AC	
N-MWCNTs/AuNPs[a]	3.0	0.35	This work
(N-DHPB)/CPE[b]	0.2	10	Ref [217]
SiCuNP/CPE[c]	41.8		Ref [218]
Fe_3O_4/RGO/GCE[d]	11.1		Ref [219]
Fe_3O_4/GO/GCE[e]	25.0		Ref [220]
Co/Graphene/GCE[f]	890		Ref [221]
Co/GCE[g]	410		Ref [221]
$Co(OH)_2$/GCE[h]	220		Ref [222]
CA/SPCE[i]		13	Ref [223]
PVC/TTF-TCNQ[j]		0.66	Ref [224]
PANI/MWCNTs/GCE[k]		0.25	Ref [225]
Ni/CE[l]		0.60	Ref [226]
TiO_2/GCE[m]		2.0	Ref [227]

a Composite N-MWCNTs/AuNPs film fabricated in the present work.

b Carbon paste electrode modified with N-(3,4-dihydroxyphenethyl)-3,5-dinitrobenzamide (N-DHPB), (concentration linear range, 0.5–200 μmol L^{-1} NAC and 15.0–270 μmol L^{-1} AC).

c Carbon paste electrode modified with copper nitroprusside/3- aminopropylsilica (concentration linear range, 0.099–0.89 mM; sensitivity, 30.2 mA M^{-1}).

d Magnetite/reduced graphene oxide composite-modified glassy carbon electrode (concentration linear range, 0.10–10.0 mM; sensitivity, 21.64 μAM^{-1} cm^{-2}).

e Magnetite/graphene oxide composite-modified glassy carbon electrode (concentration linear range, 0.12–13.3 mM; sensitivity, 146.25 μA mM^{-1} cm^{-2}).

f Cobalt nanoparticles attached to graphene modified glassy carbon electrode (concentration linear range, 2.42–10.67 mM; sensitivity, 18.25 μAM^{-1} cm^{-2}).

g Cobalt nanoparticles attached glassy carbon electrode (concentration linear range, 2.42–11.17 mM; sensitivity, 10.99 μAM^{-1} cm^{-2}).

h Cobalt hydroxide nanoparticles modified glassy carbon electrode (concentration linear range, 0.25–10.1 mM).

i Cellulose acetate screen-printed carbon electrode (concentration linear range, 0–2.0 mM; sensitivity, 9.98 μA $mmol^{-1}$).

j Poly (vinyl chloride)/TTF-TCNQ salt composite electrode modified with gold nanoparticles (concentration linear range, 1–800 μM; sensitivity 53 mA M^{-1}).

k Glassy carbon electrode modified with poly (aniline)-multi-walled carbon nanotubes (concentration linear ranges, 1–100 μM and 250–2.000 μM).

l Carbon-coated nickel magnetic nanoparticles (concentration linear range, 7.8–110 μM).

m Glassy carbon electrode modified with poly (acid yellow 9)-nano-TiO_2 (concentration linear range, 12–120 μM).

4.2.4 Characterization of N-MWCNTs modified with rhodium, palladium, iridium, platinum, silver and gold nanoparticles.

4.2.4.1 Scanning electron microscopy and transmission electron microscopy

SEM images taken for N-MWCNTs modified with MNPs (M: Rh, Pd, Ir, Pt, Ag, and Au) reveal that the deposited MNPs dispersed homogeneously on the surface of N-MWCNTs without agglomeration. The modified films show quite net structure that is always favorable for electron transfer processes. The metal nanoparticles can be recognized in SEM micrographs as small bright dots deposited on the outer walls of carbon nanotubes (Fig.38).

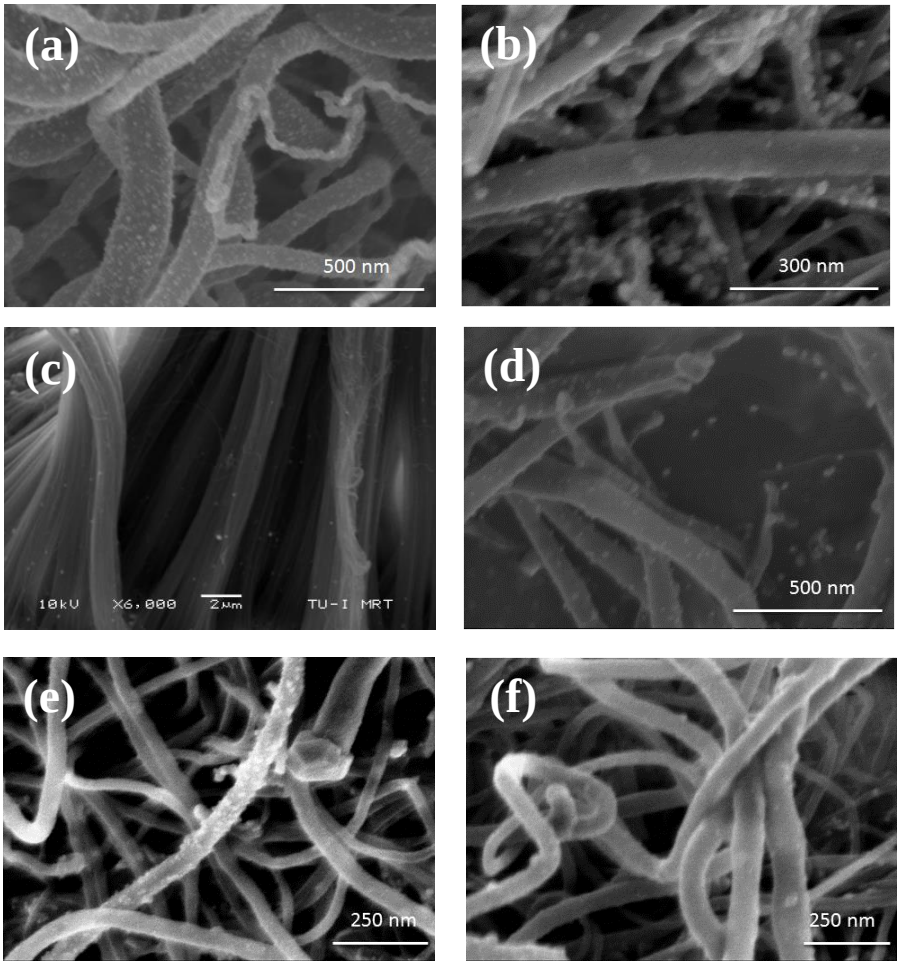

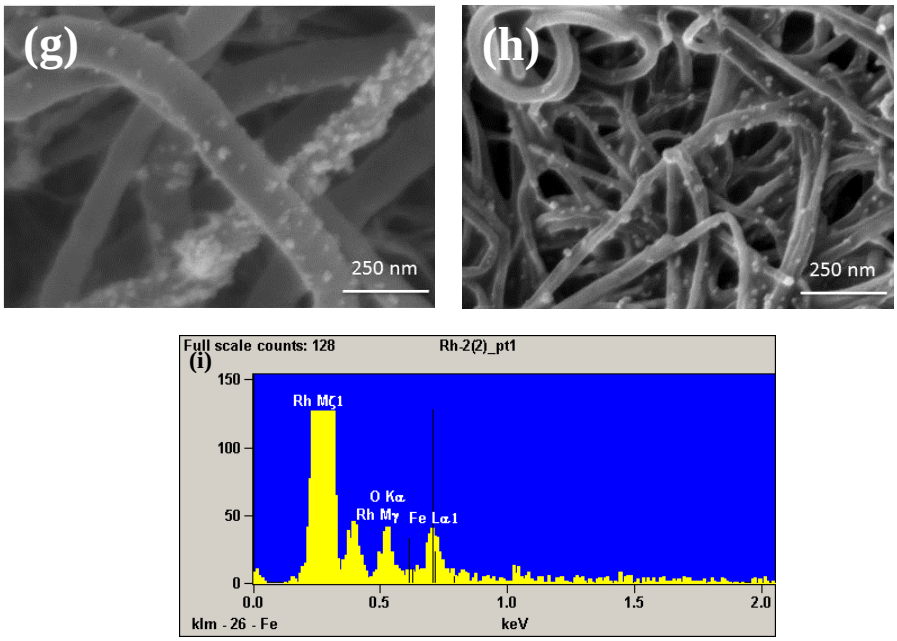

Fig. 38 SEM micrographs for N-MWCNTs/AuNPs **(a)**, N-MWCNTs/AgNPs **(b)**, N-MWCNTs/PtNPs **(c,d)**, N-MWCNTs/PdNPs **(e,f)**, N-MWCNTs/IrNPs **(g)**, N-MWCNTs/RhNPs **(h)**, composite films, and representative EDX spectrum recorded for N-MWCNTs/RhNPs **(h)**.

TEM analysis performed for N-MWCNTs/AuNPs confirms the homogeneously dispersion of nanoparticles on the tubes which still have the "bamboo structure" after their decoration with MNPs. EDX spectra confirms more that these nanoparticles consist of gold (Fig.39).

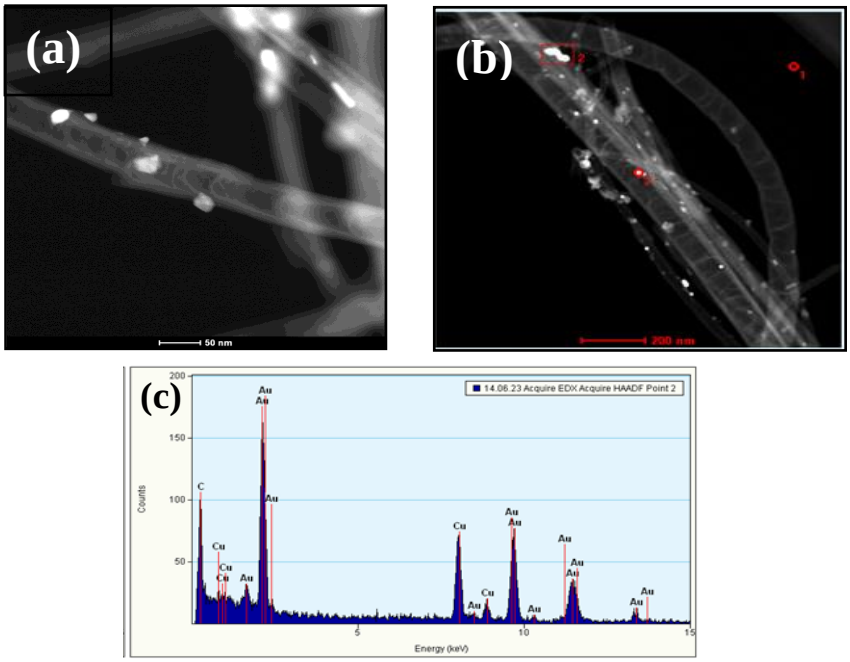

Fig. 39 TEM images for N-MWCNTs/AuNPs **(a,b)**, EDX spectrum recorded for N-MWCNTs/AuNPs composite film **(c)**.

4.2.4.2 Cyclic voltammetry

The standard redox system $[Fe(CN)_6]^{3-/4-}$ (1.0 M KCl) was investigated on the modified films N-MWCNTs/MNPs (M: Rh, Pd, Pt, and Ag) by means of cyclic voltammetry. Representative CVs were recorded in the concentration range of 0.099- 0.990 mM on N-MWCNTs/MNPs (M: Rh, Pd, Pt, and Ag), respectively are shown in Figs.40-43. The results show that quite symmetrical CVs were obtained consist of oxidation peak at about 0.32 V (vs. Ag/AgCl), and reduction peak occurs at about 0.24 V (vs. Ag/AgCl), corresponding to the one electron oxidation $[Fe(CN)_6]^{4-}$ to $[Fe(CN)_6]^{3-}$ and the inverse to reduction of $[Fe(CN)_6]^{3-}$ to $[Fe(CN)_6]^{4-}$.

It is remarkable that on all modified films, the redox couple tends to be reversible and the current response enhances with the increase of the concentration of redox system with slight shift to more anodic potential and more cathodic potential of the oxidation and reduction peaks, respectively. Consequently, the peak potential difference ($\Delta E_p = E_p^{ox} - E_p^{red}$) increases with increasing the concentration of redox system. This can be attributed to the resistance of the cell which remains uncompensated and increases with increasing the concentration of $[Fe(CN)_6]^{3-/4-}$.

It must be mentioned that the oxidation and reduction peak currents remain constant for large number of cycles, demonstrating that there are no chemical reactions coupled with the electron transfer and confirming that the studied electro-active species are stable in the time frame of the experiment and that the charge-transfer process occurring on studied composite films is reversible. Furthermore, the peak current ratio of forward and reverse scans is equal to unity (within experimental error) and is independent of the scan rate applied for recording the CVs indicating that there are no parallel chemical reactions coupled to electrochemical process. The average value of oxidation and reduction potentials $E_{1/2}$ was estimated to be stable ($E_{1/2}$ = 0.280 V vs. Ag/AgCl) with the experimental error on all modified composite films, something which is quite common for reversible system.

It is very interesting to mention that the oxidation-reduction peak potential separation of the investigated redox system on the N-MWCNTs modified with PdNPs, PtNPs, and AgNPs, determined to be 0.062, 0.060 and 0.059 V respectively, that is within experimental error very close to the expected theoretical ΔE_p value for Nernstian reversible system. Whereas on the N-MWCNTs modified with RhNPs was estimated to be ($\Delta E_p \approx 0.078$ V). However, this value still smaller compared to that obtained on unmodified N-MWCNTs 0.083 V. These findings demonstrate that the kinetic of electron transfer tends to enhance upon modification with metal nanoparticles. A relation between the kinetic of the redox system and the type of the metal nanoparticles used in modification was also observed.

The heterogeneous electron-transfer rate constants were estimated by means of electrochemical absolute rate relation that is based on degree of peak potential separation between the forward and reverse scans. As it is well known, ΔE_p varies inversely with the heterogeneous electron-transfer rate constant (k_s), and thus, with the kinetics of charge-transfer process occurring onto composite films. Namely, the highest rate for electron transfer for $[Fe(CN)_6]^{3-/4-}$ exhibits the lowest ΔE_p.

In this work, it was observed that the kinetic of the redox process involving $[Fe(CN)_6]^{3-/4-}$ on the modified films tend to be improved with the following order: N-MWCNTs < N-MWCNTs/RhNPs < N-MWCNTs /PdNPs < N-MWCNTs/PtNPs < N-MWCNTs/AgNPs.

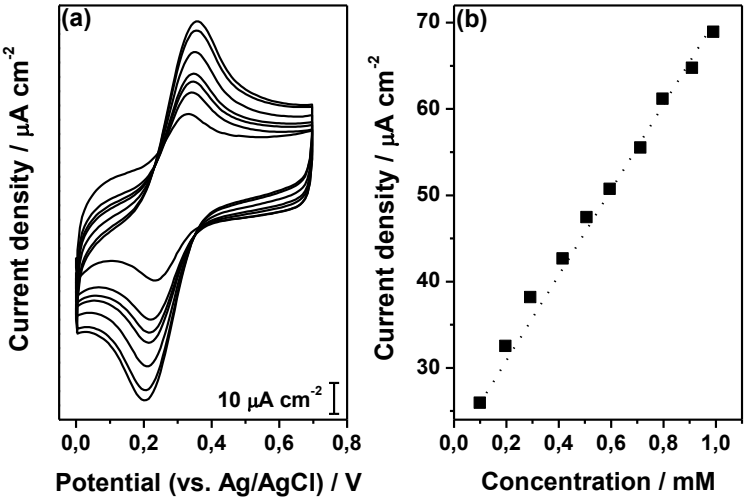

Fig. 40 (a) CVs recorded for various concentrations of $[Fe(CN)_6]^{3-/4-}$ (1.0 M KCl) (from inner to outer: 0.099, 0.291, 0.415, 0.506, 0.712, 0.909, and 0.990 mM) on N-MWCNTs/RhNPs composite film at the scan rate of 0.02 $V.s^{-1}$; **(b)** Variation of oxidation peak current of $[Fe(CN)_6]^{3-/4-}$ with its concentration in the range of 0.099-0.990 mM.

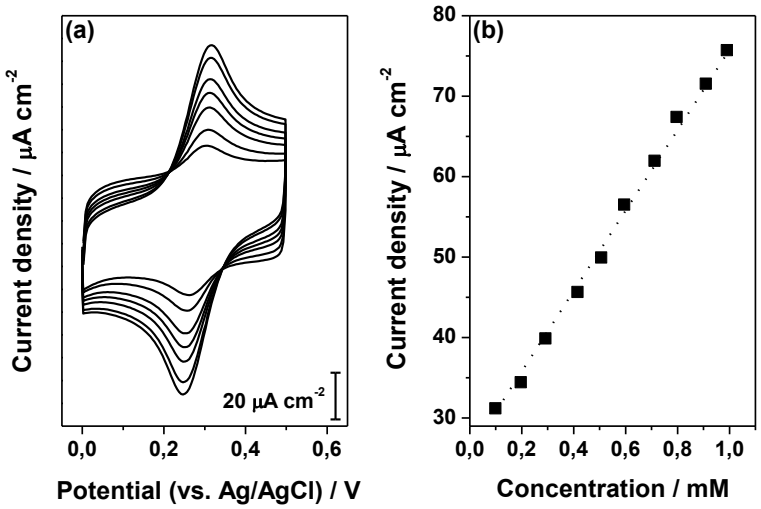

Fig. 41 (a) CVs recorded for various concentrations of $[Fe(CN)_6]^{3-/4-}$ (1.0 M KCl) (from inner to outer: 0.099, 0.291, 0.506, 0.595, 0.712, 0.909, and 0.990 mM) on N-MWCNTs/PdNPs composite film at the scan rate of 0.02 $V.s^{-1}$; **(b)** Variation of oxidation peak current of $[Fe(CN)_6]^{3-/4-}$ with its concentration in the range of 0.099-0.990 mM.

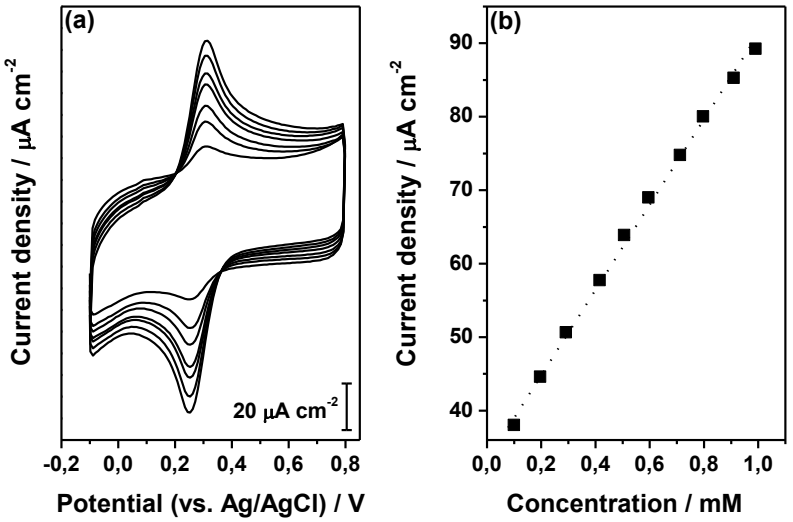

Fig. 42 (a) CVs recorded for various concentrations of $[Fe(CN)_6]^{3-/4-}$ (1.0 M KCl) (from inner to outer: 0.099, 0.196, 0.415, 0.506, 0.595, 0.712, and 0.990 mM) on N-MWCNTs/PtNPs composite film at the scan rate of 0.02 $V.s^{-1}$; **(b)** Variation of oxidation peak current of $[Fe(CN)_6]^{3-/4-}$ with its concentration in the range of 0.099-0.990 mM.

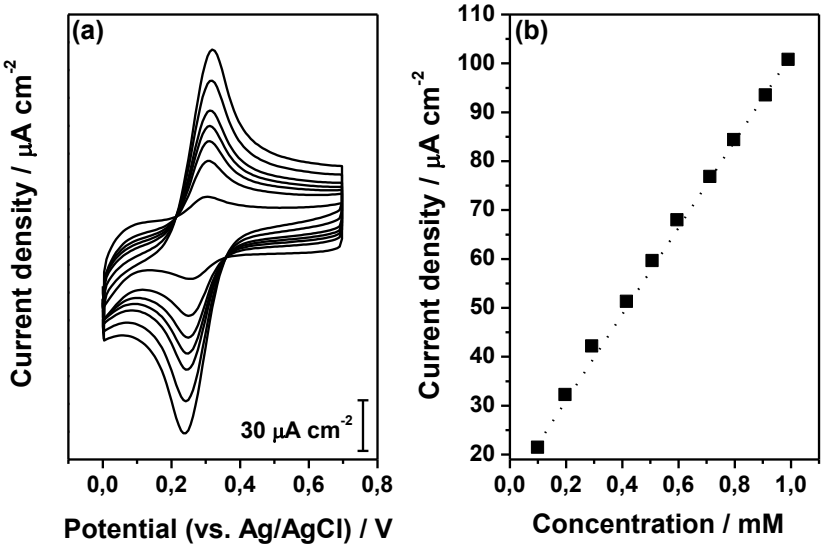

Fig. 43 (a) CVs recorded for various concentrations of $[Fe(CN)_6]^{3-/4-}$ (1.0 M KCl) (from inner to outer: 0.099, 0.196, 0.415, 0.506, 0.595, 0.797, and 0.990 mM) on N-MWCNTs/AgNPs composite film at the scan rate of 0.02 $V.s^{-1}$; **(b)** Variation of oxidation peak current of $[Fe(CN)_6]^{3-/4-}$ with its concentration in the range of 0.099-0.990 mM.

The heterogeneous electron-transfer rate constants were determined by means of the Nicholson equation [196]. However, this procedure the approximate values of k_s can be determined, because this equation is limited to the planar diffusion flat electrode, and our fabricated electrode have porous structure and rough surface, as well as, the cell resistance which stay uncompensated and affect consequently the potential peak difference ΔE_p. For this reason, we have calculate it in another method depending on the data extracted from impedance spectroscopy.

The estimated electrochemical parameters extracted for the interpretation of recorded CVs are presented in Table 7. To compare the determined values of k_s on the different type of modified films, the results were presented graphically in histogram shown in Fig.44b. It is obvious that the highest electron transfer rate was obtained on the N-MWCNTs modified with silver nanoparticles. Namely, the rate for electron transfer of $[Fe(CN)_6]^{3-/4-}$ on various composite films increases with the order :N-MWCNTs < N-MWCNTs/RhNPs < N-MWCNTs/PdNPs < N-MWCNTs/PtNPs < N-MW CNTs/AgNPs.

Table 7 Parameters extracted from CVs and EIS for N-MWCNTs/MNPs (M: Rh, Pd, Pt, and Ag) composite films towards $[Fe(CN)_6]^{3-/4-}$ (1.0 M KCl).

Parameters	N-MWCNTs/MNPs			
	RhNPs	**PdNPs**	**PtNPs**	**AgNPs**
E_p^{ox} (V)[a]	0.319	0.311	0.310	0.309
E_p^{red} (V)[a]	0.241	0.249	0.250	0.250
$E_{1/2}$ (V)[b]	0.280	0.280	0.280	0.280
ΔE_p (V)	0.078	0.062	0.060	0.059
A (cm^2)	5.56	6.10	6.37	6.96
I_p^{ox} ($\mu A\ cm^{-2}$)	65	78	90	101
I_p^{ox}/i_p^{red}	1.00	1.01	0.98	1.00
k_s (10^{-2} cm s^{-1})[c]	0.77	3.61	4.49	5.03
k_s (10^{-2} cm s^{-1})[d]	1.41	3.04	4.22	6.98
R_{ct} (Ω)[e]	43	12	10	2
LOD (lM)[f]	0.232	0.185	0.157	0.138
S (A M^{-1} cm^{-2})	0.603	0.696	0.766	0.836

a All potentials are reported with respect the Ag/AgCl (KCl sat.) reference electrode.

b The $E_{1/2}$ values were determined as the average values of E_p^{ox} and E_p^{red}.

c The k_s values were determined from electrochemical absolute rate relation: $\Psi=(D_o/D_R)^{a/2}k_s(n\pi FvD_o/RT)^{-1/2}$, where Ψ is kinetic parameter, a the charge-transfer coefficient ($a \approx 0.5$), D_o, D_R the diffusion coefficients of oxidized and reduced species, respectively ($D_o \approx D_R$), and n the number of electrons involved in the redox reaction (n = 1) [196]

d The k_s values were determined from EIS parameters according to relation: $R_{ct} = RT/n^2F^2Ak_sc$, where R_{ct} is the charge-transfer resistance, A the active surface area, and c the concentration of redox system [198]

e The EIS parameters were determined using the equivalent electrical circuit ($R_s + (C_{dl}/(R_{ct} + Z_w))$) (software Thales, version 4.15).

f The detection limits were estimated on the basis of signal-to-noise (S/N) ratio of 3 by means of CV technique.

The findings demonstrate that the electrochemical response of the fabricated films enhances obviously upon modification with metal nanoparticles. The k_s values of $[Fe(CN)_6]^{3-/4-}$ estimated in the present work on N-MWCNTs/MNPs composite films appear to be significantly greater (in some cases up to 15 times greater) compared to those reported in literature for the same redox system on either bare gold ($k_s \approx 0.26\times10^{-2}$ cm s^{-1}) or modified gold electrode ($k_s \approx 0.29\times10^{-2}$ cm s^{-1}) [228].

Furthermore, the electrochemical current response of modified N-MWCNTs/MNPs films towards $[Fe(CN)_6]^{3-/4-}$ is also improved. For comparison reason, the response of one concentration of the investigated system was compared on the unmodified N-MWCNTs films and modified films with various nanoparticles (Fig.46). As it can be seen, an improvement in the current density

occurs with the modification, which confirms the important role of the nanoparticles in facilitating the redox process and increasing the conductivity of the films. The anodic current density of $[Fe(CN)_6]^{3-/4-}$ redox system onto unmodified and modified with metal nanoparticles N-MWCNTs films is presented graphically in histogram in (Fig.44a).

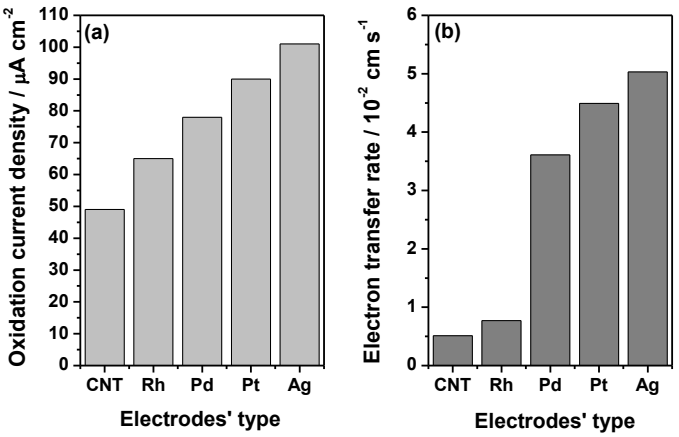

Fig. 44 Histograms showing the oxidation current density **(a)** and the heterogeneous electron-transfer rate constant **(b)** of 0.990 mM $[Fe(CN)_6]^{3-/4-}$ (1.0 M KCl) on N-MWCNTs (symbolized in diagram as CNT) and N-MWCNTs/MNPs (M: Rh, Pd, Pt, and Ag) composite films (symbolized in diagram as Rh, Pd, Pt, and Ag).

The results indicate once more that this improvement depends strongly on the type of the metal nanoparticles. Namely, with the modification of N-MWCNTs films with RhNPs an increase of about 33 % is observed in anodic current density compared to unmodified films. A modification of the N-MWCNTs films with PdNPs results to an improvement of anodic current density of about 59 %, while the decoration of N-MWCNTs with PtNPs leads to an enhancement of oxidation peak current density of about 84 %. Finally, upon modification of N-MWCNTs film with AgNPs an improvement of the oxidation current density of about 106 % occurs.

It was also remarkable that the active surface area of the modified electrode is higher than the active surface area of unmodified electrode, something that is related to the nanoparticles which decorate the surface of the N-MWCNTs and probably increase the defects and consequently increase the active surface area.
In order to estimate the lower limit of detection and the sensitivity of the synthesized modified films, the current density response of the films towards $[Fe(CN)_6]^{3-/4-}$ were investigated in large concentration range of 0.099–0.990 mM. The determined values of the detection limit and sensitivity are included in Table.7, and are presented graphically in Fig.45.

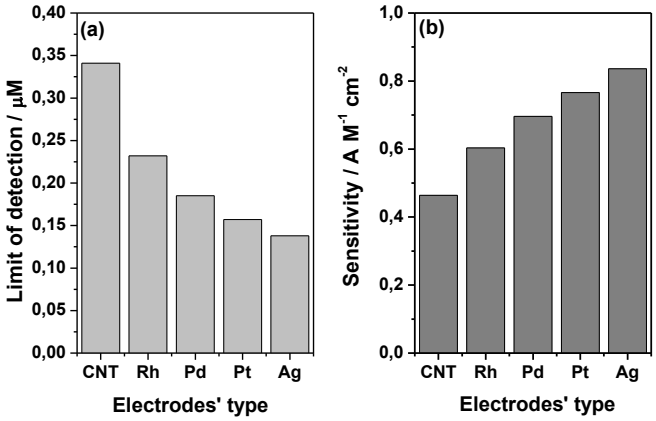

Fig. 45 Histograms showing the lower limit of detection **(a)** and the sensitivity **(b)** of N-MWCNTs (symbolized in diagram as CNT) and N-MWCNTs/MNPs (M: Rh, Pd, Pt, and Ag) composite films (symbolized in diagram as Rh, Pd, Pt, and Ag) towards $[Fe(CN)_6]^{3-/4-}$ (1.0 M KCl).

An improvement in the detection capability of the N-MWCNTs films occurs with their modification with metal nanoparticles. The capability of MNPs to enhance the film's electrocatalytic activity increases with the following order: N-MWCNTs < N-MWCNTs/RhNPs < N-MWCNTs/PdNPs < N-MWCNTs/PtNPs < N-MWCNTs/AgNPs. Specifically, upon modification of N-MWCNTs with RhNPs, PdNPs, PtNPs, and AgNPs an improvement of film's detection capability of about 32, 46, 54 and 60 %, respectively, occurs. Furthermore, it can be seen that the sensitivity of the N-MWCNTs films enhances for about 29, 50, 65 and 80 %, with its modification with PdNPs, PtNPs, and AgNPs, respectively. It must be mentioned that the electrochemical response of N-MWCNTs modified with IrNPs (2.7 nm) and AuNPs (12.5 nm) toward the redox system $[Fe(CN)_6]^{3-/4-}$ was already reported in literature [229]. An improvement in the electrode electrochemical response as well as the kinetic of electron transfer was observed. The detection limit and sensitivity values of 0.170 µM, 0.75 A M^{-1} cm^{-2} and 0.130 µM, 0.886 A M^{-1} cm^{-2} on N-MWCNTs/IrNPs, N-MWCNTs/AuNPs, respectively, were estimated.

Furthermore, CVs for single concentration of $[Fe(CN)_6]^{3-/4-}$ (0.990 mM) onto unmodified N-MWCNTs and modified N-MWCNTs/MNPs (M: Rh, Pd, Pt, and Ag) films are presented in Fig.46. It is obvious that the current response of modified films towards the oxidation of redox system is higher than those on unmodified film measured under the same conditions.

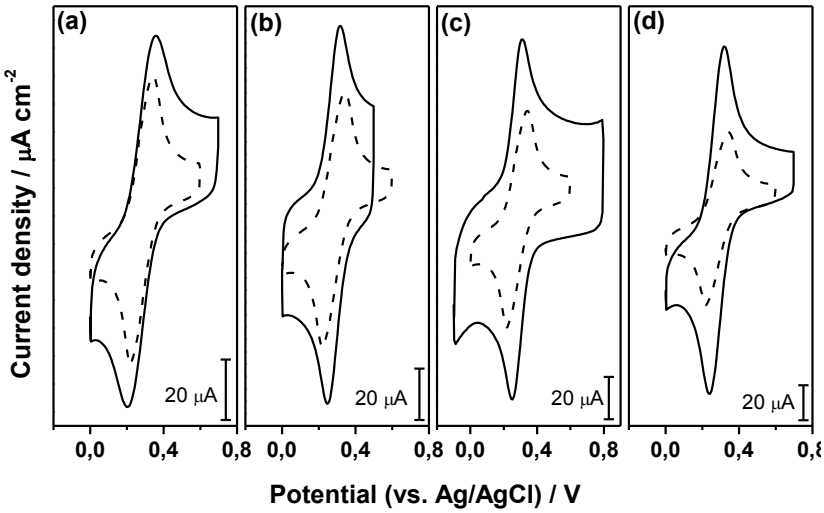

Fig. 46 CVs recorded for 0.990 mM $[Fe(CN)_6]^{3-/4-}$ (1.0 M KCl) on N-MWCNTs/RhNPs (a), N-MWCNTs/PdNPs (b), N-MWCNTs/PtNPs (c), N-MWCNTs/AgNPs (d) composite films at the scan rate of 0.02 V s^{-1}. For comparison reasons the CVs recorded for 0.990 mM $[Fe(CN)_6]^{3-/4-}$ (1.0 M KCl) on N-MWCNTs composite film (dashed line) are also included.

It would be interesting to compare the limits of detection of N-MWCNTs/MNPs (M: Rh, Pd, Pt, and Ag) towards $[Fe(CN)_6]^{3-/4-}$ with those reported in literature for other novel composite films. The comparison demonstrates that the MWCNTs/MNPs films exhibit greater detection ability (lower detection limit) towards $[Fe(CN)_6]^{3-/4-}$ compared to other novel electrodes reported in literature. For instance, electrode modified with 1-butyl-4-methylpyridinium tetrafluoroborate towards $[Fe(CN)_6]^{3-/4-}$ [230] seems to be significantly poorer compared to that obtained on our N-MWCNTs/MNPs films. In addition, the detection limit of 100 μM reported for carbon paste electrode modified with sodium dodecyl sulphate towards $[Fe(CN)_6]^{3-/4-}$ [231] is likewise considerably poorer compared to that measured on our N-MWCNTs/MNPs. Furthermore, the detection limit of 30 μM reported for glass capillary ultra-microelectrode towards $[Fe(CN)_6]^{3-/4-}$ [232] seems to be noticeably poorer compared to that measured on our novel N-MWCNTs/MNPs. Besides, the detection limit of glassy carbon electrode modified with titan dioxide and MWCNTs towards $[Fe(CN)_6]^{3-/4-}$ was reported as 48.6 and 1.10 μM [233], which appears to be also significantly poorer compared to that measured on our N-MWCNTs/MNPs. From this comparison, it can be clearly seen that the detection capability of N-MWCNTs/ MNPs (M: Rh, Pd, Pt, and Ag) films appears to be obviously better compared to other composite films reported in literature. These results demonstrate the excellent response of N-MWCNTs-based films ‘‘decorated’’ with metal nanoparticles.

4.2.4.3 Impedance spectroscopy

In order to estimate the barrier for electron transfer occurring on N-MWCNTs/MNPs (M: Rh, Pd, Pt, and Ag) films, electrochemical impedance spectra were recorded for $Fe(CN)_6]^{3-/4-}$ (1.0 M KCl) in the investigated concentration range of 0.099–0.990 mM.

EIS spectra recorded on N-MWCNTs/MNPs (M: Rh, Pd, Pt, and Ag) films (presented as Nyquist plots), are shown in Figs 47-50, respectively. The EIS spectra were recorded at the half-wave potential of $[Fe(CN)_6]^{3-/4-}$ (+0.280 V vs. Ag/AgCl).

As it can be seen, the spectra include a part of depressed semicircle followed by a straight line. The depressed semicircle, observed at higher frequencies (it is almost not observable), corresponds to the electron-transfer limited process, whereas the linear part that can be seen in lower frequencies represents the diffusion limited electron-transfer process.

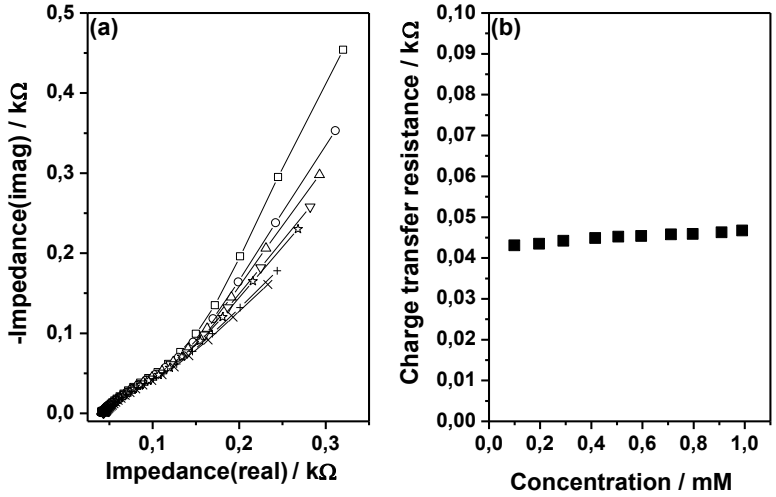

Fig. 47 (a) EIS spectra recorded for various concentrations of $[Fe(CN)_6]^{3-/4-}$ (1.0 M KCl) on N-MWCNTs/RhNPs composite film at the frequency range from 0.1 Hz to 100 kHz. The symbols are denoted as follows: 0.099 mM (open square); 0.196 mM (open circle); 0.291 mM (open upward triangle); 0.415 mM (open downward triangle); 0.595 mM (star); 0.797 mM (plus symbol); 0.990 mM (X symbol); **(b)** Variation of charge transfer resistance of $[Fe(CN)_6]^{3-/4-}$ with its concentration in the range of 0.099-0.990 mM

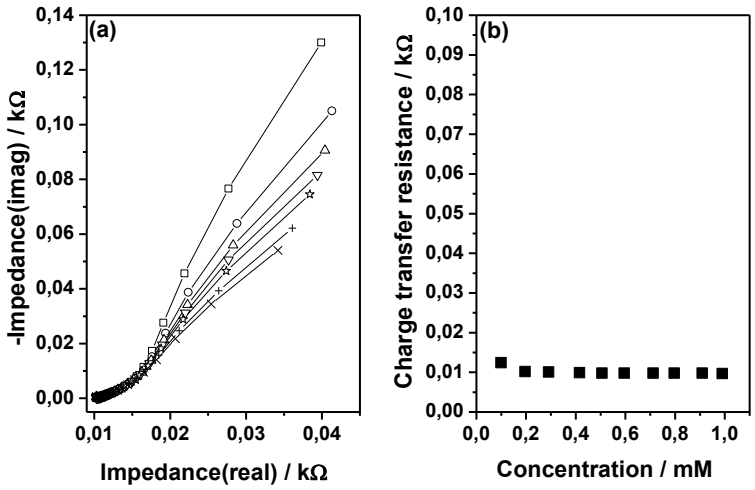

Fig. 48 (a) EIS spectra recorded for various concentrations of $[Fe(CN)_6]^{3-/4-}$ (1.0 M KCl) on N-MWCNTs/PdNPs composite film at the frequency range from 0.1 Hz to 100 kHz. The symbols are denoted as follows: 0.099 mM (open square); 0.291 mM (open circle); 0.415 mM (open upward triangle); 0.506 mM (open downward triangle); 0.595 mM (star); 0.797 mM (plus symbol); 0.990 mM (X symbol); **(b)** Variation of charge transfer resistance of $[Fe(CN)_6]^{3-/4-}$ with its concentration in the range of 0.099-0.990 mM**.**

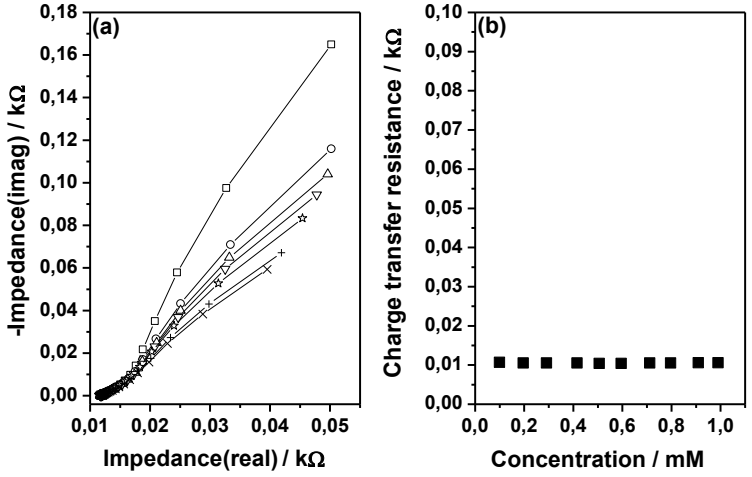

Fig. 49 (a) EIS spectra recorded for various concentrations of $[Fe(CN)_6]^{3-/4-}$ (1.0 M KCl) on N-MWCNTs/PtNPs composite film at the frequency range from 0.1 Hz to 100 kHz. The symbols are denoted as follows: 0.099 mM (open square); 0.196 mM (open circle); 0.291 mM (open upward triangle); 0.415 mM (open downward triangle); 0.506 mM (star); 0.712 mM (plus symbol); 0.990 mM (X symbol); **(b)** Variation of charge transfer resistance of $[Fe(CN)_6]^{3-/4-}$ with its concentration in the range of 0.099-0.990 mM

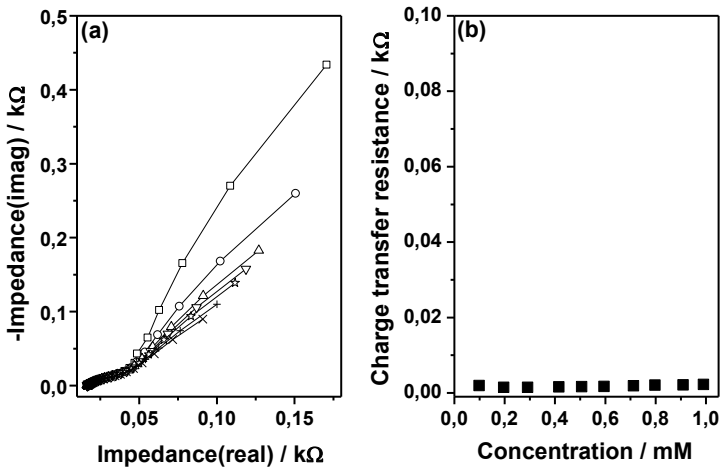

Fig. 50 (a) EIS spectra recorded for various concentrations of $[Fe(CN)_6]^{3-/4-}$ (1.0 M KCl) on N-MWCNTs/AgNPs composite film at the frequency range from 0.1 Hz to 100 kHz. The symbols are denoted as follows: 0.099 mM (open square); 0.196 mM (open circle); 0.415 mM (open upward triangle); 0.506 mM (open downward triangle); 0.595 mM (star); 0.797 mM (plus symbol); 0.990 mM (X symbol); **(b)** Variation of charge transfer resistance of $[Fe(CN)_6]^{3-/4-}$ with its concentration in the range of 0.099-0.990 mM.

It is well known that in case of very fast electron-transfer process, the EIS spectrum includes only the linear part, whereas very slow electron-transfer procedure results to semicircle with a great diameter that is not accompanied by a straight line. The recorded EIS spectra on N-MWCNTs/MNPs show that the linear part prevails over the semicircle, demonstrating that the electron transfer process on this film is quite fast (reversible Nernstian process). However, on unmodified N-MWCNTs films, an obvious semicircle can be recognized in high-frequency region of the spectrum demonstrating that a limited electron-transfer process takes place onto this particular electrode (Fig.51).

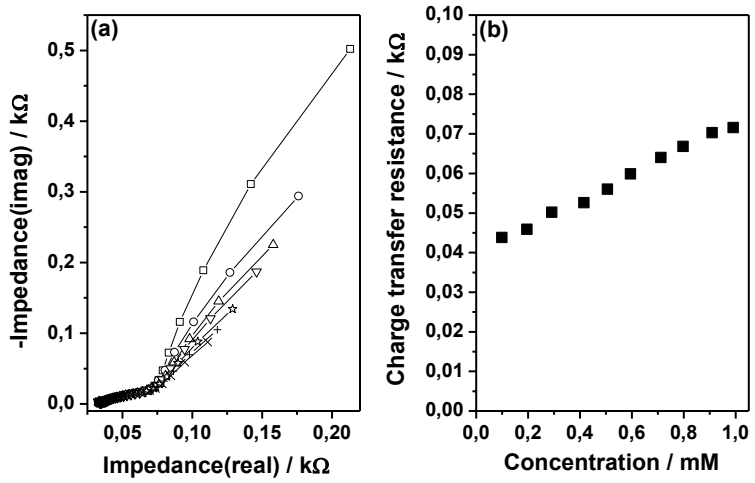

Fig. 51 (a) EIS spectra recorded for various concentrations of $[Fe(CN)_6]^{3-/4-}$ (1.0 M KCl) on N-MWCNTs composite film at the frequency range from 0.1 Hz to 100 kHz. The symbols are denoted as follows: 0.099 mM (open square); 0.196 mM (open circle); 0.291 mM (open upward triangle); 0.415 mM (open downward triangle); 0.595 mM (star); 0.797 mM (plus symbol); 0.990 mM (X symbol); **(b)** Variation of charge transfer resistance of $[Fe(CN)_6]^{3-/4-}$ with its concentration in the range of 0.099-0.990 mM.

The recorded EIS spectra were simulated using the electrical circuit (R_s+ (C_{dl}/(R_{ct} + Z_w) (Fig.52). The circuit's elements were already explained in (4.1.2.2).

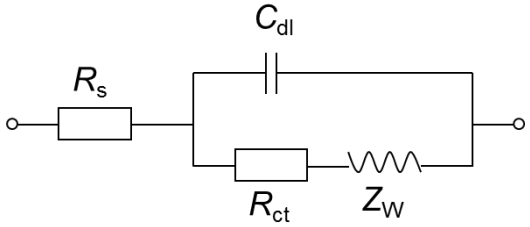

Fig. 52 Equivalent electrical circuit model (R_s+(C_{dl}/R_{ct}+Z_w)) used for the simulation of electrochemical impedance spectra recorded for $[Fe(CN)_6]^{3-/4-}$ (1.0 M KCl) on N-MWCNTs/MNPs (M: Rh, Pd, Pt, and Ag) composite films.

For comparison reasons, the EIS spectra recorded for 0.990 mM $[Fe(CN)_6]^{3-/4-}$ (1.0 M KCl) on N-MWCNTs composite film are showed and included in EIS spectra recorded for 0.990 mM $[Fe(CN)_6]^{3-/4-}$ (1.0 M KCl) on N-MWCNTs/RhNPs, N-MWCNTs/PdNPs, N-MWCNTs/PtNPs, and N-MWCNTs/AgNPs, respectively (Fig.53).

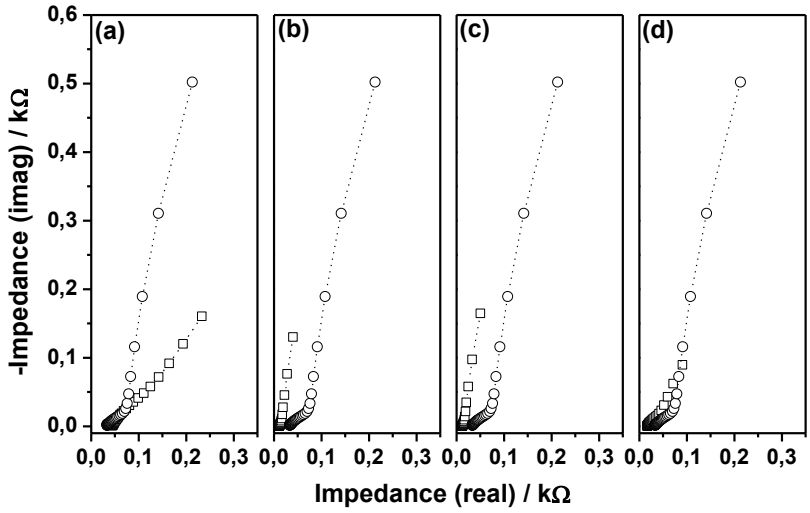

Fig. 53 EIS spectra recorded for 0.990 mM $[Fe(CN)_6]^{3-/4-}$ (1.0 M KCl) on N-MWCNTs/RhNPs **(a)** (open square), N-MWCNTs/PdNPs **(b)** (open square), N-MWCNTs/PtNPs **(c)** (open square), and N-MWCNTs/AgNPs **(d)** (open square) composite films. The EIS spectra recorded for 0.990 mM $[Fe(CN)_6]^{3-/4-}$ (1.0 M KCl) on N-MWCNTs (open circle) composite are also included.

The obtained results demonstrate that the charge-transfer resistance increases slightly with the rise of the concentration of electro-active substance. This observation that is more obvious on unmodified N-MWCNTs can be connected to the interruption of the electron-transfer process caused by the uncompensated resistance effect, which becomes more significant with increasing the concentration of redox system. The values of charge transfer resistance are included in Table.7.

The findings clearly demonstrate that with the modification of N-MWCNTs films with metal nanoparticles the charge-transfer resistance decreases indicating faster interfacial electron transfer onto modified with MNPs films compared to unmodified N-MWCNTs film. It is very interesting to mention that the R_{ct} decreases for about 26, 79, 83 and 97 % upon modification of the N-MWCNTs films with RhNPs, PdNPs, PtNPs, and AgNPs, respectively, demonstrating that the metal nanoparticles promote the electron transfer between the analyte and the electrode surface due to the smaller electron-transfer barrier introduced with the modification of N-MWCNTs with metal nanoparticles. Namely, the R_{ct} decreases with the following order: N-MWCNTs > N-MWCNTs/RhNPs > N-MWCNTs/PdNPs > N-MWCNTs/ PtNPs > N-MWCNTs/AgNPs.

The k_s values of $[Fe(CN)_6]^{3-/4-}$ redox system on N-MWCNTs/MNPs composite films were once more estimated from the impedance parameters. The values are

included in Table 7. As was expected, the determined values of k_s by means of EIS technique differ somewhat from those approximated by means of electrochemical absolute rate relation (due to the reasons explained in (4.1.2.2)). However, the variation of k_s with the type of metal nanoparticles has the same trend and thus the results in absolute accordance with the extracted CV results. The greatest k_s value was obtained on the N-MWCNTs/AgNPs to be 6.98×10^{-2} $cm.s^{-1}$, indicating the faster kinetic of electron transfer on this particular film. It is interesting to mention that on N-MWCNTs/AuNPs, the k_s was estimated to be 8.0×10^{-2} $cm.s^{-1}$ [233], which illustrate even faster kinetic and less barrier for electron transfer upon modification with AuNPs.

A comparison of our results with literature was made. For instance, Li and Chen [234] reported for $[Fe(CN)_6]^{3-/4-}$ (PBS, pH 7.0) on bare glassy carbon electrode a charge-transfer resistance of 1.91 kΩ that is greater compared to that obtained in the present work on either unmodified N-MWCNTs or modified N-MWCNTs/MNPs. Wang et al.[235] studied the impedance behavior of $[Fe(CN)_6]^{3-/4-}$ (0.1 M KCl) on conventional gold electrode modified with colloidal gold particles. These authors reported for this composite electrode a charge-transfer resistance of R_{ct} = 1.24 kΩ that appears to be significantly greater compared to the charge-transfer resistance estimated in the present work. Furthermore, Zhang and Oyama [236] probed their nanostructured indium tin oxide film modified with gold nanoparticles towards $[Fe(CN)_6]^{3-/4-}$ (0.1 M PBS, pH 7.0) and reported charge-transfer resistance values lying in the range from 13.46 to 29.22 kΩ, which are considerably greater compared to those estimated in present work for the same redox system on N-MWCNTs/MNPs composite films. This comparison demonstrates that the barrier for electron transfer on N-MWCNTs/ MNPs (M: Rh, Pd, Pt, and Ag) appears to be significantly smaller compared to that on other electrodes reported in literature.

4.2.5 Application of N-MWCNTs/MNPs in Bioanalysis

4.2.5.1 Electrochemical oxidation of acetaminophen and *N*-acetylcysteine on N-MWCNTs/PtNPs

A novel composite films consist of N-MWCNTs decorated with PtNPs (3 nm) were fabricated and applied for electrochemical analysis of acetaminophen (AC) and *N*-acetylcysteine (NAC) in phosphate buffer solution (pH 7.0). For comparison reasons, electrochemical studies on conventional platinum (Pt) electrode were also carried out.

The CV of various concentrations of AC was recorded on platinum electrode by means of cyclic voltammetry (Fig.54a). As it can be seen, AC is electrochemically

active, and therefore, it can be easily oxidized at relatively low anodic potential (+0.525 V vs. Ag/AgCl). A slight shift in the oxidation potential to more positive potential was found with increasing the concentration of AC, resulting to the increase of the peak potential separation $\Delta E_p = E_p^{ox} - E_p^{red}$. It is well known that the slow electron transfer is independent on the concentration, whereas the effect of uncompensated resistance dependents on concentration. Namely, this slight shift can be attributed to the cell resistance that remains uncompensated. It is interesting that a high value of $\Delta E_p \approx 0.473$ V was measured in the small concentration of AC ($c < 0.2$ mM), where the uncompensated resistance effect seems to be negligible. This value is higher than the theoretical ΔE_p value indicating that the electrochemical oxidation of AC is rather irreversible on Pt electrode [237]. Once more the current ratio values of oxidation and reduction peaks were much less than unity (~0.46), demonstrating the irreversibility of investigated redox system.

The effect of the variation of concentration of AC on anodic peak current of recorded CV-curves is displayed graphically in Fig.54b. It can be seen that the variation is not linear in the whole investigated concentration range. Two different linears with two different slopes were obtained in ranges of 0.166–0.819 mM and 0.819–1.61 mM, namely, it was remarkable that for concentrations of AC greater than ~ 0.9 mM the increase of oxidation current with AC concentration slightly slows down and the slope of the calibration curve decreases. The values of the limit of detection and sensitivity were determined from the first linear part 0.166–0.819 mM (with correlation coefficient of 0.9887) to be 7.0 μM, and 0.4011 $A \cdot M^{-1} \cdot cm^{-2}$, respectively.

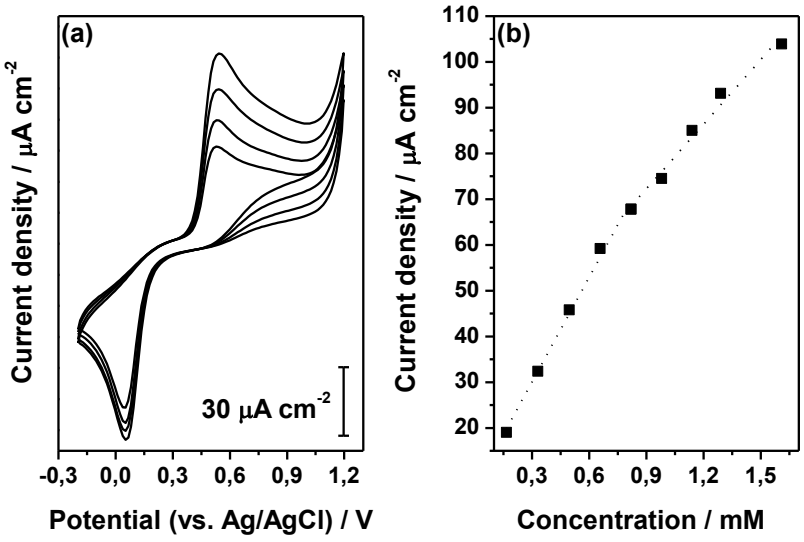

Fig. 54 (a) Representative CVs recorded for various concentrations of AC on conventional Pt electrode (PBS, pH 7.0) at 0.02 $V.s^{-1}$ (from inner to outer: 0.495, 0.657, 0.980, and 1.29 mM); **(b)** Variation of oxidation peak current density of AC with its concentration in the studied concentration range of 0.166-1.61 mM.

NAC was also investigated on conventional platinum electrode. CVs recorded for different concentrations of NAC in the range of 0.196–1.60 mM at the scan rate of 0.05 V. s^{-1} are shown in Fig.55a. NAC can be electrochemically oxidized to disulphide, *N*, *N*-diacetylcystine [238]. As it can be seen, NAC oxidized at about +0.785 V (vs. Ag/AgCl) for *c* = 0.196 mM, namely at about 230 mV more positive potential than AC. Besides, slight deviation of the peak oxidation to more positive potential with increasing the concentration of NAC was observed, as like in the case of AC. Namely, the oxidation peak of NAC lying at about +0.785 V (vs. Ag/AgCl) at *c*=0.196 mM shifts to the more positive potential of +0.808 V (vs. Ag/AgCl) with the increase of the concentration up to *c*=1.60 mM (an increase of overpotential of about ~23 mV occurs).

The value of peak potential separation was also estimated to be in the range of 0.742– 0.788 V, which seem to be greater than those determined for AC. It can be, consequently, concluded that the kinetic of electrochemical oxidation of NAC is slower compared to the oxidation of AC on Pt electrode. In addition, the electrode's current response towards AC is somehow higher compared to NAC. As a result, it can be concluded that the Pt electrode is somehow more sensitive towards oxidation of AC. From the current-concentration dependence which presented graphically in Fig.55b, a linear relationship (with correlation coefficient of 0.9989) in the whole investigated range can be observed. The detection limit and the sensitivity were determined to be 20 μM, and 0.1368 $A \cdot M^{-1} \cdot cm^{-2}$, respectively.

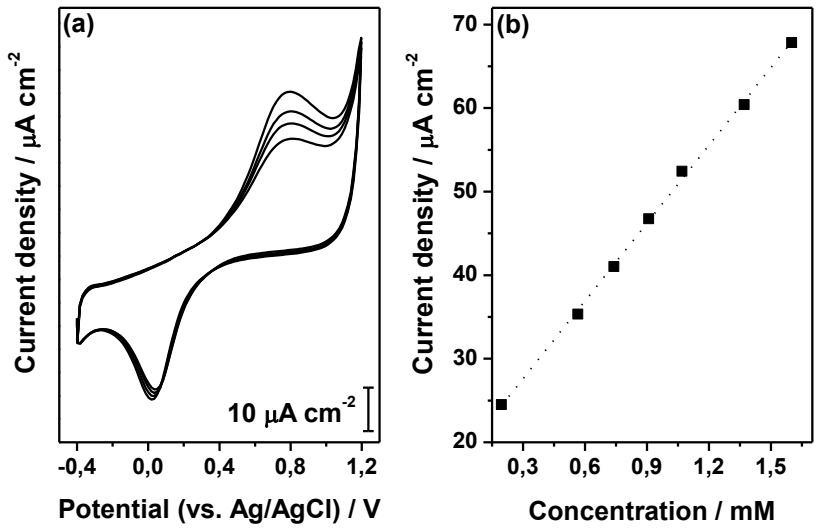

Fig. 55 (a) Representative CVs recorded for various concentrations of NAC on conventional Pt electrode (PBS, pH 7.0) at 0.05 $V.s^{-1}$ (from inner to outer: 0.566, 0.740, 0.909, and 1.07 mM); **(b)** Variation of oxidation peak current density of NAC with its concentration in the studied concentration range of 0.196-1.60 mM.

The electrochemical behavior of AC and NAC onto Pt electrode in PBS (pH 7.0) was investigated by means of impedance spectroscopy. Nyquist plots for different concentrations of AC in the range of 0.331–1.14 mM, and also for NAC in the range of 0.740–1.37 mM were recorded (Fig.56).

As it can be seen from recorded spectra, the impedance is mainly controlled by the interfacial electron transfer in the whole investigated frequency range.
The estimated value of R_{ct} decreases with increasing the concentration of AC and NAC, which demonstrate that the barrier for electron transfer slightly decreases, and consequently the charge transfer rate increases. It is interesting to compare the R_{ct} values for the oxidation of AC and NAC on Pt electrode at the same condition. For instance, the charge transfer resistance of ∼11 kΩ estimated for AC (c = 0.331 mM) appear to be about 9 times smaller compared to the charge transfer resistance of ∼98 kΩ estimated for NAC (c = 0.566 mM). These findings explain that the barrier for oxidation of AC on Pt electrode is smaller compared to that of NAC, demonstrating the greater electrode's response towards oxidation of AC.

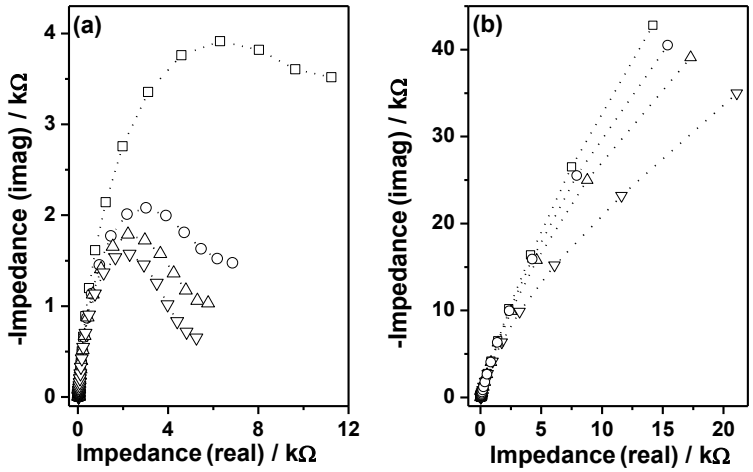

Fig. 56 (a) Representative EIS spectra recorded for 0.331 mM (open square), 0.495 mM (open circle), 0.657 mM (open upward triangle), and 1.14 mM (open downward triangle) AC on conventional Pt electrode (PBS, pH 7.0); **(b)** Representative EIS spectra recorded for 0.740 mM (open square), 0.909 mM (open circle), 1.07 mM (open upward triangle), and 1.37 mM (open downward triangle) NAC on conventional Pt electrode (PBS, pH 7.0).

The electrochemical oxidation of AC and NAC was studied on novel thin N-MWCNTs/PtNPs film (PtNPs: 3 nm) in aqueous PBS (pH 7.0). Representative CVs recorded at 0.02 $V.s^{-1}$ are presented in Figs 57a, 58a, respectively.
As it can be seen, AC oxidized at about 0.441 V (vs. Ag/AgCl), which is about 84 mV less anodic compared to that on conventional Pt electrode (+0.525 V vs.

Ag/AgCl) and almost similar within experimental error to oxidation potential of AC obtained on unmodified N-MWCNTs film in this work (+0.440 V vs. Ag/AgCl). It was also observed that the oxidation potential is shifted to more positive potential with the increase of AC concentration. This can be related to the cell's resistance which remains uncompensated. The ΔE_p value for AC was estimated for the lowest studied concentration of 0.166 mM, (where the uncompensated resistance has minimum effect) to be (0.160 V), indicating that the redox processes taking place onto N-MWCNTs/PtNPs film can be considered as quasi-reversible (in contrast to those occurring on conventional Pt electrode that were characterized as irreversible).

The variation of anodic peak current with the concentration of AC is displayed graphically in (Fig.57b). As it can be seen, the variation of the oxidation current of AC with its concentration was not linear in the whole investigated concentration range of 0.166–1.61 mM. Namely, as was already observed for the oxidation of AC onto Pt electrode, two dissimilar concentration-current linear dependences having different slopes in concentration ranges of 0.166–0.819 mM and 0.819–1.61 mM, were recognized.

The film's detection limit and sensitivity towards oxidation of AC were estimated by means of linear concentration-current curve in concentration range of 0.166–0.819 mM (with correlation coefficient of 0.9950) to be 0.395 μM and 0.9890 $A.M^{-1}.cm^{-2}$, respectively.

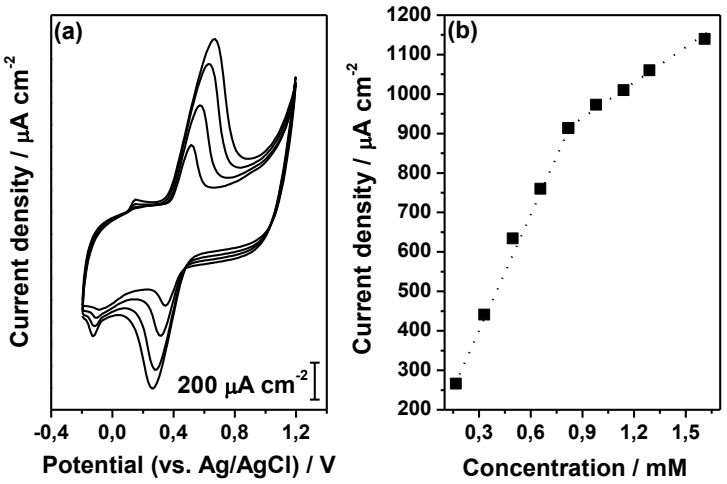

Fig. 57 (a) Representative CVs recorded for various concentrations of AC on N-MWCNTs/PtNPs film (PBS, pH 7.0) at 0.02 $V.s^{-1}$ (from inner to outer: 0.166, 0.331, 0.495, and 0.657 mM); **(b)** Variation of oxidation peak current density of AC with its concentration in the studied concentration range of 0.166-1.61 mM.

Furthermore, as it can be seen in CVs shown in Fig.58a, NAC oxidized on N-MWCNTs/PtNPs and its oxidation peak lies at about +0.199 V (vs. Ag/AgCl) at *c*

=0.196 mM, which is clearly less positive (namely about 586 mV less anodic) compared to that measured for NAC on conventional Pt electrode for the same concentration (+0.785 V vs. Ag/AgCl; c = 0.196 mM). These results verify the strong electrocatalytic activity of electrodes consisting of carbon nanomaterials modified with metal nanoparticles. A shift of oxidation peak to more positive values with the increase of concentration occurs also for NAC, as like in the case of AC, due to the uncompensated resistance effect. The ΔE_p values for NAC (0.328 V) estimated for the lowest studied concentrations of 0.196 mM, appear to be significantly smaller compared to those obtained on conventional Pt electrode (under the same conditions) indicating that the redox processes taking place onto N-MWCNTs/PtNPs film can be considered as quasi-reversible.

In addition, the estimated ΔE_p value for NAC (0.328 V) appears to be two times greater compared to that determined for AC (0.160 V) indicating that the kinetic of electrochemical oxidation of NAC on N-MWCNTs/PtNPs is rather slower compared to that of AC (similar behavior was observed on Pt electrode). Furthermore, the film's current response towards oxidation of AC appears to be somehow greater compared to that for NAC. Namely, the oxidation peak current density of about 1141 $\mu A \cdot cm^{-2}$ measured for AC (c = 1.61 mM) on N-MWCNT/PtNPs film appears to be more than four times greater from that measured for NAC (c = 1.60 mM) on the same electrode (252 $\mu A \cdot cm^{-2}$). Anyhow, the current response of N-MWCNTs/PtNPs for both compounds appears to be significantly greater compared to that of conventional Pt electrode.

The relationship between the current response and concentration was linear in the concentration range of 0.196–1.60 mM (with correlation coefficient of 0.9880) (Fig.58b). The limit of detection and sensitivity of N-MWCNTs/PtNPs film towards oxidation of NAC were estimated to be 10 μM and 0.1740 $A \cdot M^{-1} \cdot cm^{-2}$, respectively. The detection ability of N-MWCNTs/PtNPs film towards NAC seems to be weaker compared to AC, something that is in absolute accordance with the different current responses observed for studied biomolecules.

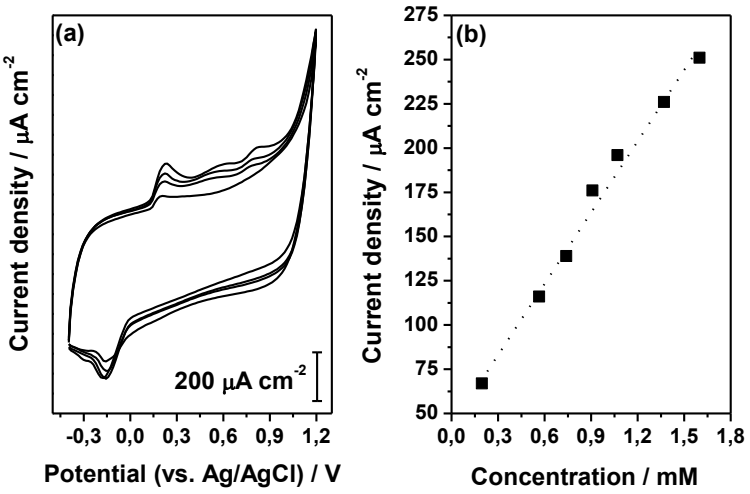

Fig. 58 (a) Representative CVs recorded for various concentrations of NAC on N-MWCNTs/PtNPs film (PBS, pH 7.0) at 0.02 $V.s^{-1}$ (from inner to outer: 0.196, 0.740, 1.07, and 1.60 mM); **(b)** Variation of oxidation peak current density of NAC with its concentration in the studied concentration range of 0.196-1.60 mM.

It was remarkable that on N-MWCNTs/PtNPs, the peak potential separation between AC and NAC was about 250 mV, demonstrating the ability to analyze AC and NAC in a single experiment. Consequently two well separated peaks were observed for AC and NAC on N-MWCNTs/PtNPs permitting the simultaneous determination of both biomolecules (Fig.59a). It is interesting to mention that on Pt electrode a single peak for both AC and NAC was observed (Fig.59b).

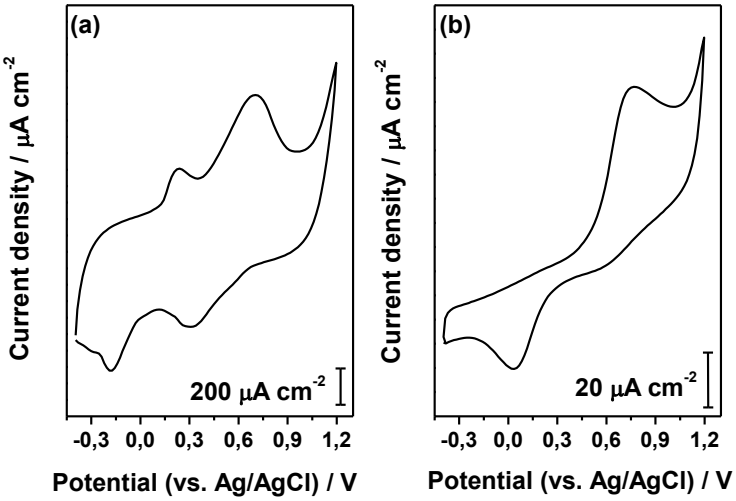

Fig. 59 CVs recorded for AC and NAC binary mixtures (NAC: 1.60 mM; AC: 0.495 mM) on either N-MWCNTs/PtNPs film **(a)** or conventional Pt electrode **(b)** at 0.02 $V.s^{-1}$ (PBS, pH 7.0).

A comparison of detection limits and sensitivities obtained in present work for conventional Pt electrode and N-MWCNTs/PtNPs film towards AC and NAC (PBS, pH 7.0) with those reported in literature for other novel electrodes is shown in Table 8.

Table 8 The comparison of limits of detection (LOD) and sensitivities (S) obtained in the present work for conventional Pt electrode and N-MWCNTs/PtNPs film towards AC and NAC (PBS, pH 7.0) with literature values**.**

Electrode	*LOD*/μM		S/A ·M^{-1} ·cm^{-2}		References
	AC	NAC	AC	NAC	
Pt[a]	7.0	20.0	0.4011	0.1368	This work
N-MWCNTs/PtNPs[a]	0.395	10.0	0.9890	0.1740	This work
N-MWCNTs[b]	0.485		0.8406		This work
MWCNTs[b]	0.950		0.6010		This work
CPE/G[c]	0.60		0.2820		[239]
CFE[d]	1.50		0.1800		[240]
GCE/G/Nd[e]	14.22		0.5310		[241]
GCE[f]	19.85				[242]
GC/TiO_2[g]	2.0				[227]
GC/Cu/TTCA[h]	5.0				[243]
VCPE[i]	88.0				[244]
PGE/MIP[j]	0.79				[209]
CP/CNT[k]	1.10				[245]
MWCNTs/FC[l]		0.60			[246]
MWCNTs/PE/DNB[m]	10.0	0.20			[217]
CP/MWCNTs/EFC[n]		0.08			[247]
CP/SiCuNP[o]		41.8		0.0302	[248]
CP/CuHCF[p]		63.0			[249]

a Pt and N-MWCNTs/PtNPs electrodes used in present work

b Pristine MWCNTs- and N-MWCNTs-based films used in this work

c Carbon paste electrode modified with grapheme

d Carbon fiber electrode modified with electro-copolymerization of ophenylenediamine and aniline

e Glassy carbon electrode modified with grapheme oxide and neodymium hexacyanoferrate

f Glassy carbon electrode

g Glassy carbon electrode modified with TiO_2 nanoparticles

h Glassy carbon electrode modified with copper ions/terthiophene carboxylic acid polymer

I Vaseline carbon paste electrode modified with avocado tissue (Persea americana)

j Pencil graphite electrode modified with molecularly imprinted polypyrrole

k Carbon paste electrode modified with carbon nanotubes and poly(3-aminophenol)

l MWCNTs paste electrode modified with ferrocene

m MWCNTs paste electrode modified with *N*-(3,4-dihydroxyphenethyl)-3,5-dinitrobenzamide

n Carbon paste electrode modified with MWCNTs and ethynylferrocene

o Carbon paste electrode modified with copper nitroprusside adsorbed on 3-Aminopropylsilica

p Carbon paste electrode modified with copper(II) hexacyanoferrate(III)

The comparison exhibits that in general the detection ability and sensitivity of novel N-MWCNTs/PtNPs is quite enhanced. It is very interesting that the modification of N-MWCNTs with PtNPs leads to an improvement of its detection ability towards oxidation of AC. Namely, as it can be observed from the values reported in Table 8, the detection limit of N-MWCNTs/PtNPs appears to be about 19% smaller compared to that of unmodified N-MWCNTs. Furthermore, the sensitivity of N-MWCNTs/PtNPs towards AC seems to be about 18% greater compared to that of unmodified N-MWCNTs. The findings exhibit that the fabricated N-MWCNTs/PtNPs film decreases the overpotentials and improves the kinetics for oxidation of studied compounds. The investigated biomolecules can be also successfully oxidized on N-MWCNTs/PtNPs and can be analyzed in a single experiment.

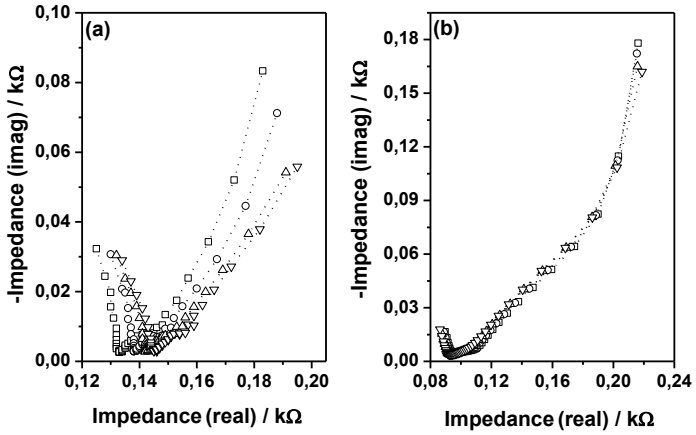

Fig. 60 (a) Representative EIS spectra recorded for 0.495 mM (open square), 0.819 mM (open circle), 1.14 mM (open upward triangle), and 1.29 mM (open downward triangle) AC on N-MWCNTs/PtNPs film; **(b)** EIS spectra recorded for 0.566 mM (open square), 0.740 mM (open circle), 1.07 mM (open upward triangle), and 1.37 mM (open downward triangle) NAC on N-MWCNTs/PtNPs film.

EIS spectra for various concentrations of AC and NAC in the range of 0.495-1.29 mM and 0.566-1.37 mM, respectively, were recorded in (PBS, pH 7.0) on the modified N-MWCNTs/PtNPs (Fig.60). The observed results indicate that the charge transfer resistance gradually decreases (slightly) with the increase of concentration of redox compounds, demonstrating that the barrier for electron transfer slightly decreases, and thus, the charge transfer rate of redox processes increases with increasing concentration of AC and NAC. Once more, it is remarkable that the R_{ct} values for the oxidation of either AC or NAC on N-MWCNTs/PtNPs film appear to be significantly smaller compared to those measured onto conventional Pt electrode for the same redox systems under the same conditions. For example, the R_{ct} values of 0.044 kΩ and 0.095 kΩ estimated

for AC (1.61 mM) and NAC (1.60 mM), respectively, on N-MWCNTs/PtNPs film seem to be considerably smaller (more than 90% smaller) from those obtained on conventional Pt electrode.

4.2.5.2 Electrochemical detection of AA, DA, and UA on N-MWCNTs/MNPs (M: Rh, Pd, Ir, Pt, and Au)

The electrochemical response of N-MWCNTs/MNPs (M: Rh, Pd, Ir, Pt, Au) composite films, towards simultaneous oxidation of (AA), (DA), and (UA) was investigated in (PBS, pH 7.0) by means of cyclic voltammetry technique (CV). The electrochemical oxidation of AA, DA, and UA takes place according to the following reactions (Fig. 61).

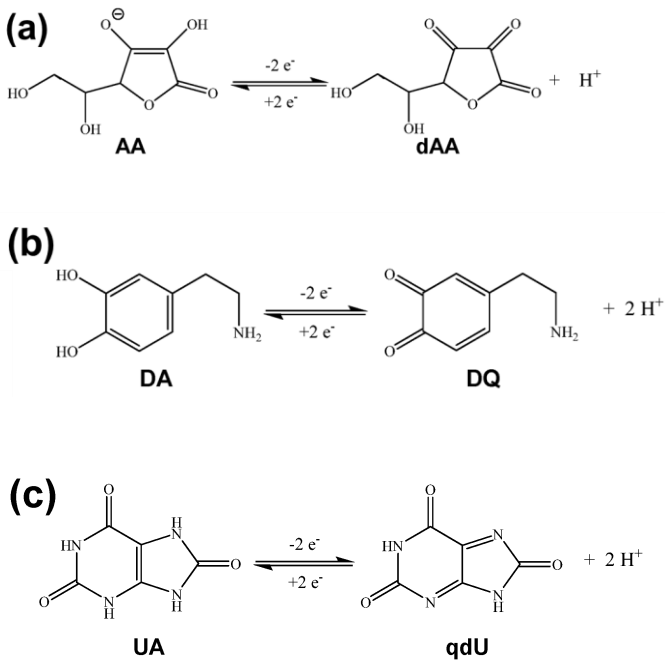

Fig. 61 Electrochemical oxidation of (a) AA (b) DA, and (c) UA on N-MWCNTs/MNPs composite films [250- 252].

Firstly, the oxidation of DA in the presence of AA and UA was studied on unmodified N-MWCNTs and modified N-MWCNTs/MNPs composite films. For this purpose, CVs were recorded by varying the concentration of DA in the range from 0.012 to 0.322 mM while keeping the concentration of AA (0.5 mM) and UA (0.1 mM) constant. It must be mentioned that the concentration of AA was higher from those of DA and UA due to the limited sensitivity of composite films towards oxidation of AA. CVs recorded for the ternary mixtures AA, DA, and UA are presented in Fig.62.

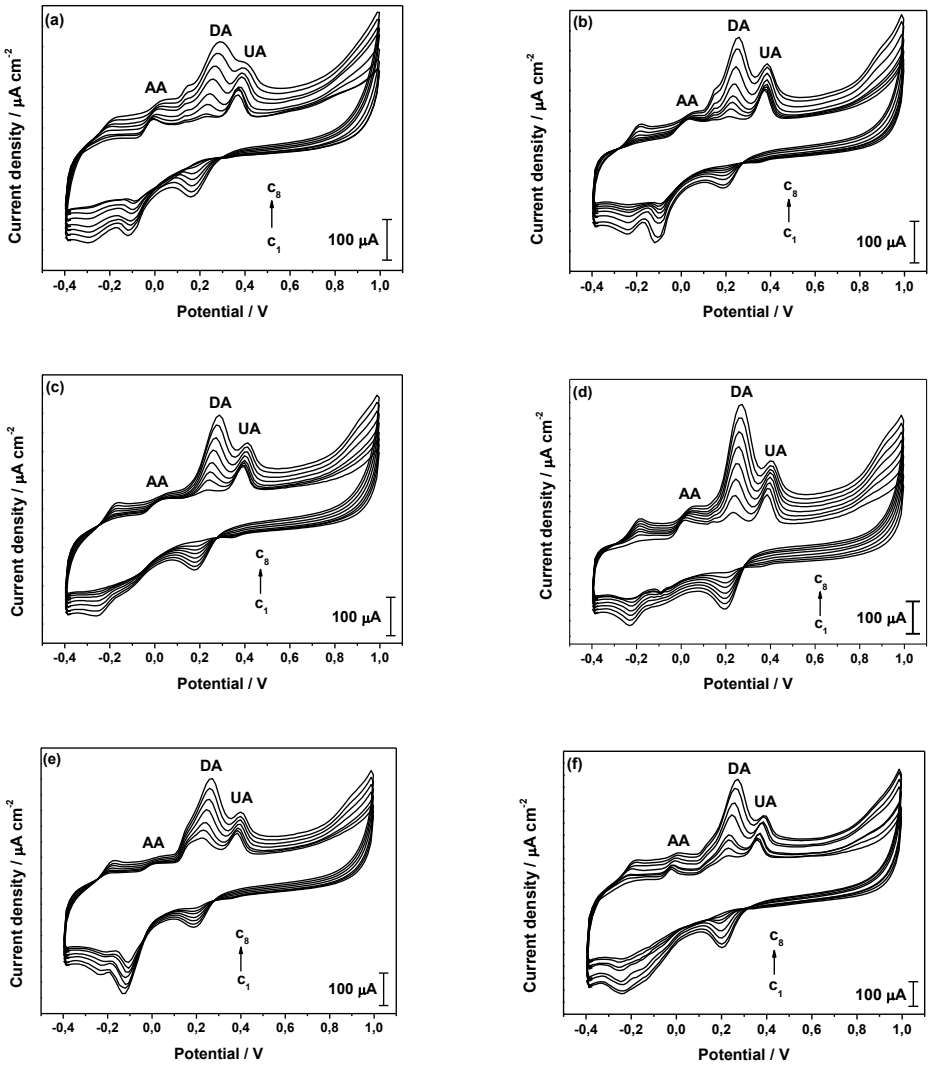

Fig. 62 CVs recorded for different concentrations of DA (in the range of 0.012-0.322 mM) in the presence of AA (0.5 mM) and UA (0.1 mM) in phosphate buffer solution (pH 7.0) at the scan rate of 0.02 $V \cdot s^{-1}$ on N-MWCNTs (a), N-MWCNTs/RhNPs (b), N-MWCNTs/PdNPs (c), N-MWCNTs/IrNPs (d), N-MWCNTs/PtNPs (e), and MWCNTs/AuNPs (f) composite films. The potentials are reported *versus* Ag/AgCl (saturated KCl) reference electrode.

As it can be seen, the three obtained oxidation peaks corresponding to oxidation of AA, DA, and UA are well separated. The oxidation of DA takes place at about 0.225 V (vs. Ag/AgCl) and the oxidation peak is followed by a reduction peak at about 0.196 V (vs. Ag/AgCl) (both oxidation and reduction potential are estimated for the lowest concentration 0.012 mM). It is well known that DA can be oxidized to dopamine-o-quinone (DAQ) with two electron transfer (Fig.61b). The two other oxidation waves, which lie in the potential ranges of -0.021- 0.017

V (vs. Ag/AgCl) and 0.361- 0.397 V (vs. Ag/AgCl), are attributed to the electrochemical oxidations of AA and UA, respectively.

The peak potential separation ($\Delta E_p = E_p^{ox} - E_p^{red}$) for oxidation of DA was estimated to be about $\Delta E_p \approx 0.029$ V which is very close to the expected theoretical ΔE_p value of 2.3RT/*n*F (*n*=2) demonstrating that the electro-oxidation of DA to DAQ tends to be reversible on N-MWCNTs and N-MWCNTs/MNPs composite films. However, the oxidation and reduction peak current ratio (i_P^{ox}/i_P^{red}) appears to be slightly greater that unity (deviation from reversibility) indicating that the redox system DA/DAQ is quasi-reversible onto studied composite films. It is, thus, probable that a parallel chemical reaction takes place disturbing the reversibility of DA/DAQ redox system. It was remarkable that in general the ΔE_p values tend to increase with increasing the concentration of DA. For instance, on N-MWCNTs/AuNPs the ΔE_p increases from 0.029 V up to 0.070 V when the concentration of DA increases from 0.012 mM up to 0.322 mM (the highest studied concentration of DA). This behavior can be attributed to the cell resistance that remains uncompensated, and it has been also observed for the other studied molecules.

It would be very interesting to compare the ΔE_p values for oxidation of DA obtained onto unmodified N-MWCNTs and modified N-MWCNTs/MNPs composite films. On unmodified N-MWCNTs films, ΔE_p values of 0.060 V and 0.107 V were obtained for the DA concentrations of 0.012 mM and 0.322 mM, respectively, while on modified N-MWCNTs/AuNPs, ΔE_p values of 0.029 and 0.070 V were obtained for the DA for the same concentrations 0.012 mM and 0.322 mM, respectively. The findings demonstrate that the ΔE_p value onto N-MWCNTs is almost two times greater compared to those measured under the same conditions onto N-MWCNTs/AuNPs.

Considering that ΔE_p is connected to heterogeneous electron transfer rate constant (k_s) through the electrochemical absolute rate relation (ΔE_p is inversely analogous to k_s) [253], the findings indicate that the kinetic for oxidation of DA to DAQ onto unmodified N-MWCNTs film is significantly slower compared to that on N-MWCNTs/MNPs. Thus, the estimated k_s values confirm that the kinetic of DA/DAQ redox system on N-MWCNTs ($k_s \approx 8\times10^{-3}$ cm.s^{-1}) is about 78% slower compared to that on N-MWCNTs/MNPs ($k_s \approx 38\times10^{-3}$ cm.s^{-1}).

CVs recorded on all types of N-MWCNTs/MNPs composite films reveal three well-separated (not overlapped) anodic CV-waves corresponding to progressive oxidation of AA, DA, and UA. A slight overlapping of oxidation waves of DA and UA can be seen on unmodified N-MWCNTs film at elevated concentrations of DA. Besides, it is obvious that within the investigated MNPs, the modification of N-MWCNTs with AuNPs leads to pronounced decrease of oxidation overpotential of AA (-0.021 V vs. Ag/AgCl), and thus, to greater peak potential

separation (~0.248 V) between oxidation waves of interfering AA and DA analytes. In addition, the oxidation current of DA appears to be about 46% and 25-40% greater on N-MWCNTs/AuNPs compared to that measured onto N-MWCNTs and other N-MWCNTs/MNPs (M: Rh, Pd, Ir, Pt) composite films, respectively (comparison was always done for same concentration and scan rate). These findings demonstrate that the electrocatalytic activity of N-MWCNTs/AuNPs towards simultaneous oxidation of AA, DA, and UA is quite enhanced.

It must be noted that the oxidation potential of AA is shifted to less anodic potential (more than 0.250 V) either on unmodified N-MWCNTs or other N-MWCNTs/ MNPs films compared to that on conventional GC and Pt electrodes demonstrating once more the greater electrocatalytic activity of carbon nanomaterials towards oxidation of studied biomolecules.

It is interesting to mention that on N-MWCNTs/MNPs (M: Rh, Pd, Ir, Pt) the overpotential for oxidation of AA is similar (within experimental error) to that measured onto unmodified N-MWCNTs. It can be concluded that the ability of these particular nanoparticles (RhNPs, PdNPs, IrNPs, PtNPs) to decrease the overpotential of AA is limited compared to AuNPs.

The interpretation of CVs recorded with various concentrations of DA in the presence of AA and UA demonstrate that the oxidation peak current of DA increases linearly with the increase of its concentration in the range of 0.012 - 0.322 mM on N-MWCNTs and N-MWCNTs/ MNPs composite films. From the linear current-concentration variation, the lower limit of detection at signal-to-noise ratio of 3 (*S/N*=3) of N-MWCNTs and N-MWCNTs/ MNPs composite films towards oxidation of DA to DAQ in the presence of AA and DA was determined. The results are shown in Table.9 and are presented graphically in histogram in Fig.65a. The results demonstrate that the detection ability of fabricated composite films towards DA/DAQ redox system in presence of AA and UA enhances with the following order: N-MWCNTs < N-MWCNTs/RhNPs < N-MWCNTs/PdNPs < N-MWCNTs/IrNPs < N-MWCNTs/PtNPs < N-MWCNTs/AuNPs. These findings demonstrate the greater electrocatalytic activity of N-MWCNTs modified with AuNPs for analysis of DA in presence of AA and UA.

Furthermore, the electrochemical response of N-MWCNTs and N-MWCNTs/MNPs (M: Rh, Pd, Ir, Pt, Au) composite films towards oxidation of UA in the presence of AA and DA was investigated. Various concentrations of UA in the range of 0.049-0.313 mM in the presence of AA (0.5 mM) and DA (0.1 mM) were recorded by means of CV technique in phosphate buffer solution (pH 7.0) at the scan rate of 0.02 $V \cdot s^{-1}$ (Fig.63). As already mentioned in the previous paragraph, the concentration of AA was high due to the limited sensitivity of composite films towards oxidation of AA.

A peak corresponding to oxidation of UA can be seen in recorded CVs in the range from 0.361 V to 0.397 V (vs. Ag/AgCl) (within experimental error). This wave can be attributed to the oxidation of UA to its diamine (UADI) (Fig.61) [254]. The two other oxidation waves that lie, the first in the potential region of -0.021 to 0.017 V (vs. Ag/AgCl) and the second at about 0.225 V (vs. Ag/AgCl), can be attributed to the electrochemical oxidations of AA and DA, respectively.

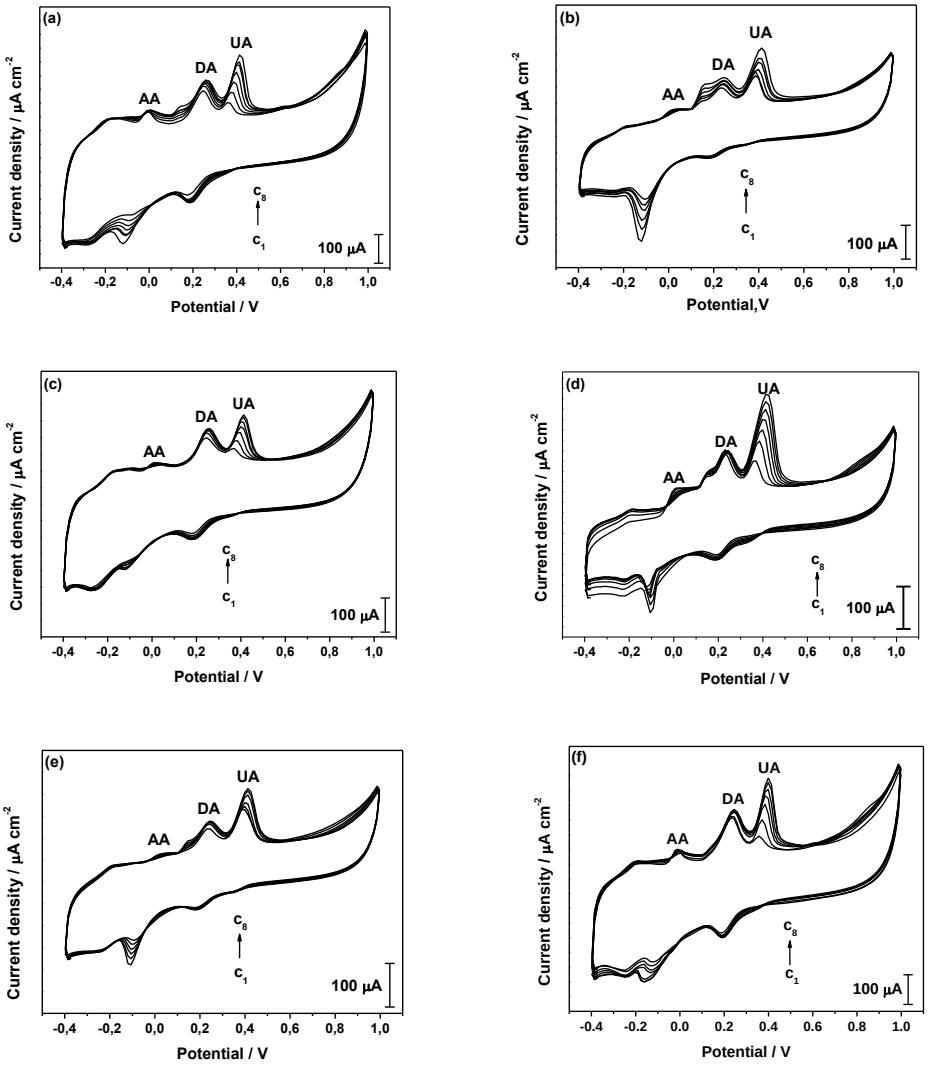

Fig. 63 CVs recorded for different concentrations of UA (in the range of 0.049–0.313 mM) in the presence of AA (0.5 mM) and DA (0.1 mM) in phosphate buffer solution (pH 7.0) at the scan rate of 0.02 V s^{-1} on N-MWCNTs (a), N-MWCNTs/RhNPs (b), N-MWCNTs/PdNPs (c), N-MWCNTs/IrNPs (d), N-MWCNTs/PtNPs (e), and N-MWCNTs/AuNPs (f) composite films. The potentials are reported *versus* Ag/AgCl (saturated KCl) reference electrode.

The electrochemical oxidation of UA appears to be completely irreversible on composite films studied, and thus, no reduction wave can be observed in recorded

CVs even at low scan rates. It is well known that the electrochemical oxidation of UA is followed by a chemical reaction that interrupts the reversibility of the redox system. Namely, UADI the oxidation product of UA, reacts fast with water to give imine alcohol that is reduced at more cathodic potential than diamine (at about -1.0 V vs. Ag/AgCl) [255].

From the recorded CVs presented in Fig.63, three well-separated waves can be seen for the oxidation of AA, DA, and UA onto investigated N-MWCNTs and N-MWCNTs/MNPs composite films permitting their simultaneous analysis in a single measurement. Anyhow, it is noticeable that on N-MWCNTs/AuNPs film the oxidation peaks of three analytes are better separated and the oxidation current density of UA on this particular film is greater compared to either N-MWCNTs or other N-MWCNTs/MNPs films at the same concentration of analyte (Table 9). This result is an indication of greater electrocatalytic activity of AuNPs.

Table 9 Oxidation peak potentials (E_p^{ox}) of AA, DA, UA analytes and oxidation peak potential differences (ΔE_p^{ox}) of AA-DA and DA-UA analytes estimated on N-MWCNTs, N-MWCNTs/RhNPs, N-MWCNTs/PdNPs, N-MWCNTs/IrNPs, N-MWCNTs/PtNPs, and N-MWCNTs/AuNPs composite films in phosphate buffer solution (pH 7.0) at the scan rate of 0.02 $V.s^{-1}$.

Electrode Material	E_p^{ox} /V[(a)(b)]	E_p^{ox} /V[(a)(c)]	E_p^{ox} /V[(a)(d)]	E_p^{ox} /V[(e)]	E_p^{ox} /V[(f)]
N-MWCNTs	0.017	0.227	0.361	0.210	0.134
N-MWCNTs/RhNPs	0.008	0.225	0.378	0.217	0.153
N-MWCNTs/PdNPs	0.014	0.225	0.367	0.211	0.142
N-MWCNTs/IrNPs	0.014	0.029	0.380	0.215	0.151
N-MWCNTs/PtNPs	0.017	0.225	0.383	0.208	0.158
N-MWCNTs/AuNPs	-0.021	0.227	0.397	0.248	0.170

[(a)] All potentials are reported *versus* Ag/AgCl (saturated KCl) reference electrode
[(b)] Oxidation peak potential of AA/DHAA redox system
[(c)] Oxidation peak potential of DA/DAQ redox system
[(d)] Oxidation peak potential of UA/UADI redox system
[(e)] Oxidation peak potential difference of AA-DA analytes
[(f)] Oxidation peak potential difference of DA-UA analytes

Namely, the potential separation of oxidation waves of interfering AA and DA compounds appears to be about 0.248 V (about 30-40 mV greater compared to that onto other composite films), while the oxidation current of UA on N-

MWCNTs/AuNPs seems to be about 45% and 5.0-32% greater compared to that measured on N-MWCNTs and other N-MWCNTs/MNPs (M: Rh, Pd, Ir, Pt) composite films, respectively (comparison was done at same concentration and scan rate).

The results exhibit clearly that the electrocatalytic activity of N-MWCNTs/AuNPs composite film towards oxidation of UA in presence of DA and AA is greater compared to other studied films. The analysis of CVs recorded at various concentrations of UA (in the range of 0.049-0.313 mM) exhibits that the oxidation current of UA increases linearly with its concentration in the investigated concentration range. The lower limits of detection (*S/N*=3) of N-MWCNTs and N-MWCNTs/MNPs composite films towards oxidation of UA in the presence of AA and DA were estimated from the linear oxidation current-concentration diagram and the obtained results are presented in Table 10 and are shown graphically in histogram in Fig.65b. The findings demonstrate that the lower limit of detection of composite films towards oxidation of UA in the presence of AA and DA tends to decrease with the following order: N-MWCNTs > N-MWCNTs/RhNPs > N-MWCNTs/PdNPs > N-MWCNTs/IrNPs >N-MWCNTs/PtNPs > N-MWCNTs/AuNPs.

Table 10 Lower limits of detection (*LOD*) estimated at signal-to-noise ratio of 3 (*S/N*=3) for N-MWCNTs, N-MWCNTs/RhNPs, N-MWCNTs/PdNPs, N-MWCNTs/PtNPs, and N-MWCNTs/AuNPs composite films towards simultaneous electrochemical oxidation of AA, DA, and UA in phosphate buffer solution (pH 7.0).

Electrode Material	***LOD* / μM**		
	AA[(a)]	**DA**[(b)]	**UA**[(c)]
N-MWCNTs	8.7	1.4	5.9
N-MWCNTs/RhNPs	7.9	1.1	4.1
N-MWCNTs/PdNPs	6.8	0.8	3.6
N-MWCNTs/IrNPs	6.1	0.7	3.1
N-MWCNTs/PtNPs	3.1	0.6	2.1
N-MWCNTs/AuNPs	0.9	0.3	0.4

(a) Estimated in concentration range of 0.099-0.600 mM
(b) Estimated in concentration range of 0.012-0.322 mM
(c) Estimated in concentration range of 0.049-0.313 mM

These findings are in a very good agreement with those obtained from the analysis of DA in presence of AA and UA (see previous paragraph); and verify the greater electrocatalytic activity of N-MWCNTs/AuNPs composite film for analysis of

UA in the presence of AA and DA. The electrochemical determination of AA in the presence of DA and UA was also investigated. CVs recorded for different concentrations of AA in the concentration range of 0.099-0.600 mM in the presence of DA (0.05 mM) and UA (0.05 mM) either on unmodified N-MWCNTs or N-MWCNTs/MNPs (M: Rh, Pd, Ir, Pt, Au) composite films in (PBS, pH 7.0) at the scan rate of 0.02 $V \cdot s^{-1}$ are shown in Fig.64.

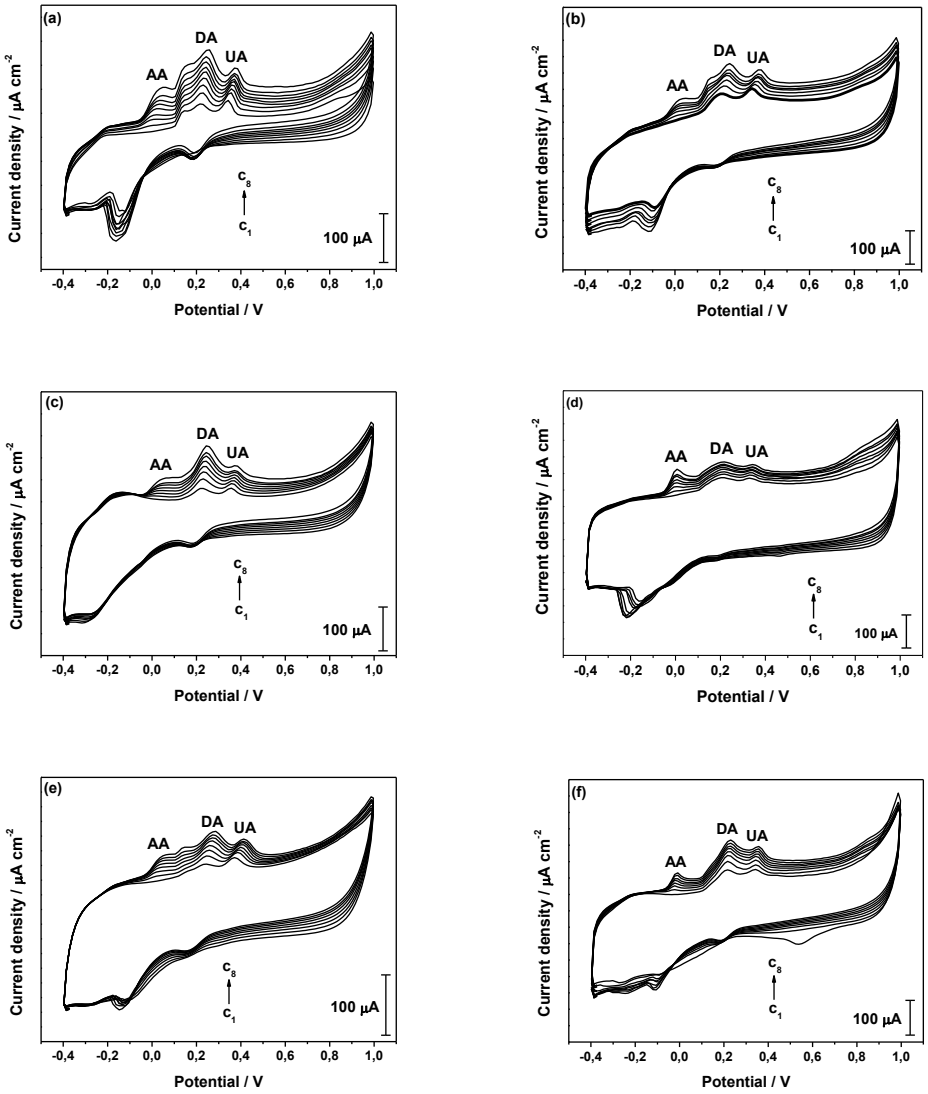

Fig. 64 CVs recorded for different concentrations of AA (in the range of 0.099–0.600 mM) in the presence of DA (0.05 mM) and UA (0.05 mM) in phosphate buffer solution (pH 7.0) at the scan rate of 0.02 V s^{-1} on (a) N-MWCNTs, (b) N-MWCNTs/RhNPs, (c) N-MWCNTs/PdNPs, (d) N-MWCNTs/IrNPs, (e) N-MWCNTs/PtNPs, and (f) N-MWCNTs/AuNPs composite films. The potentials are reported *versus* Ag/AgCl (saturated KCl) reference electrode.

The CVs were recorded with higher concentration of AA since the sensitivity of composite films towards oxidation of AA is limited. The interpretation of

recorded CVs demonstrates that the oxidation of AA on unmodified N-MWCNTs occurs at about 0.017 V (vs. Ag/AgCl), while its oxidation onto N-MWCNTs/MNPs composite films modified with RhNPs, PdNPs, IrNPs, PtNPs, and AuNPs takes place at about 0.008 V, 0.014 V, 0.014 V, 0.017 V, and -0.021 V (vs. Ag/AgCl), respectively.

The mechanism for the electrochemical oxidation of AA was already discussed by many researchers and reported in literature [256,257]. According to previously published reports, the quasi-reversible electrochemical oxidation of AA leads to the formation of dehydro-L-ascorbic acid (DHAA) via two electron transfer process that is followed by an irreversible chemical reaction (Fig.61). Thus, the reduction peak appearing in the potential range from -0.105 to -0.136 V (vs. Ag/AgCl) (depending on type of composite film) corresponds to the inverse process, namely to the reduction of DHAA to AA.

The data extracted from recorded CVs demonstrate that the anodic and cathodic peak potential separation $\Delta E_p = E_p^{ox} - E_p^{red}$ of AA on N-MWCNTs and N-MWCNTs/MNPs estimated in the range of 0.098-0.153 V (lowest concentration of 0.099 mM and scan rate of 0.02 $V.s^{-1}$) appears to be significantly greater than the expected theoretical value of $59/n$ mV (for n=2 at 25^{o}C). Furthermore, the oxidation and reduction peak current ratio (i_P^{ox}/i_P^{red}) for electrochemical oxidation of AA appears to be significantly greater than unity.

Consequently, according to these findings the redox system AA/DHAA can be considered as irreversible on novel N-MWCNTs and N-MWCNTs/MNPs composite films. In addition, the estimated k_s values for AA/DHAA ($k_s \approx 6\times10^{-3}$ $cm.s^{-1}$), that appear to be significantly smaller than those of reversible DA/DAQ redox system, confirm the great deviation of AA/DHAA from reversibility.

It was also observed that the electrochemical current response of N-MWCNTs and N-MWCNTs/MNPs composite films towards DA and UA is always greater compared to AA at the same concentration of analytes. Namely, the oxidation current of AA appears to be always about 20-30% smaller compared to that of DA and UA analytes (measured at the same concentration and scan rate). These findings demonstrate the lower sensitivity of studied composite films towards the oxidation of AA. It is interesting to mention that on N-MWCNTs/AuNPs composite film, the oxidation overpotential of AA decreases significantly. Namely, the oxidation peak of AA lies in negative potential region (-0.021 V vs. Ag/AgCl). Consequently, on N-MWCNTs/AuNPs film the potential difference between oxidation waves of interfering AA and DA analytes appears to be great (~0.248 V) resulting to huge separation of oxidation waves of AA and DA. Similarly, onto this particular film the separation between DA and UA oxidation waves appears to be the greatest (~0.170 V). It must be noted, however, that onto unmodified N-MWCNTs and other modified N-MWCNTs/MNPs composite films

the separation between oxidation waves of AA and DA is also enough large (~0.210-0.217 V) and thus no interference of AA in analysis of DA (and the inverse, interference of DA in analysis of AA) can be observed. Thus, it can be concluded that the simultaneous determination of AA, DA, and UA can be successfully carried out on novel N-MWCNTs/MNPs in a single measurement.

The electrochemical responses of N-MWCNTs and N-MWCNTs/MNPs composite films towards oxidation of AA increase linearly with increasing concentration of AA in the investigated concentration range from 0.099 to 0.600 mM. The relationship between current and concentration appears to be linear and thus the lower limit of detection (*S/N*=3) of novel composite films towards the redox system AA/DHAA in the presence of DA and UA was estimated from this linear dependence. The obtained detection limits are included in Table 10 and are presented graphically in histogram Fig.65c.

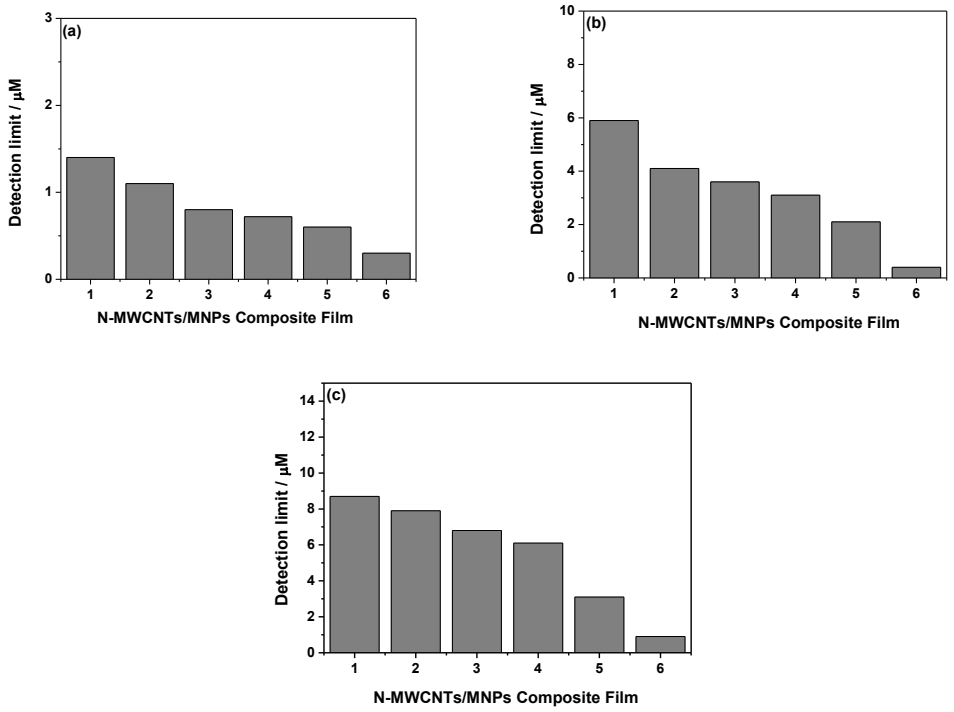

Fig. 65 Histograms showing the detection limits (S/N = 3) of N-MWCNTs (1), N-MWCNTs/RhNPs (2), N-MWCNTs/PdNPs (3), N-MWCNTs/IrNPs (4), N-MWCNTs/PtNPs (5), and N-MWCNTs/AuNPs (6) composite films towards electrochemical oxidation of (a) DA in the presence of AA and UA, (b) UA in the presence of AA and DA, and (c) AA in the presence of DA and UA (phosphate buffer solution, pH 7.0).

The findings exhibit that the detection ability of N-MWCNTs and N-MWCNTs/MNPs composite films towards AA/DHAA redox system in the presence of DA and UA is improved with the same order found for DA/DAQ and

UA/UADI redox systems. Namely, the lower limit of detection of composite films towards oxidation of AA decreases with the following order: N-MWCNTs > N-MWCNTs/RhNPs > N-MWCNTs/PdNPs > N-MWCNTs/IrNPs > N-MWCNTs/PtNPs > N-MWCNTs/AuNPs.

The results verify once more the greater affinity of AuNPs to improve the sensitivity and electrocatalytic activity of N-MWCNTs for simultaneous analysis of AA, DA, and UA. It is very interesting to mention that the detection ability of N-MWCNTs and N-MWCNTs/MNPs composite films towards oxidation of studied compounds is always enhanced with the order AA < UA < DA.

Fig.66 displays the dependence of detection limits (*S/N*=3) of N-MWCNTs/MNPs (M: Rh, Pd, Ir, Pt, Au) composite films towards oxidation of AA, DA, and UA on density of states of corresponding metal nanoparticles, calculated from the model band structures and reported in literature by Smith *et al*. [258].

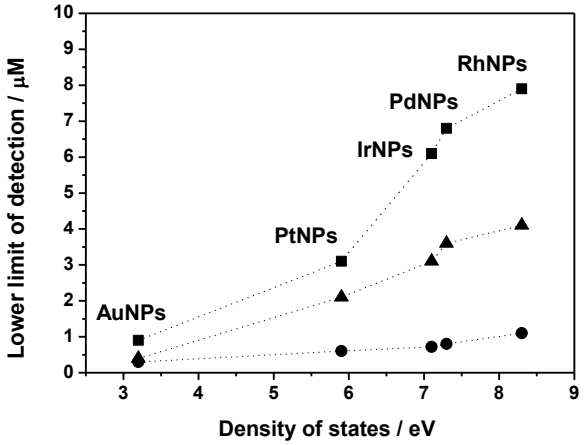

Fig. 66 Diagrams showing the variation of detection limits (*S/N*=3) of N-MWCNTs/RhNPs, N-MWCNTs/PdNPs, N-MWCNTs/IrNPs, N-MWCNTs/PtNPs, and N-MWCNTs/AuNPs composite films towards electrochemical oxidation of AA (■), DA (●), and UA (▲) (phosphate buffer solution, pH 7.0) *versus* the density of states reported in literature by Smith *et al* [255]. The density of states was calculated from the model band structures. The zero of energy corresponds to the Fermi level.

From this diagram is can be clearly seen that the detection ability, and thus the sensitivity of composite film, is related to density of states of metals. Namely, the smallest density of states of AuNPs (3.2 eV) leads to the lowest detection limit (greatest sensitivity), while the greatest density of states of RhNPs (8.3 eV) results to the highest detection limit (lowest sensitivity).

In addition, the simultaneous electrochemical analysis of AA, DA, and UA was studied on standard conventional working electrodes such as glassy carbon (GC)

and platinum (Pt). Specifically, ternary mixture of AA, DA, and UA with concentration ratio of 1:1:1 was electrochemically investigated. Initially the oxidation of AA was electrochemically studied for estimating its overpotential. Representative CVs recorded for AA in (phosphate buffer solution, pH 7.0) on GC and Pt electrodes are shown in Figs.67a, 67b, respectively. Afterwards a ternary mixture of AA, DA, and UA was investigated in phosphate buffer solution, pH 7.0. CVs recorded for the ternary mixture shown in Fig.67a-b, respectively.

The results demonstrate that on GC and Pt electrodes the oxidation of AA requires a potential of about 0.301 V (vs. Ag/AgCl) and 0.392 V (vs. Ag/AgCl), respectively, which is clearly more anodic (positive) compared to that required for the oxidation of AA onto either unmodified N-MWCNTs (0.017 V vs. Ag/AgCl) or N-MWCNTs/MNPs (in the range from −0.021 to 0.017 V vs. Ag/AgCl) (Table 9). These findings are in absolute accordance with the literature reports that the direct electrochemical oxidation of AA on conventional electrodes requires higher potential than the expected oxidation potential of AA, namely it needs the so-called overpotential. For instance, the equilibrium potential of oxidation of AA lies at about −0.185 V vs. SCE [259], and according to literature, the oxidation of AA on either GC or Pt electrodes requires potentials of about 0.400 and 0.600 V vs. SCE, respectively [260].

It is noticeable that on novel either unmodified N-MWCNTs or modified N-MWCNTs/MNPs films the oxidation overpotential of AA decreases significantly from that required on GC and Pt electrodes. As a result, on GC and Pt electrodes the oxidation peak of AA overlaps with the oxidation peak of DA that appears in the same potential region (~0.270 V vs. Ag/AgCl), and thus, a significant interference of AA in electrochemical detection of DA (and the inverse, interference of DA in analysis of AA) occurs on these particular electrodes. The CVs recorded for AA, DA, and UA ternary mixture on GC electrode (Fig.68a) reveal two separated anodic peaks that correspond to the oxidations of both AA and DA (first overlapped oxidation wave at about 0.264 V vs. Ag/AgCl) and the oxidation of UA (second single oxidation wave at about 0.532 V vs. Ag/AgCl). Similarly, on Pt electrode two anodic waves that lie at about 0.266 V (vs. Ag/AgCl) (overlapped oxidation wave of AA and DA) and 0.610 V (vs. Ag/AgCl) (oxidation wave of UA) can be clearly seen in Fig.68b.

In contrast to GC and Pt conventional electrodes, the electrocatalytic activity of unmodified N-MWCNTs and N-MWCNTs/MNPs (M: Rh, Pd, Ir, Pt, Au) composite films towards simultaneous oxidation of AA, DA, and UA is significantly more enhanced and all three analytes can be simultaneously electrochemically determined since their oxidation waves are well separated and do not overlap each other.

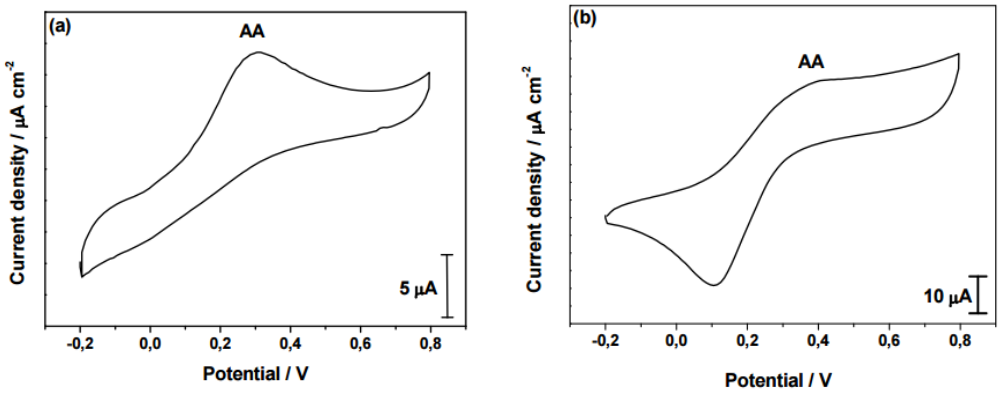

Fig. 67 CVs recorded for AA (0.5 mM) in phosphate buffer solution (pH 7.0) at the scan rate of 0.02 $V.s^{-1}$ on **(a)** GC and **(b)** Pt electrodes.

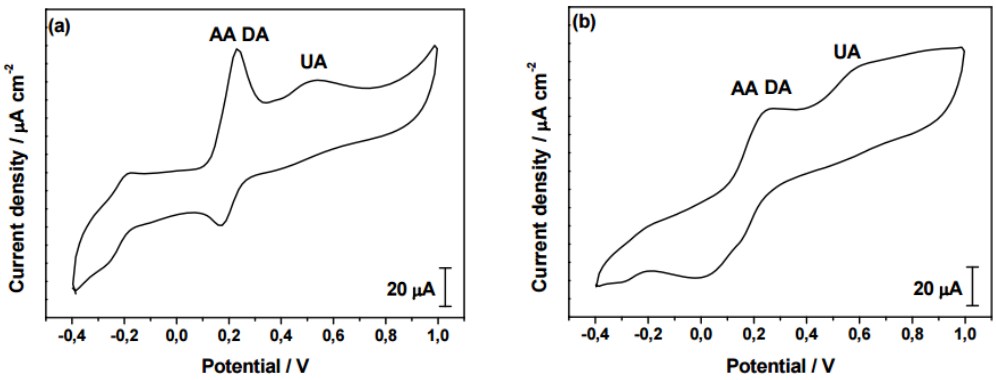

Fig. 68 CVs recorded for AA, DA, and UA ternary mixture (1:1:1; 0.5 mM) in phosphate buffer solution (pH 7.0) at the scan rate of 0.02 $V.s^{-1}$ on **(a)** GC and **(b)** Pt electrodes.

For comparison reasons, the detection limits obtained in the present work for N-MWCNTs and N-MWCNTs/MNPs towards simultaneous oxidation of AA, DA, and UA are compared with those reported in literature for other novel electrode materials in Table 11.

Table 11 Comparison of lower limits of detection (*LOD*) estimated at signal-to-noise ratio of 3 (*S/N=3*) for N-MWCNTs, N-MWCNTs/RhNPs, N-MWCNTs/PdNPs, N-MWCNTs/IrNPs, N-MWCNTs/PtNPs, and N-MWCNTs/AuNPs films towards simultaneous oxidation of AA, DA, and UA (PBS, pH 7.0) with literature values.

Electrode Material	***LOD* / μM**			
	AA	**DA**	**UA**	**Ref**
N-MWCNTs	8.7	1.4	5.9	This work
N-MWCNTs/RhNPs	7.9	1.1	4.1	This work
N-MWCNTs/PdNPs	6.8	0.8	3.6	This work
N-MWCNTs/IrNPs	6.1	0.7	3.1	This work
N-MWCNTs/PtNPs	3.1	0.6	2.1	This work
N-MWCNTs/AuNPs	0.9	0.3	0.4	This work
GCE/RGO[(a)]	0.7	0.1	1.0	[261]
SPGNE[(b)]	0.95	0.12	0.20	[262]
GCE/MWCNTs/PtNPs[(c)]	20	0.048	0.35	[263]
GCE/AgNPs/PPy[(d)]	1.8	0.1	0.5	[264]
GCE/GN/PtNPs[(e)]	7.4	1.2	1.4	[265]
GCE/MWCNTs/SDS[(f)]	3.0	0.01	0.04	[266]
GCE/ATD[(g)]	2.01	0.33	0.19	[267]
GCE/HCNTs[(h)]	0.92	0.80	1.5	[268]
GCE/Ch/GR[(i)]	50	1.0	2.0	[269]
GP/MWCNTs/AuNC[(j)]	40	0.67	0.23	[270]
GCE/PABA[(k)]	5.0	1.0	0.5	[271]

[(a)]Glassy carbon electrode modified with reduced graphene oxide [261]

[(b)]Screen-printed graphene electrode [262]

[(c)]Glassy carbon electrode modified with multi-walled carbon nanotubes and platinum nanoparticles [263]

[(d)]Glassy carbon electrode modified with silver nanoparticles and polypyrrole nanofibers [264]

[(e)]Glassy carbon electrode modified with graphene and platinum nanoparticles [265]

[(f)]Glassy carbon electrode modified with sodium dodecyl sulfate and multi-walled carbon nanotubes [266]

[(g)]Glassy carbon electrode modified with polymerized 2-amino-1,3,4- thiadiazole [267]

[(h)]Glassy carbon electrode modified with helical carbon nanotubes [268]

[(i)]Glassy carbon electrode modified with chitosan and graphene [269]

[(j)]Graphene-multi-walled carbon nanotubes-gold nanocluster composite film [270]

[(k)]Glassy carbon electrode modified with polymerized 4-aminobutyric acid [271]

In general, this comparison exhibits that the detection capability of N-MWCNTs/MNPs appears to be significantly greater compared to other composite films reported in literature. For instance, the detection limits of glassy carbon electrode modified with PtNPs, AuNPs, and 1-cysteine towards simultaneous analysis of AA (103 μM), DA (24 μM), and UA (21 μM) reported by Thiagarajan and Chen [272] seem to be significantly poorer compared to those obtained on our N-MWCNTs/MNPs (M: Rh, Pd, Ir, Pt, Au) composite films.

In addition, the detection limit of composite film consisting of phosphorylated zirconia-silica mixed oxide particles modified with methylene blue towards oxidation of AA (8.3 μM), DA (1.7 μM), and UA (3.7 μM) reported by Arguello *et al*.[273] seem to be poorer compared to those measured on N-MWCNTs/MNPs (M: Rh, Pd, Ir, Pt, Au) composite films.

4.2.6 Stability study of some metal nanoparticles on N-MWCNTs

To evaluate the stability of the metallic nanoparticles on the N-MWCNTs wafers, four different type of nanoparticles RhNPs, PdNPs, PtNPs, and AuNPs possessing diameter 2.7, 2.6, 2.7, and 14 nm, respectively were used to modify four N-MWCNTs films, further denoted as N-MWCNTs/MNPs (M: Rh, Pd, Pt, Au). The electrochemical responses of composite films towards constant concentration (1.0 mM) of $[Fe(CN)_6]^{3-/4-}$ in KCl solution (1.0 M) were investigated using CV technique (Fig.69). The measurements were repeated for each type of modified electrode several times (five times) in four months by using the same conditions. It must be mentioned that the composite films used as working electrode were washed with distilled water and left to dry in the room temperature and afterwards were used again for the next measurement.

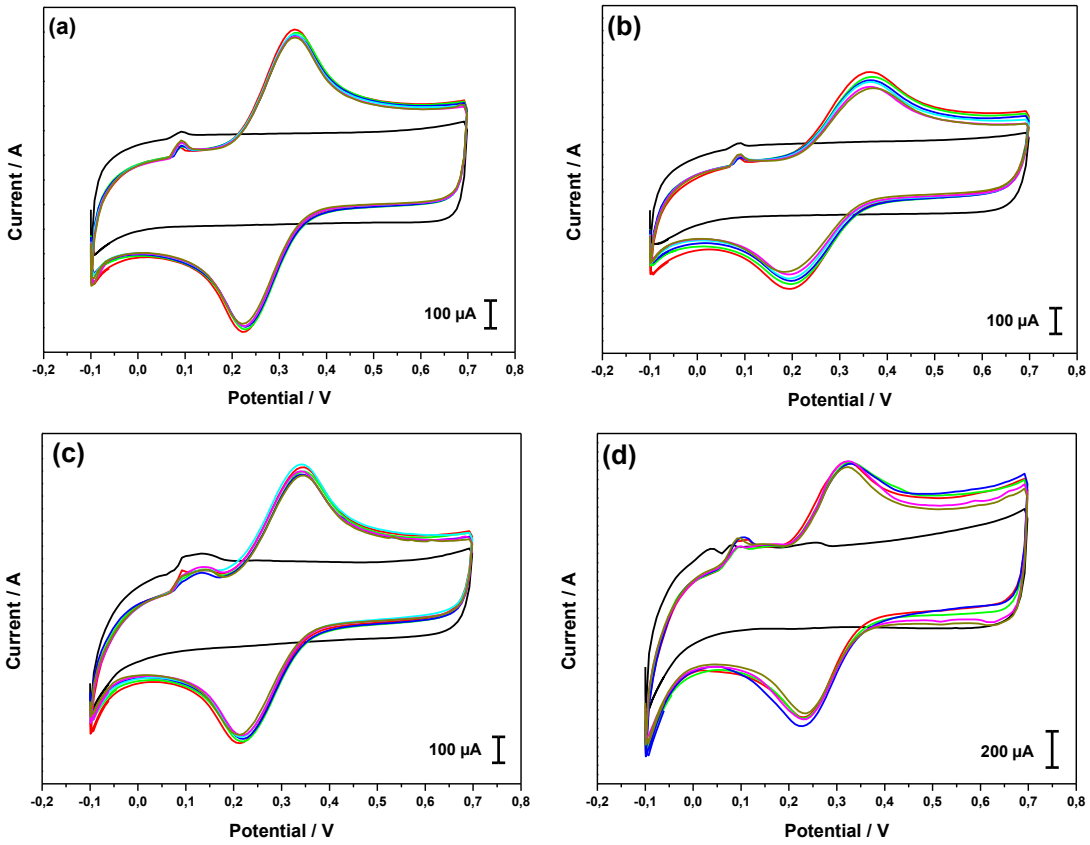

Fig. 69 CVs recorded for 1.0 mM $[Fe(CN)_6]^{3-/4-}$ (1.0 M KCl) on N-MWCNTs modified with (a) RhNPs (b) PdNPs (c) PtNPs (d) AuNPs at the scan rate of 0.05 V. s^{-1} in four months.

As it can be seen in Fig.69, symmetric CVs curves represented a pair of reversible redox peaks (oxidation and reduction peaks of studied redox system) appears to be at the same potential. Furthermore, the anodic and cathodic current responses of redox system tend to decrease with repeating the experiment (Fig.70). The relative

standard deviation for repeated five measurements recorded on N-MWCNTs/MNPs films toward 1.0 mM $[Fe(CN)_6]^{3-/4-}$ (1.0 M KCl) is calculated to be 2.81, 6.09, 3.81, and 1.79 % for N-MWCNTs/RhNPs, N-MWCNTs/PdNPs, N-MWCNTs/PtNPs, and N-MWCNTs/ AuNPs, respectively. It can be concluded that the N-MWCNTs/AuNPs film has the lowest standard deviation value, demonstrating that this particular film is quite stable.

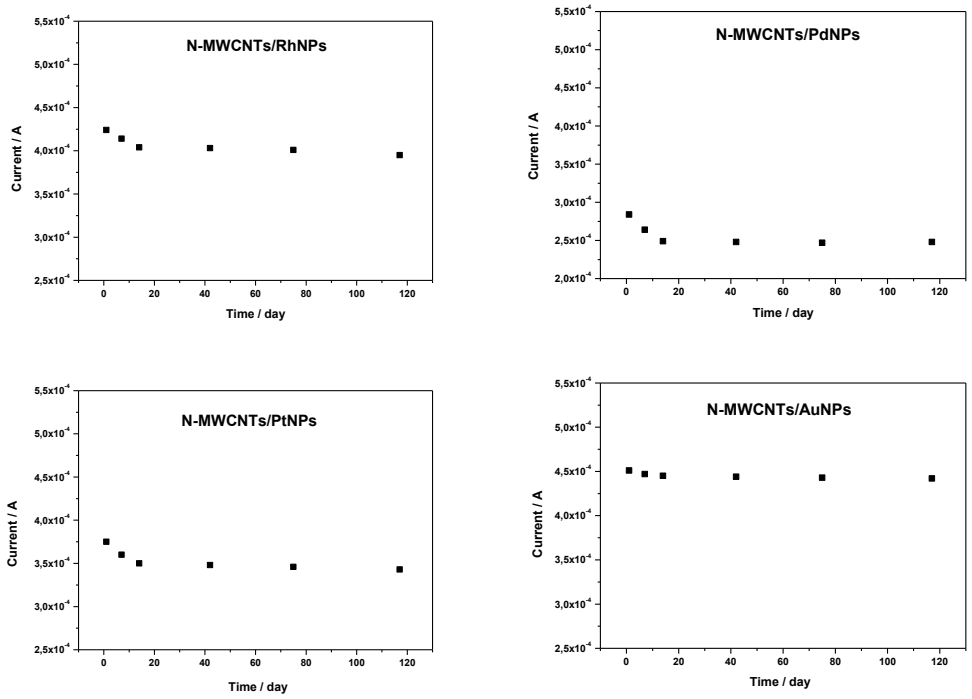

Fig. 70 Stability of the current response on modified N-MWCNTs/MNPs (M: Rh, Pd, Pt, Au) films.

It is interesting to mention that in this study, no peak related to redox system $[Fe(CN)_6]^{3-/4-}$ was found in background after using the same N-MWCNTs/MNPs film (Fig.71).

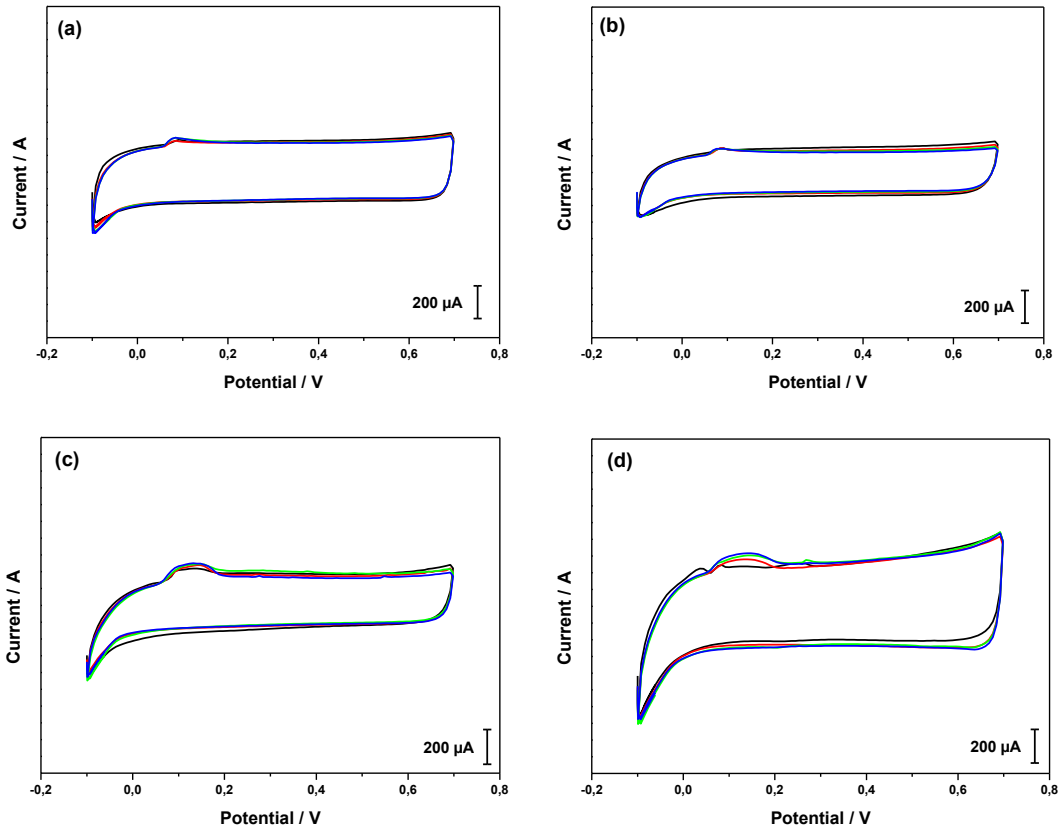

Fig. 71 Repeated CVs recorded in background (1.0 M KCl) on N-MWCNTs modified with (a) RhNPs (b) PdNPs (c) PtNPs (d) AuNPs at the scan rate of 0.05 V. s^{-1}.

In addition, to study the stability of nanoparticles on the surface of films, SEM images were taken for each modified wafer before the first measurement and after the last one, namely, after four months (Fig.72). The metal nanoparticles can be recognized in SEM micrographs as small bright dots deposited on the outer walls of carbon nanotubes. The SEM images reveal that the deposited metal nanoparticles are dispersed homogenously onto the surface of N-MWCNTs and that no agglomeration of nanoparticles takes place, expect the RhNPs, where some agglomeration of RhNPs on the carbon nanotubes can be seen (Fig.72b). It must be reported that it was quite difficult to take a SEM image for all wafers at the same position that was done before their application.

Generally, the structure of N-MWCNTs/MNPs did not change at all, namely, the structure of carbon nanotubes remains unaffected and some nanoparticles can be recognized. It is interesting to mention that the distribution of AuNPs on the N-MWCNTs is still homogenous after four months. The findings reveal strong evidence that the more stable nanoparticles are AuNPs.

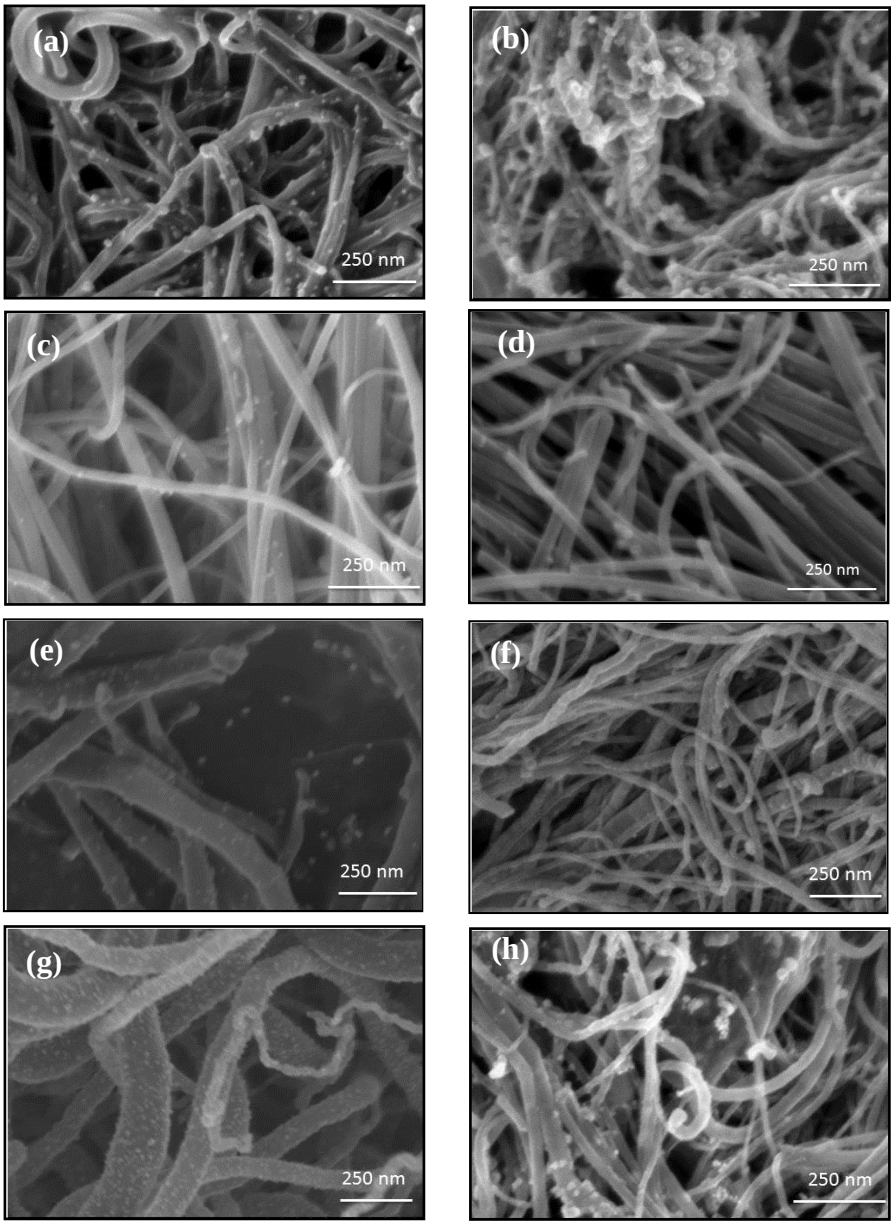

Fig. 72 SEM micrographs taken for (a,b) N-MWCNTs/RhNPs, (c,d) N-MWCNTs/PdNPs, (e,f) N-MWCNTs/PtNPs, and (g,h) N-MWCNTs/AuNPs films before use (left), and after their use for four months (right).

The modified films were further analyzed by means of EDX analysis in order to get information about the elemental composition of the surface. It should be noticed that EDX spectrum is better to be recorded for large surface area of the sample for preferable representation, in other words, lower errors. The EDX spectra of N-MWCNTs/MNPs films demonstrate that the main elements present within the inspection field are carbon, iron and metallic nanoparticles. The carbon comes from the CNT; iron results from rest of the catalyst nanoparticles (embedded in the tubes) and the most important the metallic nanoparticles that remain on the surface of CNTs even after using of the modified films several

times for analysis. A typical EDX spectrum is displayed as a plot of x-ray counts vs. energy (in keV) (Energy peaks correspond to the elements in the sample) (Fig.73).

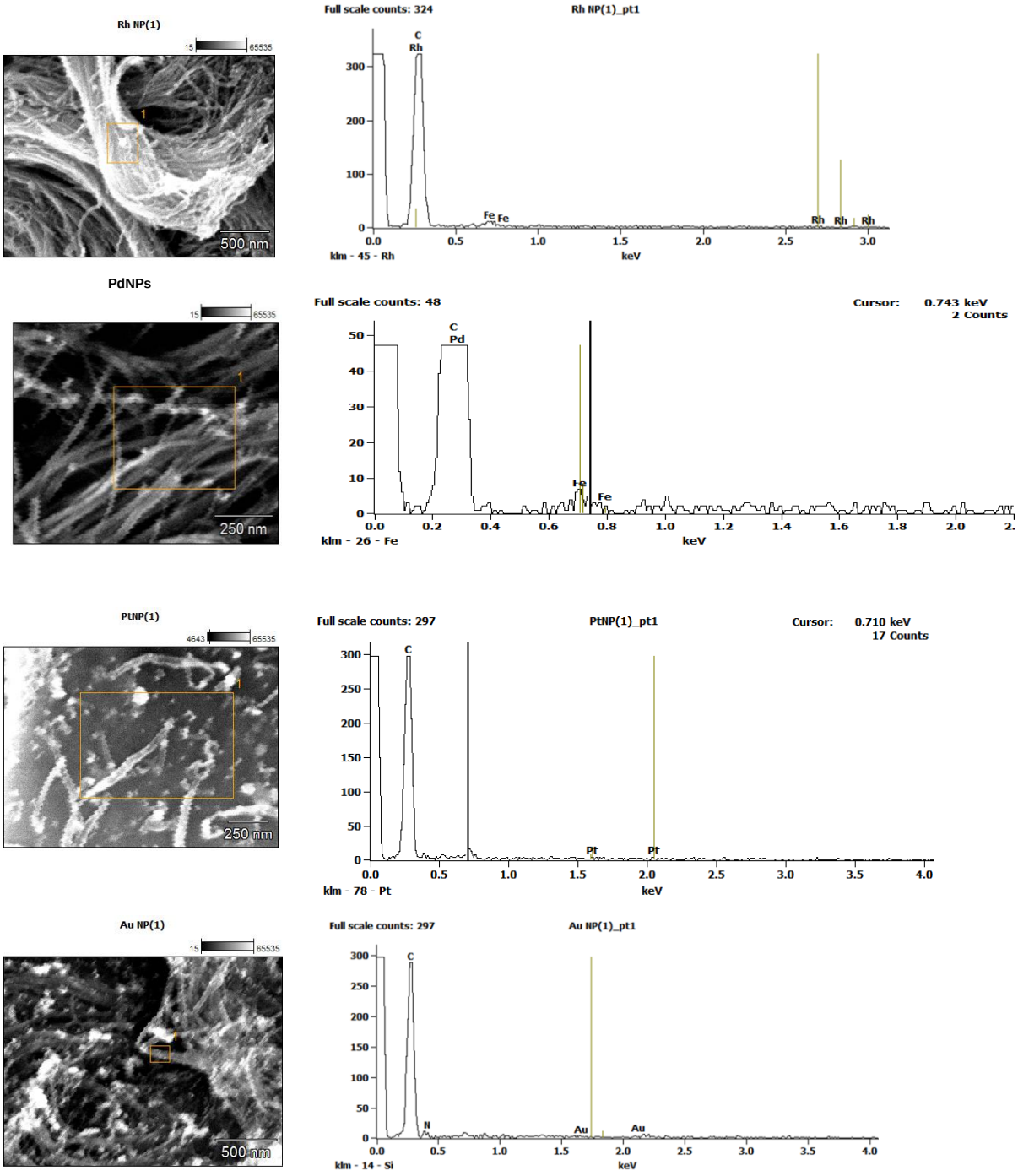

Fig. 73 Energy dispersive X-ray (EDX) spectra of the composite N-MWCNT/MNPs (M: Rh, Pd, Pt and Au), respectively.

These results show that the modified electrode possessed excellent stability, indicating its interesting electrochemical performance.

It must be noted that no detachment of film's contacting occurred during the measurement. In addition, the electrodes were quite stable and remained in very good state after the experiments. The results revealed that the stability of the proposed sensors is acceptable.

4.2.7 Dilution of AuNPs solution

In order to study the effect of AuNPs concentration on the electrocatalytic activity of carbon nanotubes, the stock solution of AuNPs (**2.33×10^{12})** particles/ml was diluted with double distilled water according to the following AuNPs: H_2O ratio of 1:1, 1:10, 1:100, and 1:300.

The same modification procedure was applied to decorate the N-MWCNT films with AuNPs. Namely, N-MWCNTs wafers were modified by using AuNPs solution with various dilution ratios (1:1, 1:10, 1:100, 1:300, and 1:1000).

As was expected, the SEM micrographs taken for N-MWCNTs/AuNPs reveal that the deposited nanoparticles are still dispersed homogenously onto the surface and the number of AuNPs is decreased in the following order: 1:1 > 1:10 > 1:100 > 1:300 (Fig.74).

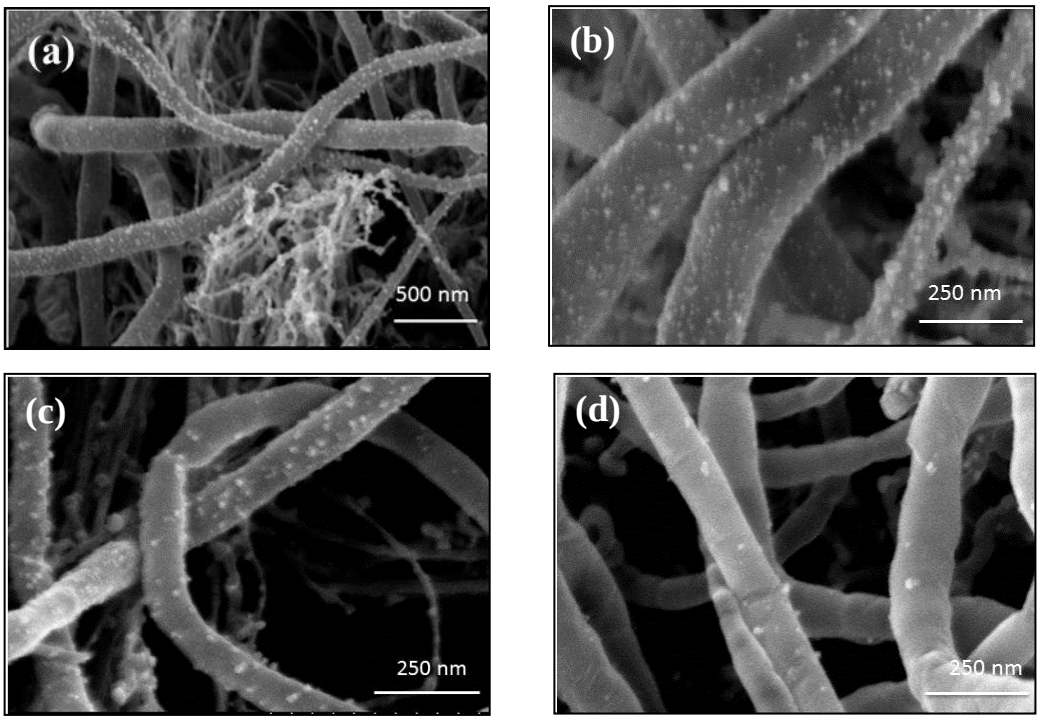

Fig.74 Representative SEM micrographs of N-MWCNTs/AuNPs 1:1 (a), N-MWCNTs/AuNPs 1:10 (b), N-MWCNTs/AuNPs 1:100 (c), N-MWCNTs/AuNPs 1:300 (d).

The images demonstrate that the AuNPs still stable and visible up to dilution ratio of about 1:300. It must be mentioned that the dilution ratio of 1:1000 was also investigated and no AuNPs were seen in SEM image. In the next step, CVs of standard redox system $[Fe(CN)_6]^{3-/4-}$ in large concentration range (0.099–0.990 mM) in potassium chloride solution (1.0 M) on the modified N-MWCNTs/AuNPs films (different dilution ratio) were recorded. For comparison reason, the CVs curves on N-MWCNTs/AuNPs without dilution of AuNPs solution were also recorded (Fig.75).

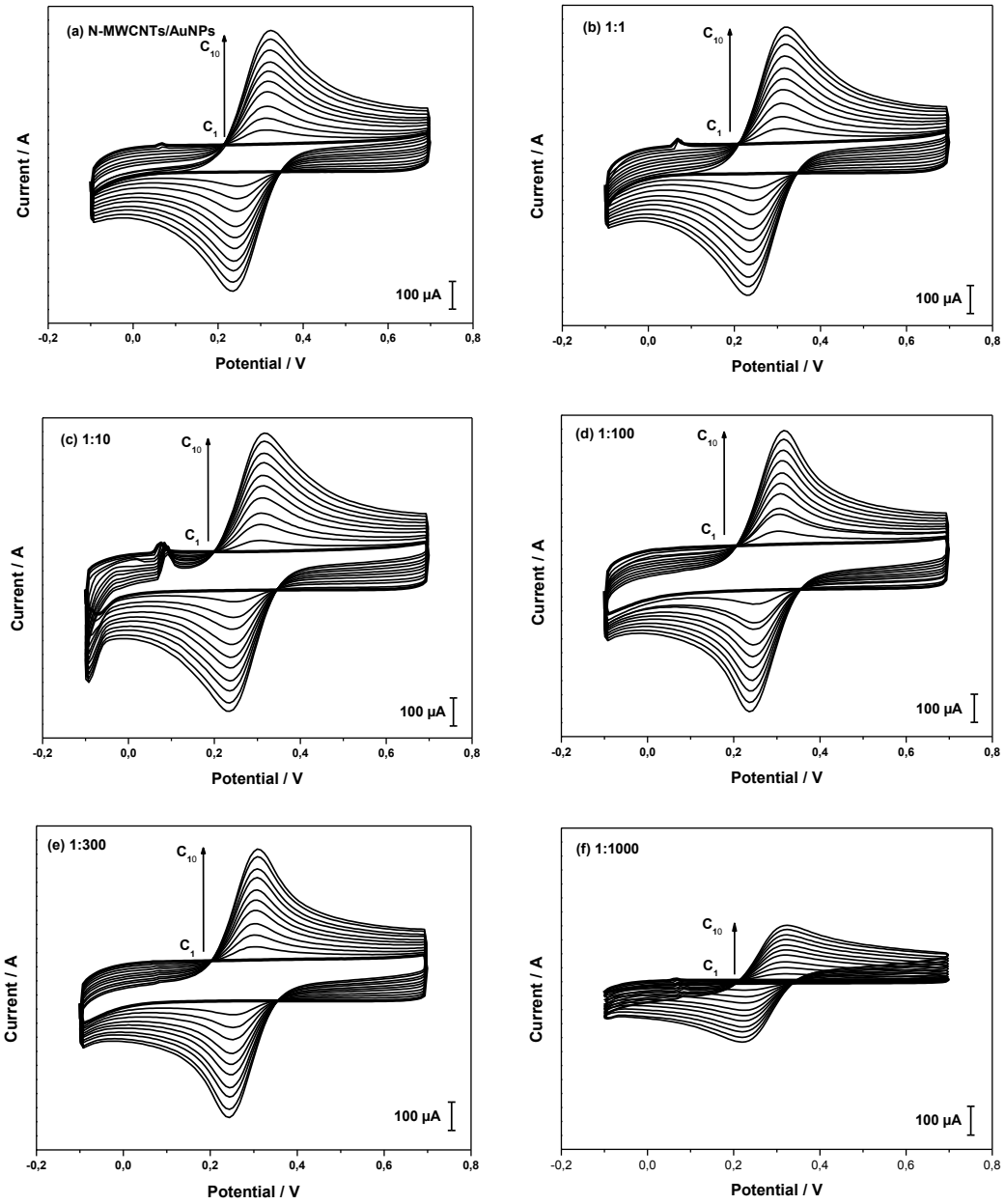

Fig. 75 Representative CVs recorded for $[Fe(CN)6]^{3-/4-}$ (1.0 M KCl) in the range of 0.099- 0.990 mM) on modified N-MWCNTs/AuNPs films without dilution (a), and with dilution of 1:1 (b), 1:10 (c), 1:100 (d), 1:300 (e), 1:1000 (f), at the scan rate 0.02 $V.s^{-1}$

As it can be seen, symmetrical CVs were obtained on all modified films, consisting of reversible oxidation and reduction peaks. The findings demonstrate clearly that no significant change in the current response and peak potential difference can be seen on all N-MWCNTs modified with AuNPs (1:1, 1:10, 1:100, 1:300). Anyhow, it is remarkable that in case of N-MWCNTs/AuNPs (dilution ratio 1:1000) an obvious decrease of current response (about 57%) occurs.

The findings reveal that the potential peak separation ΔE_p for the standard redox system on the modified N-MWCNTs/AuNPs films is unaffected up to dilution ratio 1:300 and has the value of about 0.06 V. It was observed that the value of ΔE_p on N-MWCNTs/AuNPs modified with AuNPs (dilution ratio 1:1000) was about 0.08 V, namely, about 20 mV higher compared to that obtained on N-MWCNTs/AuNPs films modified with different dilution ratio of AuNPs (1:1, 1:10, 1:100, 1:300). The active surface area for N-MWCNTs/AuNPs films towards $[Fe(CN)_6]^{3-/4-}$ redox system were also estimated and found to be decreased with the following order: AuNPs 1:1 < AuNPs 1:10 < AuNPs 1:100 < AuNPs 1:300 < AuNPs 1:1000 The extracted data are presented in Table 12.

Besides, the EIS spectra were recorded in the whole investigated concentration range of 0.099–0.990 mM to estimate the barrier for electron transfer occurring on modified films. The measurements were recorded in the frequency range from 0.1 Hz to 100 kHz at $E_{½}$ potential of the studied redox system $[Fe(CN)_6]^{3-/4-}$ (Fig.76).

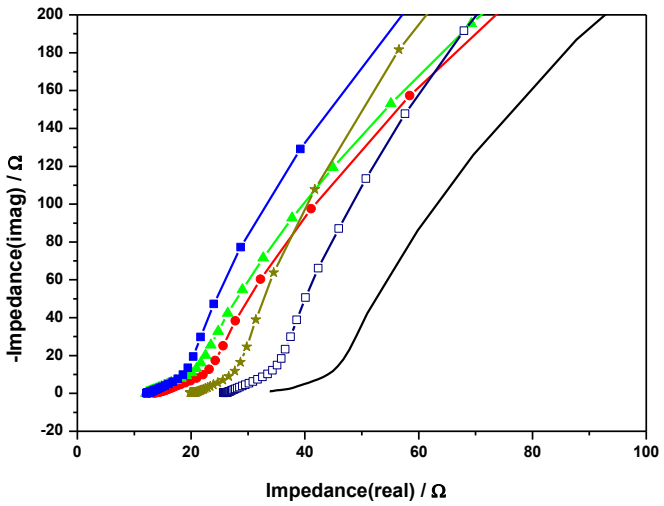

Fig. 76 Nyquist plots for C= 0.099 mM $[Fe(CN)_6]^{3-/4-}$ on N-MWCNTs and N-MWCNTs modified with AuNPs with different ratio of dilution. The symbols are denoted as follows: (straight line) N-MWCNTs, (filled circle) N-MWCNTs/AuNPs, (filled upward triangle) N-MWCNTs/AuNPs (1:1), (filled square) N-MWCNTs/AuNPs (1:10), (star) N-MWCNTs/AuNPs (1:100), (open square) N-MWCNTs/AuNPs (1:300).

As it can be seen from EIS spectra, the spectrum consists of two parts, the first part is a small depressed semicircle at high frequency area corresponding to electron transfer-limited process, and the second part is a straight line at low frequency area representing the diffusion-limited electron transfer process. The linear part prevails over the semicircle demonstrating that the electron transfer process on this film is quite fast.

The EIS results were simulated using the Randles circuit and they indicate that the charge transfer resistance R_{ct} increases slightly in this order: N-MWCNTs/AuNPs (without dilution) < AuNPs 1:1 < AuNPs 1:10 < AuNPs 1:100 < AuNPs 1:300. The estimated values of R_{ct} are included in Table 12.

A small shift in the EIS spectra to low frequency area (to the right) with the dilution of AuNPs can be seen. However, this observation can be explained with the decrease of the number of AuNPs, and thus the decrease of the catalytic activity of AuNPs leading to diminishing the electron transfer kinetic

Table 12 The electrochemical parameters extracted from recorded CVs determined for $[Fe(CN)6]^{3-/4-}$ (1.0 M KCl) on N-MWCNTs/AuNPs films (different dilution ratio).

Parameter	Stock solution	1:1	1:10	1:100	1:300	1:1000
ΔE_p (V)	0.06	0.06	0.06	0.06	0.059	0.08
A (cm^2)	4.46	4.52	4.41	4.48	4.18	2.08
R_{ct} (Ω)	2	4.2	5	7.2	9.2	30

4.2.8 Repeatability and reproducibility of N-MWCNTs/AuNPs

The repeatability and reproducibility of the modified electrode N-MWCNTs/AuNPs for the determination of dopamine (DA) were studied. The repeatability was evaluated by performing ten repeat determinations with same concentration of DA solution (1 mM) in PBS (pH 7.0) for a period of two weeks. The electrochemical response was measured daily by means of cyclic voltammetry. To study the repeatability, two electrodes were investigated. The first one was left at room temperature (further denoted as E_1), and the second one was stored in PBS (pH 7.0) at 4°C (denoted as E_2). The CVs recorded on E_1, E_2 are shown in Fig.77.

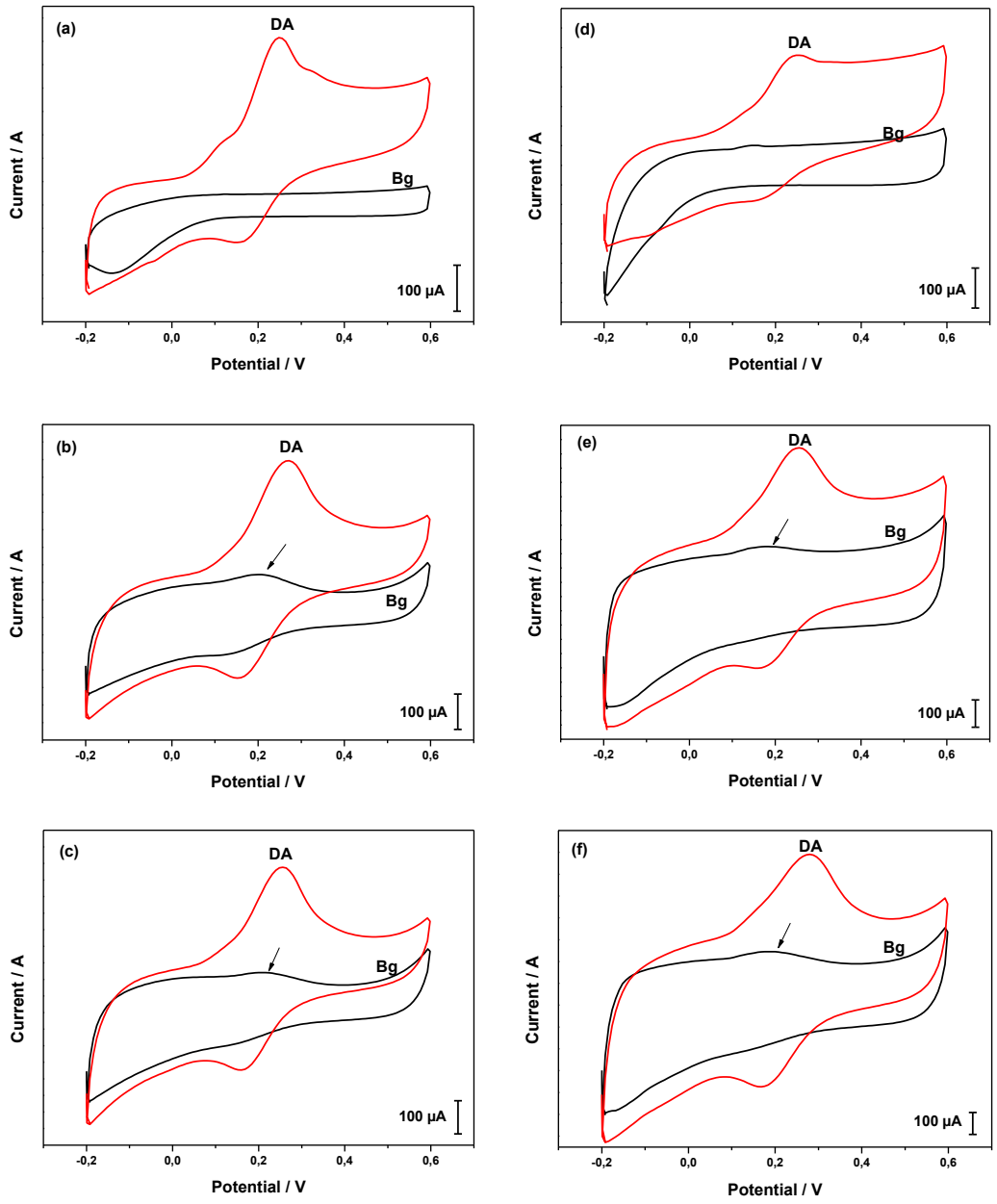

Fig. 77 CVs recorded for DA (1 mM) on N-MWCNTs/AuNPs (E_1) at (a) first day, (b) fifth day, and (c) tenth day. The same measurements recorded on (E_2), at (d) first day, (e) fifth day, and (f) tenth day.

It must be noted that the peak potentials of studied system were stable on both electrodes E_1, E_2. On E_1, the current response of DA was stable after three continuous measurements and after that an increase in the current peak was observed. Furthermore, the current response of electrode E_2 towards DA was increased. Specifically, compared to its initial current response, the modified electrode continued to exhibit a relatively high current even after ten

measurements (done with 2 weeks) (see Fig.78). This can be explained by the adsorption of dopamine (deposition of dopamine and other by-products) on the surface of synthesized films.

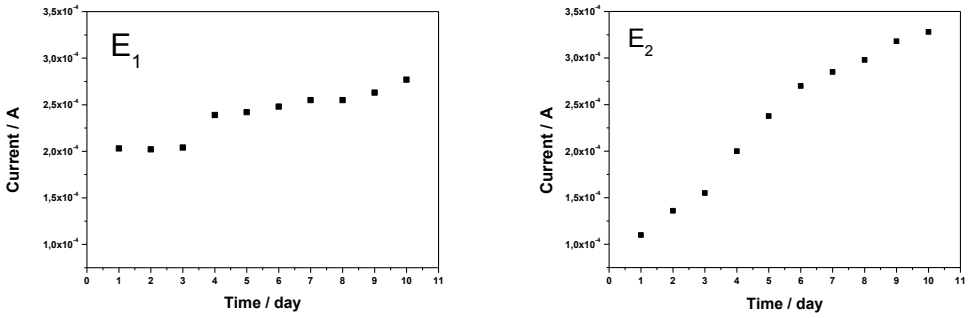

Fig. 78 The current response of E_1, E_2 toward DA (1 mM) in ten days.

Furthermore, SEM images of films were taken after their use for two weeks to check the morphology of films and to get information about the effect of the store conditions on the structure.

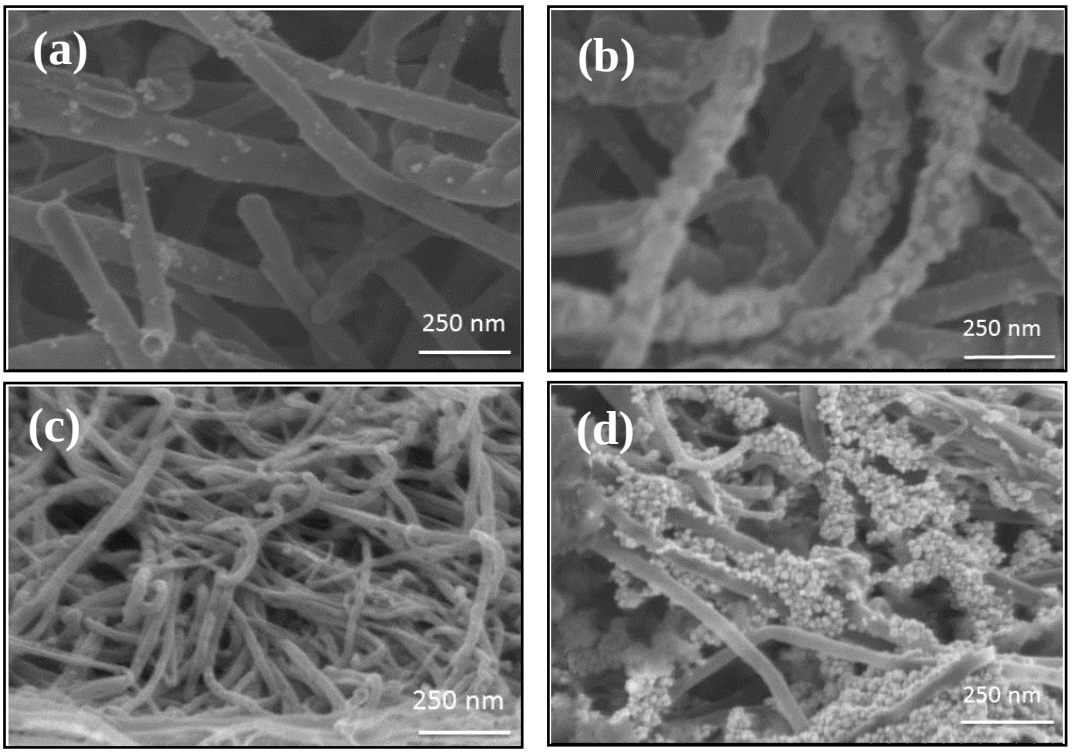

Fig. 79 SEM images after two weeks measurements of DA on N-MWCNTs/AuNPs stored at room temperature (a, b), on N-MWCNTs/AuNPs stored in (PBS, pH 7.0) at 4 ˚C (c, d).

In both stored conditions, the SEM images demonstrate the presence of some agglomeration on the tubes. This can be attributed to the deposition of DA and some by-products associated from the DA oxidation on the surface of films

(Fig.79b,d). The presence of one peak in the background of recorded CVs can be explained with this reason (Fig.77). It must be reported that although the electrode was washed with distilled water, but the removing of DA was not possible because of porous structure of film. However, the AuNPs are stable and homogeneous distributed on the tubes as it can be seen in Fig.79a.

The reproducibility of method was studied by measuring the electrochemical response of three different N-MWCNTs/AuNPs films towards oxidation of (1 mM) DA in (PBS, pH 7.0). All N-MWCNTs films were fabricated with the same procedure by means of (CVD) and modified with AuNPs (12.5 nm). The extracted results are presented in Table 13.

Table 13 parameters extracted from CVs on N-MWCNTs/AuNPs films

parameter	**N-MWCNTs/AuNPs-1**	**N-MWCNTs/AuNPs-2**	**N-MWCNTs/AuNPs-3**
ΔE_p (V)	0.08	0.075	0.085
I (µA)	115	120	85

The findings reveal that the reproducibility of the N-MWCNTs/AuNPs was acceptable.

4.3 Characterization of N-P-MWCNTs

4.3.1 Physical characterization of N-P-MWCNTs

4.3.1.1 Scanning electron microscopic analysis

In order to investigate the morphology of fabricated carbon nanotubes N-P-MWCNTs, SEM technique was used. Representative SEM images taken for the N-P-MWCNTs films synthesized with decomposition of 0.2, 0.4, 0.5, 0.6, 0.7, and 1 wt %. TPP are shown in Fig.80. As it can be seen in SEM images, the surface of films is quite homogeneous for the sample synthesized with decomposition of ACN, $FeCp_2$ and TPP (0.2 to 0.6 wt %) with a presence of some circular nodes in the tube structure. The morphology of the fabricated film starts to change with increasing the TPP content (from 0.7 up to 1 wt %. TPP). It will be like amorphous carbon and no aligned carbon nanotubes can be recognized in SEM image. It was also noticed that the length of carbon nanotubes decreased with increasing the phosphorus content from 0.2 to 1 wt %. TPP.

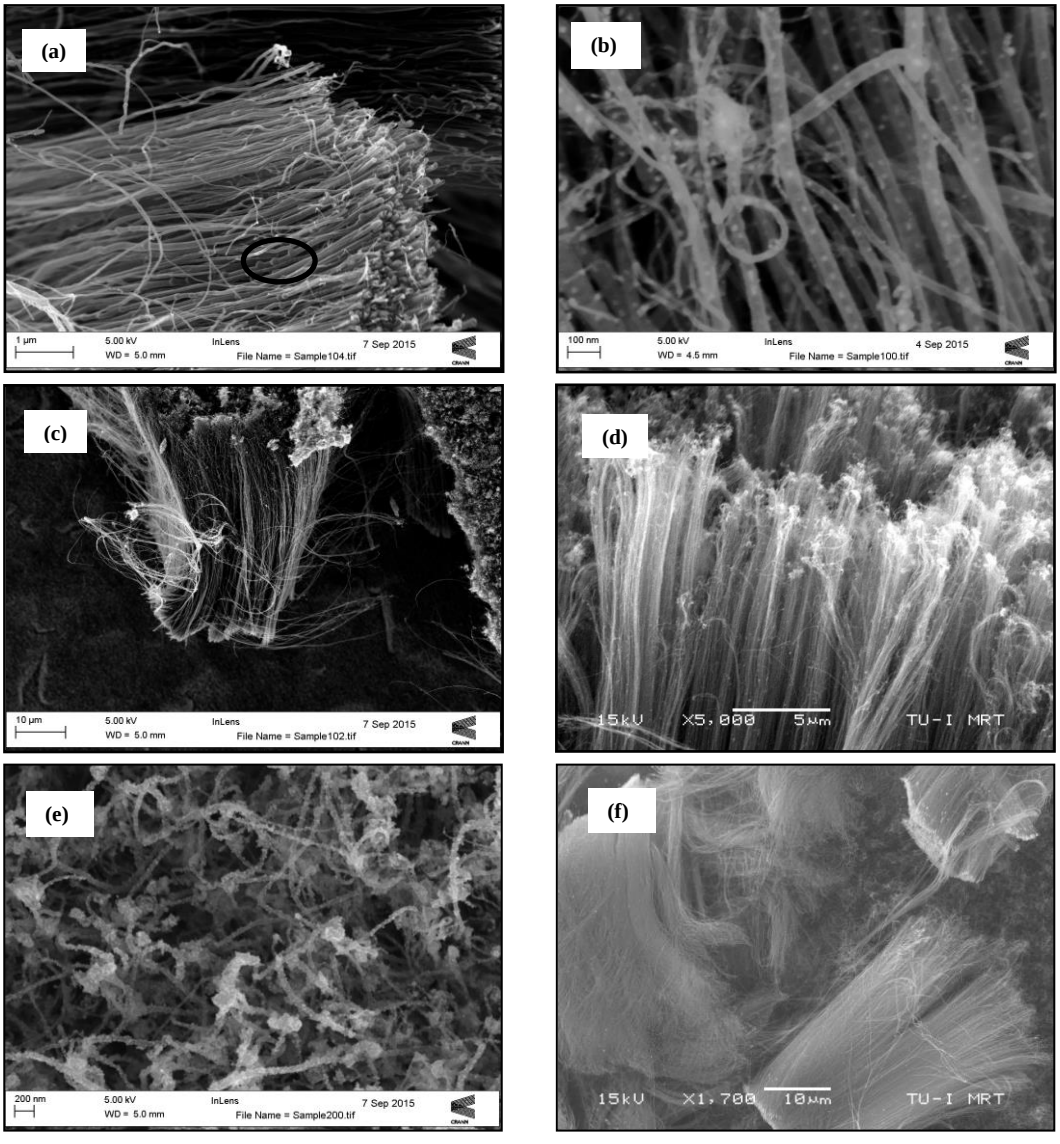

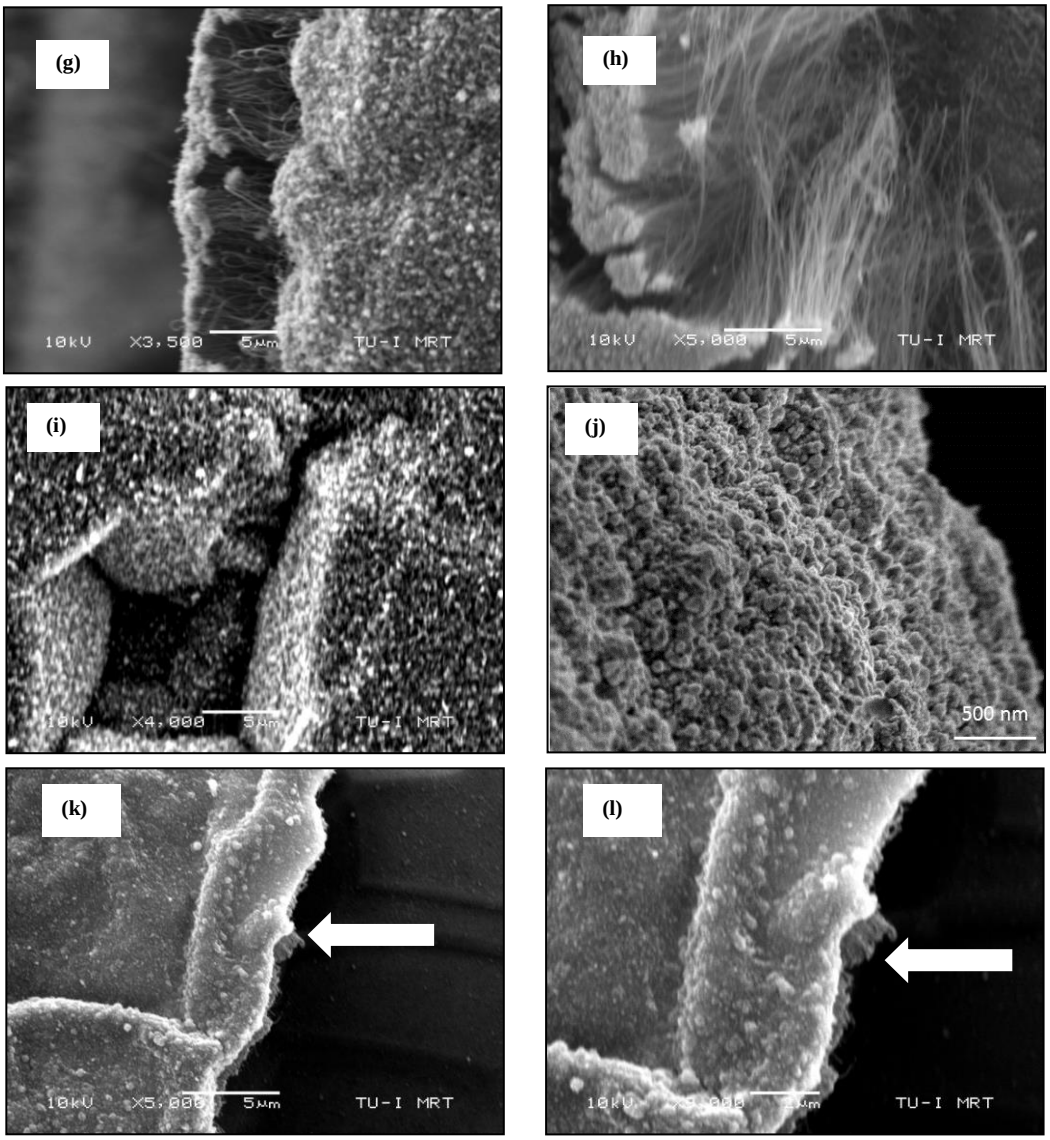

Fig. 80 SEM images of N-P-MWCNTs composite films fabricated with decomposition of 0.2 wt %. TPP (a-c), 0.4 wt %. TPP (d), 0.5 wt %. TPP (e, f), 0.6 wt %. TPP (g, h), 0.7 wt %. TPP (i), and 1 wt %. TPP (j, k, l).

4.3.1.2 Transmission electron microscopic analysis

TEM images taken of N-P-MWCNTs films fabricated with decomposition of (0.2 and 0.5 wt %. TPP) demonstrate that the carbon nanotubes are bamboo-shaped (Fig.81). Namely, the structure of pure N-MWCNTs does not change significantly with the phosphorus-doping. The catalyst nanoparticles (black capsules) were also seen inside the nanotubes.

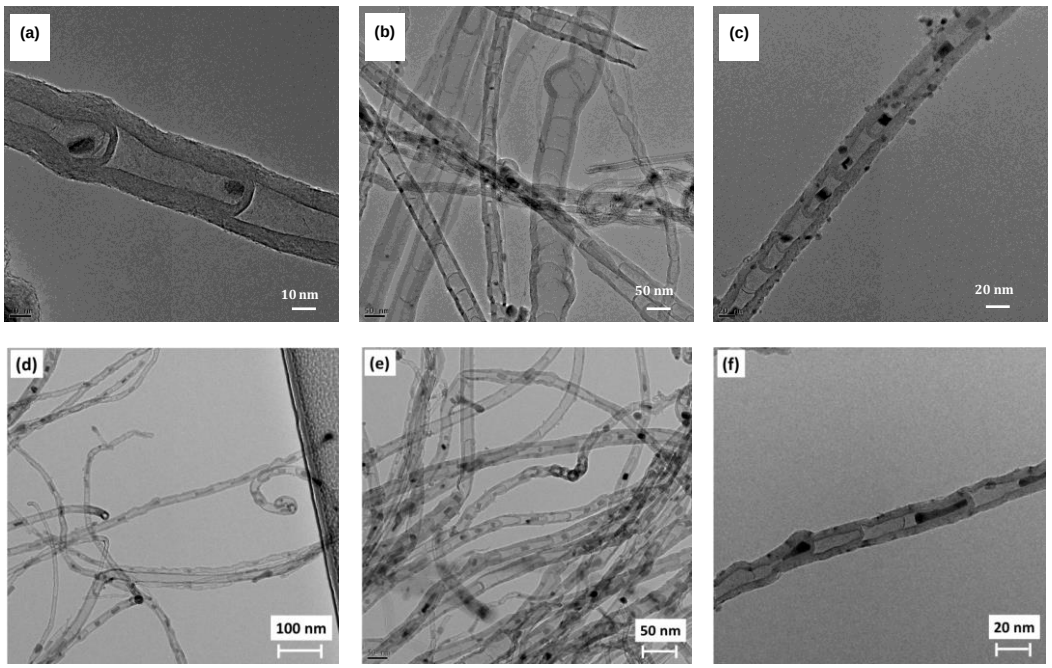

Fig. 81 TEM micrographs of N-P-MWCNTs composite film fabricated with decomposition of 0.2 wt %. TPP (a, b, c), and 0.5 wt %. TPP (d, e, f).

TEM/EDX analysis of N-P-MWCNTs confirms that the carbon nanotubes incorporate phosphorus into their structure (Fig.82).

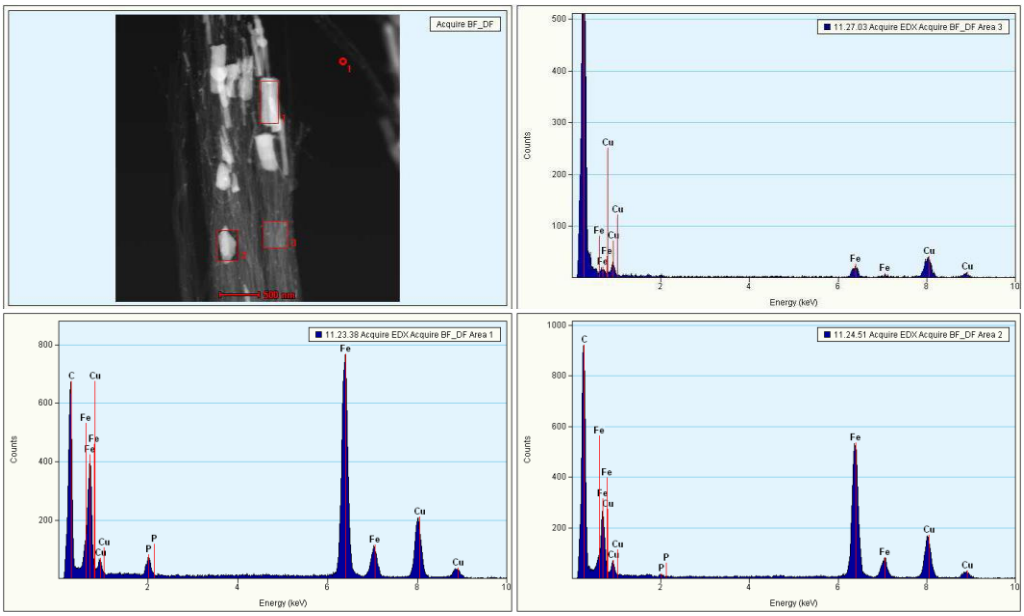

Fig. 82 Representative EDX spectra recorded for N-P-MWCNTs composite film.

It must be mentioned that the TEM image of the sample produced with greatest TPP content (0.7 wt %. TPP and 1 wt %. TPP) couldn't be measured. It's probably due to high amount of amorphous carbon that contains.

4.3.1.3 Raman spectroscopy

Raman spectra were recorded using a microscope-fitted Horiba Jobin Yvon HR800 Raman spectrometer that was calibrated using a Si substrate. The spectra were collected within the range of 1000-2000 cm^{-1} (scanning intervals of 1.66 cm^{-1}) with a slit and hole of 300 and 200 cm^{-1}, respectively. An air cooled CLDS point mode diode 532 nm laser was used and the radiation was limited to 10% to avoid damage of the carbon nanotubes samples. The spectra were averaged by 10 accumulations of 2 seconds each (using Lab Spec 6 software).

Raman spectroscopy studies were carried out for MWCNTs, N-P-MWCNTs (0.5 wt %. TPP), and N-MWCNTs. The Raman spectra of carbon nanotubes consist of two main bands, namely the so-called D-band (1336-1343 cm^{-1}) and the G-band (1567-1573 cm^{-1}), and their frequency is slightly affected by doping of nanotubes. As it well known the G-band corresponds to the high frequency E_{2g} first-order mode and can be attributed to opposing movement of two-neighboring carbon atoms in graphene sheet [274], while the D-band results from defects in curved graphene sheets, as well as from ends and finite size crystalline domains of carbon nanotubes [275].

The ratio of relative intensities of G- and D-bands (I_G/I_D) is a measure of degree of structural order. For carbon nanotubes with different surface modifications, the change in intensity ratio (I_G/I_D) can be attributed to the change in surface functionalities or local defects resulting from bond breakage between C–C bonds in nanotubes [276]. In the present work, the N-MWCNT films were found to exhibit smaller value of intensity ratio (I_G/I_D) compared to N-P-MWCNTs film, indicating greater degree of structural defects in N-MWCNTs. Namely, it was observed that the degree of defects increases with the following order: N-MWCNTs > N-P-MWCNTs > undoped MWCNTs (see Table 14). It is thus obvious that the enhanced electrochemical response of N-MWCNTs can be attributed to the greater degree of defects that these particular nanotubes possess.

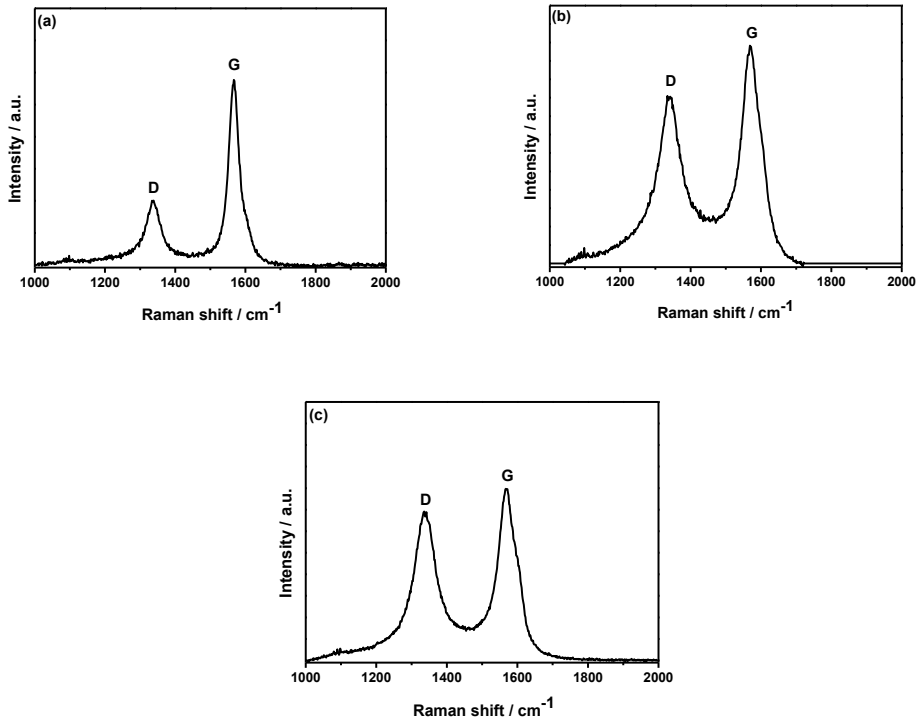

Fig. 83 Raman spectra recorded for (a) MWCNTs, (b) N-P-MWCNTs, and (c) N-MWCNTs composite films.

Table 14 Raman D-bands, G-bands, and intensity ratios of G- and D-bands (I_G /I_D) for undoped-MWCNTs, N-P-MWCNTs, and N-MWCNTs.

Composite film	**ν_D/cm^{-1}**	**ν_G/cm^{-1}**	**I_G /I_D**
MWCNTs	1336	1567	2.88
N-P-MWCNTs	1341	1571	1.30
N-MWCNTs	1339	1570	1.15

4.3.2 Electrochemical characterization of N-P-MWCNTs

4.3.2.1 Cyclic voltammetry

To study the effect of nitrogen-phosphorus doping on the electrocatalytic activity of carbon nanotube, the electrochemical response of N-MWCNTs and N-P-MWCNTs composite films toward $[Fe(CN)_6]^{3-/4-}$ in aqueous 1.0 M KCl solution was investigated.

The synthesized N-P-MWCNTs films were further denoted as N-P-MWCNTs-1, N-P-MWCNTs-2, N-P-MWCNTs-3, N-P-MWCNTs-4, and N-P-MWCNTs-5 according to the mass percent of TPP in ACN/TPP/$FeCp_2$ ternary mixture (Table 15).

Table 15 Nitrogen- and phosphor-source materials, catalyst, and volume of sprayed ACN/TPP/$FeCp_2$ ternary mixtures for the fabrication of novel N-MWCNTs and N-P-MWCNTs composite films.

Composite film	Carbon and nitrogen source	Carbon and phosphor source	Catalyst	Sprayed solution
N-MWCNTs	ACN	0.0 wt %. TPP	2 wt %. $FeCp_2$	3.0 ml
N-P-MWCNTs-1	ACN	0.2 wt %. TPP	2 wt %. $FeCp_2$	3.0 ml
N-P-MWCNTs-2	ACN	0.5 wt %. TPP	2 wt %. $FeCp_2$	3.0 ml
N-P-MWCNTs-3	ACN	0.6 wt %. TPP	2 wt %. $FeCp_2$	3.0 ml
N-P-MWCNTs-4	ACN	0.7 wt %. TPP	2 wt %. $FeCp_2$	3.0 ml
N-P-MWCNTs-5	ACN	1 wt %. TPP	2 wt %. $FeCp_2$	3.0 ml

CVs were recorded on the N-MWCNTs and various N-P-MWCNTs composite films for various concentrations of standard redox system in the range of (0.099-0.990 mM) at the scan rate of 0.02 $V.s^{-1}$ (Fig.84).

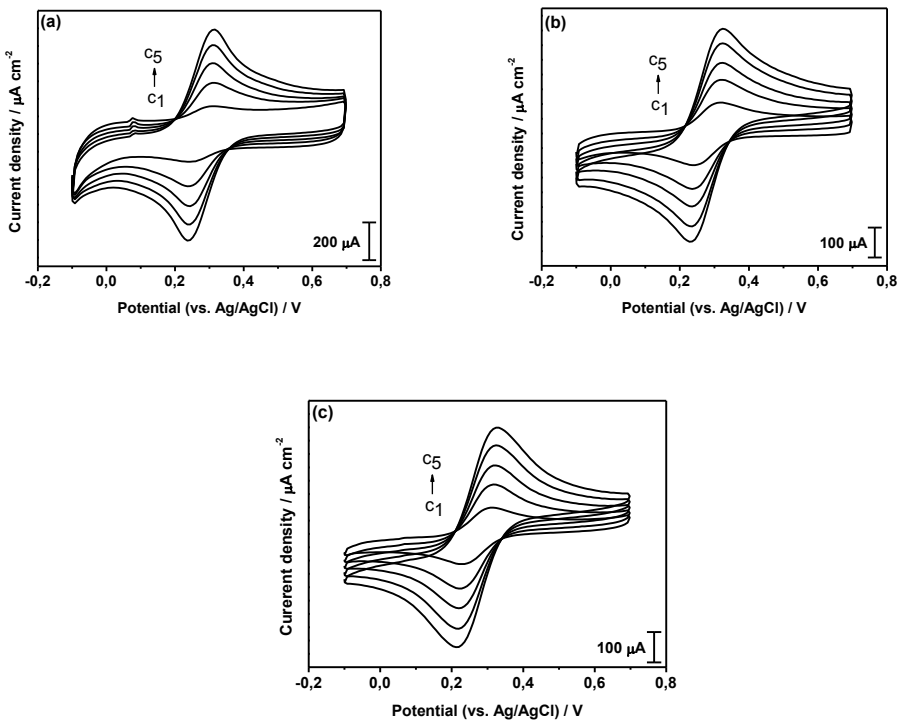

Fig. 84 CVs recorded for various concentrations of $[Fe(CN)_6]^{3-/4-}$ (1.0 M KCl) on **(a)** N-MWCNTs, **(b)** N-P-MWCNTs-3, and **(c)** N-P-MWCNTs-5 at 0.02 $V.s^{-1}$. The CVs (from inner to outer) correspond to concentrations: c_1=0.196 mM; c_2=0.415 mM; c_3=0.595 mM; c_4=0.797 mM; and c_5=0.990 mM.

The CVs curves demonstrated that the studied redox system exhibit a reversible behavior on both N-MWCNTs and N-P-MWCNTs films. Furthermore, the oxidation-reduction peak current ratio is equal to unity and it is independent of scan rate demonstrating that no parallel chemical reactions take place. The results indicate also the stability of oxidative and reductive peak currents for many cycles, confirming that no chemical reaction coupled to electron transfer process and that the charge transfer process is reversible. The half-wave potential for the redox system on the N-MWCNTs and N-P-MWCNTs was estimated to be similar within experimental error ($E_{1/2}$≈0.280 V vs. Ag/AgCl). The value of anodic and cathodic peak potential separation (ΔE_p) was also estimated to be in the range of 0.059-0.097 V. The lowest value of ΔE_p was measured on N-MWCNTs and the greatest one was obtained on N-P-MWCNTs fabricated by decomposing of 1% TPP. The results indicate that the ΔE_p increases with increase the wt %. of the TPP used in fabrication process demonstrating that the kinetic of redox system decreases with the increasing the composition of decomposed TPP used for the synthesis process in the various fabricated composite films Fig.86d.

The electrochemical response of N-MWCNTs and various N-P-MWCNTs films was plotted as oxidation peak current density *vs.* concentration of redox system and it appears to be linear in the studied range (0.099-0.990 mM) (Fig.85). From

this linear dependence the detection limit and the sensitivity of the fabricated films towards $[Fe(CN)_6]^{3-/4-}$ were estimated and presented in Table 15.

The extracted data confirms that the detection limit tends to increase, and thus, the sensitivity tends to decrease with increasing the concentration of decomposed TPP used for synthesis process. The variation of sensitivity and lower limit of detection with the wt % of decomposed TPP used for synthesis of nanotubes is presented graphically in Fig.86b and Fig.86c, respectively.

The findings demonstrate that the N-MWCNTs composite film has the lowest detection limit and thus the highest sensitivity. Furthermore, upon doping with phosphorus the sensitivity tends to decrease and the kinetic of electrochemical process decreases rapidly.

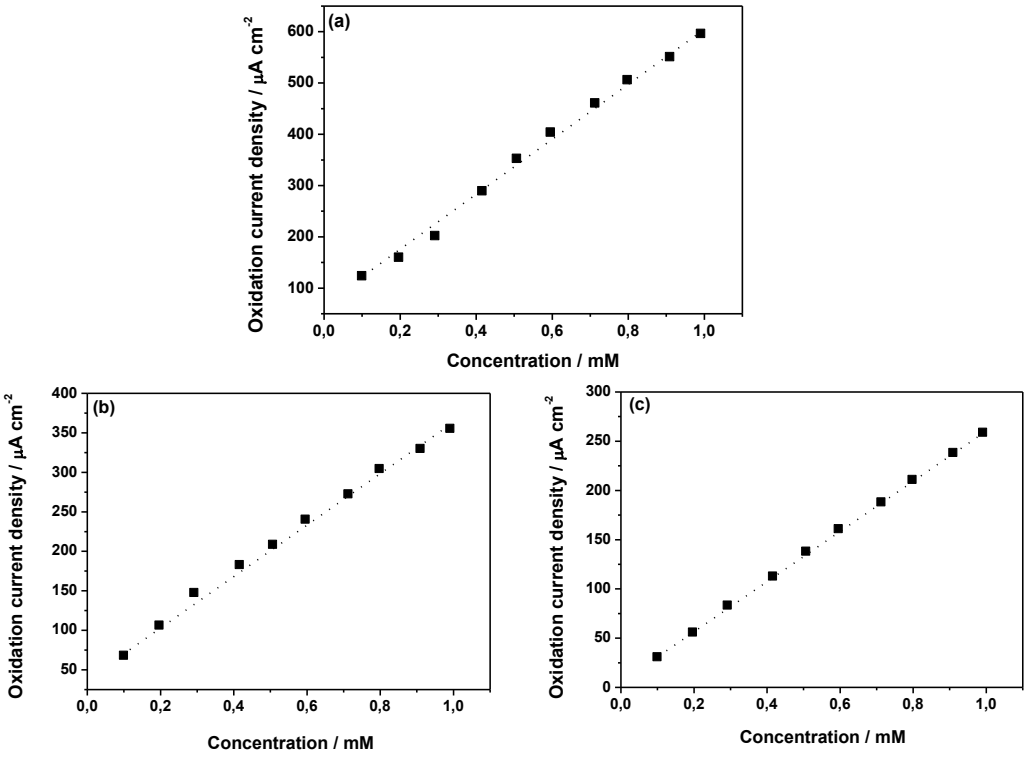

Fig. 85 Variation of oxidation peak current density with the concentration of $[Fe(CN)_6]^{3-/4-}$ (1.0 M KCl) observed on **(a)** N-MWCNTs, **(b)** N-P-MWCNTs-3, and **(c)** N-P-MWCNTs-5 composite films at the scan rate of 0.02 $V \cdot s^{-1}$.

As it was expected, the heterogeneous electron rate transfer constant (k_s) tends to decrease with the increase of wt %. of TPP. The k_s values were estimated for $[Fe(CN)_6]^{3-/4-}$ on the N-MWCNTs and N-P-MWCNTs composite films by means of electrochemical absolute rate relation to be in the range from 2×10^{-3} to 4.3×10^{-2} $cm.s^{-1}$ (Table 16). The findings indicate that the doping with phosphorus leads to

decrease of kinetic of electrochemical process occurring onto carbon nanotubes Fig.86a.

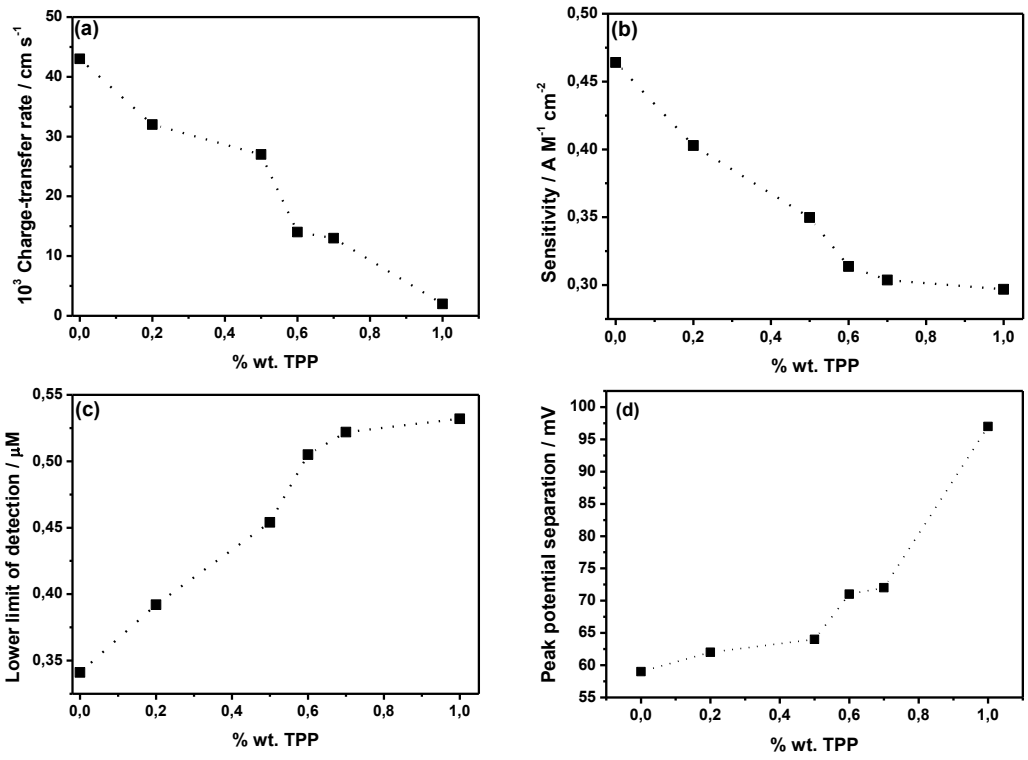

Fig. 86 Variation of **(a)** charge-transfer rate, **(b)** sensitivity, **(c)** lower limit of detection, and anodic and **(d)** cathodic peak potential separation of $[Fe(CN)_6]^{3-/4-}$ (1.0 M KCl) with the wt %. TPP used for fabrication of N-P-MWCNTs composite films.

Table 16 Electrochemical parameters determined for $[Fe(CN)_6]^{3-/4-}$ (1.0 M KCl) on novel N-MWCNTs and N-P-MWCNTs composite films at the scan rate of 0.02 $V \cdot s^{-1}$.

Composite film	$E_{1/2}$/V	ΔE_p/V	$10^3 k_s$ /cm·s^{-1}[(c)]	R_{ct}/Ω	*LOD*/µM	*S*/A·M^{-1}·cm^{-2}
N-MWCNTs[(a)]	0.277	0.059	43	4.7	0.341	0.464
N-P-MWCNTs-1[(b)]	0.280	0.062	32	8.4	0.392	0.403
N-P-MWCNTs-2[(b)]	0.278	0.064	27	14.5	0.454	0.350
N-P-MWCNTs-3[(b)]	0.280	0.071	14	16.6	0.505	0.314
N-P-MWCNTs-4[(b)]	0.280	0.072	13	16.8	0.522	0.304
N-P-MWCNTs-5[(b)]	0.278	0.097	2	19.5	0.532	0.297

[a]Data taken from this work; [b] Data from present work; [c] k_s values determined from electrochemical absolute rate relation: $\psi=(D_o/D_R)^{a/2}k_s(n\pi FvD_o/RT)^{-1/2}$, where ψ is kinetic parameter, a the charge-transfer coefficient ($a\approx0.5$), D_o and D_R the diffusion coefficients of oxidized and reduced species, respectively ($D_o\approx D_R$), and n the number of electrons involved in redox reaction (n=1) [205]

4.3.2.2 Electrochemical Impedance spectroscopy

The electrochemical behavior of $[Fe(CN)_6]^{3-/4-}$ redox system on N-MWCNTs and various N-P-MWCNTs films was further investigated by means of electrochemical impedance spectroscopy technique. EIS spectra were recorded for $[Fe(CN)_6]^{3-/4-}$ redox system on fabricated composite films at the half-wave potential of the studied redox system ($E_{1/2}$=0.280 V vs. Ag/AgCl) in the frequency range of 0.1 Hz-100 kHz. Representative EIS spectra recorded on the N-MWCNTs and two different N-P-MWCNTs composite films (N-P-MWCNTs-3 and N-P-MWCNTs-5) are represented in Fig.88a. The presentation of EIS spectra of the other N-P-MWCNTs films was skipped since only some minor differences can be observed among the EIS spectra and consequently the spectra can be overlapped.

In order to estimate the charge transfer resistance R_{ct} that is an important parameter which controls the electron transfer kinetics of redox system at electrode interface, the EIS spectra were simulated by using a modified Nyquist circuit (Fig.87). The circuit used for the simulation of impedance data can be represented as: (R_s+ C_b + (C_{dl}/(R_{ct}+Z_w)), where R_s is the solution resistance, C_b a capacitor element, due to the additional impedance between the film and the clip used for the electrical connection, C_{dl} the double-layer capacitance (constant phase element was used instead of pure capacitor), R_{ct} the charge transfer resistance, and Z_w the Warburg diffusion impedance. The R_{ct} values were estimated and represented graphically *versus* the wt %. of TPP used for synthesis of N-P-MWCNTs films in Fig.88b.

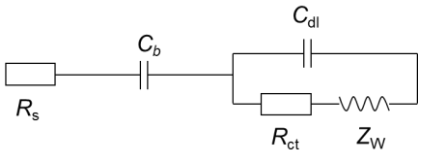

Fig. 87 Equivalent electrical circuit (R_s+ C_b + (C_{dl}/(R_{ct}+Z_w))) used for simulation of EIS spectra recorded for $[Fe(CN)_6]^{3-/4-}$ (1.0 M KCl) on N-MWCNTs and N-P-MWCNTs composite films (software Thales, version 4.15).

The findings extracted from the simulation demonstrate that the charge transfer resistance increases with doping of carbon nanotubes with phosphorus, leading therefore to slower kinetic of electrochemical process on these particular films. Namely, with increasing the mass percent wt % of decomposed TPP from 0.2 up to 1.0%, the charge transfer resistance increases with the order:

N-MWCNTs < N-P-MWCNTs-1 < N-P-MWCNTs-2 < N-P-MWCNTs-3 < N-P-MWCNTs-4 < N-P-MWCNTs-5.

It can be concluded that the increase of concentration of decomposed TPP used for fabrication of N-P-MWCNTs results to greater barrier, and thus, to lower kinetic of electron transfer and consequently the sensitivity and the detection capability of synthesized films will be also affected.

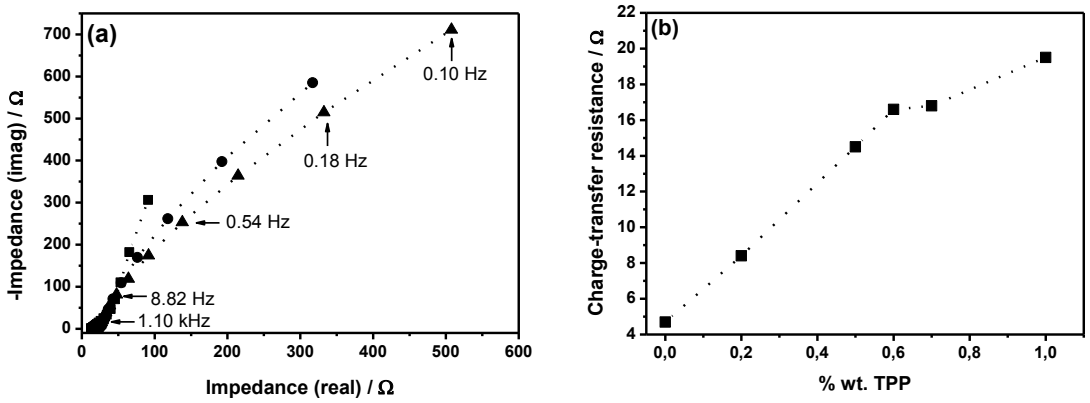

Fig. 88 (a) EIS spectra recorded for $[Fe(CN)_6]^{3-/4-}$ (1.0 M KCl) on N-MWCNTs (■), N-P-MWCNTs-3 (●), and N-P-MWCNTs-5 (▲), **(b)** Variation of charge-transfer resistance of $[Fe(CN)_6]^{3-/4-}$ (1.0 M KCl) with the wt %. TPP used for fabrication of N-P-MWCNTs composite films.

4.3.3 Application of N-P-MWCNTs for analysis of biomolecules

In this work, the response of N-P-MWCNTs (the N-P-MWCNTs fabricated upon decomposition of 1 wt %. TPP was selected) towards the oxidation of AA, DA and UA in phosphate buffer solution at pH 7.0 was studied by means of cyclic voltammetry (Fig.89).

CVs recorded for various concentrations of AA on N-P-MWCNTs-5 are shown in Fig.89a. It can be seen that the irreversible oxidation of AA on N-P-MWCNTs film occurs at the potential of about 0.228 V (vs. Ag/AgCl). Compared to N-MWCNTs, the oxidation potential of AA lies in negative region -0.014 V (vs. Ag/AgCl) which is about 240 mV less anodic than that measured for AA on N-P-MWCNTs-5. Namely, the ability of N-P-MWCNTs to decrease the oxidation overpotential of AA is clearly lesser compared to that of N-MWCNTs. It was observed that the peak current response towards oxidation of AA is low (between 30 and 40 % lesser) compared to the current response towards oxidation the same concentration of DA and UA. The detection limit of AA on N-P-MWCNTs film in the concentration range of 0.250-0.668 mM was estimated to be 11.6 μM.

Dopamine oxidation was also studied on this film. The recorded CVs show that DA oxidized at about 0.222 V (vs. Ag/AgCl) with quasi-reversible behavior (Fig.89b). This peak is very close to oxidation peak of AA measured on this film (0.228 V vs. Ag/AgCl). These results demonstrate that the analysis of AA interferes with the analysis of DA in a single measurement, and the inverse, the analysis of DA interferes with the analysis of AA. CVs with different concentrations of DA were recorded (in the range of 0.017-0.196 mM) and the detection limit was estimated to be 1.9 µM.

Furthermore, in CVs shown in Fig.89c, it can be seen that the irreversible oxidation peak of UA occurs at about +0.360 V (vs. Ag/AgCl) that lies obviously in more positive potential compared to oxidation peaks of either AA or DA. From the oxidation peak separation between AA-UA and DA-UA which is nearly the same (about 135 mV), it can be concluded that it is possible to analyze this couples in a single measurement. In order to estimate the lower limit of detection on this film towards oxidation of UA, CVs for various concentrations of UA in the range of 0.032-0.211 mM were recorded. From the linear variation of oxidation peak current density with the concentration of UA, the detection limit was found to be 7.8 µM.

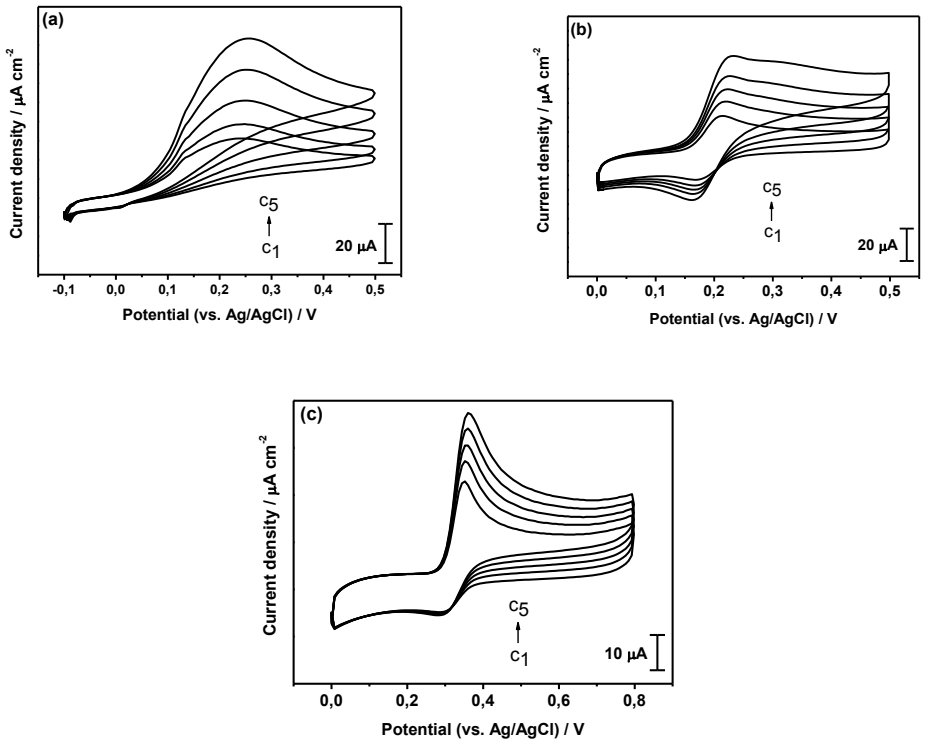

Fig. 89 CVs recorded for various concentrations of (a) AA, (b) DA, and (c) UA on N-P-MWCNTs composite film at 0.02 $V.s^{-1}$ (PBS, pH 7.0). The CVs (from inner to outer) correspond to concentrations: (a) c_1=0.250 mM; c_2=0.316 mM; c_3=0.369 mM; c_4=0.551 mM; c_5=0.668 mM; (b) c_1=0.033 mM; c_2=0.050 mM;

c_3=0.066 mM; c_4=0.099 mM; c_5=0.163 mM; (c) c_1=0.032 mM; c_2=0.062 mM; c_3=0.091 mM; c_4=0.117 mM; c_5=0.166 mM.

Compared to N-MWCNTs films, it is remarkable that the detection limit of the studied biomolecules on N-P-MWCNTs film is greater and thus the sensitivity lesser. These results support the conclusion that N-MWCNTs are more sensitive and work well in electrochemical sensing compared to N-P-MWCNTs. However, according to the comparison shown in Table 17, the fabricated N-P-MWCNTs seem to be more sensitive than other novel composite films reported in literature.

Table 17 Comparison of low limits of detection (*LOD*) of N-P-MWCNTs composite film toward oxidation of AA, DA, and UA (phosphate buffer solution, pH 7.0) with those reported in literature for other novel composite films.

Composite film	***LOD*/μM**		
	AA	**DA**	**UA**
N-P-MWCNTs-5[a]	11.6	1.9	7.8
N-MWCNTs [b]	8.7	1.4	5.9
GCE/MWCNTs/PtNPs[c]	20	0.0483	0.35
GCE/PtNPs/AuNPs/Cy[d]	103	24	21
GCE/PABA[e]	5.0	1.0	0.5
GCE/Ch/GR[f]	50	1.0	2.0
GCE/ACBK[g]	10	0.50	0.50
GCE/PEDOT[h]	7.4	1.2	1.4

[a]Nitrogen-phosphorus-doped multi-walled carbon nanotubes [this work]

[b]Nitrogen-doped multi-walled carbon nanotubes [this work]

[c]Glassy carbon electrode modified with multi-walled carbon nanotubes and platinum nanoparticles [263]

[d]Glassy carbon electrode modified with platinum nanoparticles, gold nanoparticles, and l-Cysteine [259]

[e]Glassy carbon electrode modified with polymerized 4-aminobutyric acid [271]

[f]Glassy carbon electrode modified with chitosan and graphene [269]

[g] Glassy carbon electrode modified with polymerized acid chrome blue K [277]

[h] Glassy carbon electrode modified with poly (3,4-ethylenedioxythiophene) [278]

In order to study the interference that occurs when AA and DA are measured in a single measurement, CVs for AA-DA-UA ternary mixtures were recorded (Fig.90).

As it was expected, the peak oxidation of AA and DA overlap each other hindering, thus their simultaneous electrochemical analysis. Namely, on this particular film the simultaneous analyzing of AA/UA and DA/UA binary mixture can be successfully carried out in single measurement since their oxidation peaks do not overlap each other, but the simultaneous analysis of the ternary mixture AA-DA-UA is not possible due to the wave interface of AA and DA. It is interesting that well separated redox waves can be still observed in AA/UA binary systems even if the concentration of AA is 5 times higher compared to that of UA (Fig.90a).

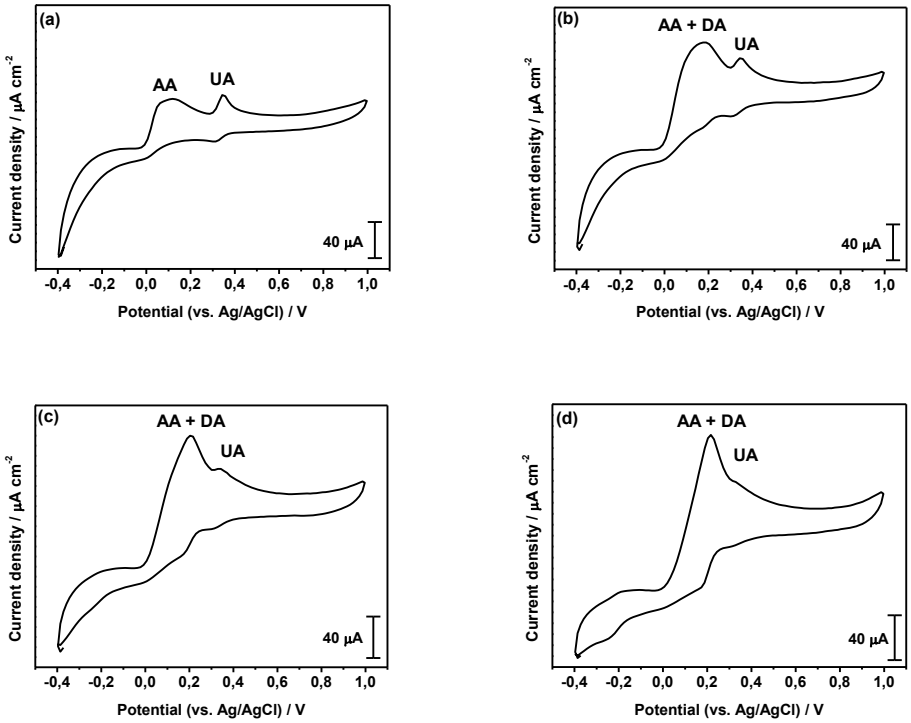

Fig. 90 CVs recorded for **(a)** binary mixtures AA/UA and **(b-d)** ternary mixtures AA/DA/UA on N-P-MWCNTs composite film at 0.02 $V.s^{-1}$ (PBS, pH 7.0). The CVs correspond to the concentrations: **(a)** AA (0.5 mM) / UA (0.1 mM); **(b)** AA (0.5 mM) / UA (0.1 mM) / DA (0.033 mM); **(c)** AA (0.5 mM) / UA (0.1 mM) / DA (0.062 mM); **(d)** AA (0.5 mM) / UA (0.1 mM) / DA (0.099 mM).

5 Summary

The synthesis of nitrogen-doped multi-walled carbon nanotubes and nitrogen-phosphorus-doped multi-walled carbon nanotubes further denoted as (N-MWCNTs) and (N-P-MWCNTs), respectively, was successfully done by using chemical vapor deposition technique (CVD). The synthesized N-MWCNTs and N-P-MWCNTs were grown on silicon / silicon oxide substrate by decomposition of either acetonitrile or acetonitrile and triphenylphosphine, respectively, in the presence of ferrocene as a catalyst. The morphology was studied using scanning electron microscopy (SEM) in combination with energy dispersive X-ray spectroscopy (EDXS), transmission electron microscopy (TEM), and Raman spectroscopy.

The SEM images show that the N-MWCNTs consist of carpet of vertically oriented carbon nanotubes and the surface of the film is quite homogeneous, whereas the TEM images show that the N-MWCNTs have the so-called bamboo structure that is a quite common structure of nitrogen-doped carbon nanotubes. Furthermore, SEM micrographs exhibit that the N-P-MWCNTs films have homogeneous structure similar to N-MWCNTs with some knots in the tube structure. The morphology of the fabricated film starts to change with increasing the phosphorus source material (between 0.7 and 1 wt %. TPP). Namely, a layer of amorphous carbon covers the carbon nanotubes and no aligned carbon nanotubes can be recognized in SEM images. It was also observed that very thin wafers from N-P-MWCNTs were obtained with increasing the phosphorus source material (1 wt %. TPP). TEM images confirm that the N-P-MWCNTs still have bamboo structure (recognizable up to an addition of 0.6 wt %. TPP). Further increase of TPP (more than 0.6 wt %. TPP), TEM images could not be taken since they contain a lot of amorphous carbon.

Raman spectroscopy analysis shows that the N-MWCNT films exhibits more defects compared to N-P- MWCNTs films.

The electrochemical characterization by means of cyclic voltammetry (CV) and electrochemical impedance spectroscopy (EIS) was carried out using the redox system $[Fe(CN)_6]^{3-/4-}$. The results show that the produced N-MWCNTs show the highest sensitivity, the smallest detection limit, and the fastest kinetics of electron transfer (the smallest charge transfer resistance) compared to the N-P-MWCNTs. The results show that the doping of carbon nanotubes with nitrogen improves the electrocatalytic properties. Furthermore, the findings indicate that the introduction of phosphorus into the structure of N-MWCNTs decrease the detection ability and thus the sensitivity, as well as the kinetic of electrochemical process on this film.

The modification of carbon-based material with metal nanoparticles MNPs was also investigated. For this purpose, rhodium (RhNPs), palladium (PdNPs),

platinum (PtNPs), and silver (AgNPs) nanoparticles were used for the decoration of surface of films. The electrochemical characterization of prepared modified films N-MWCNTs/MNPs towards the redox system $[Fe(CN)_6]^{3-/4-}$ was investigated. The results show that the modified N-MWCNTs/MNPs films show great electrochemical response since the nanoparticles act as a catalyst improving the electrocatalytic activity of the electrode. The findings exhibit that the electrocatalytic response of films enhances with the following order: N-MWCNTs < N-MWCNTs/RhNPs < N -MWCNTs/PdNPs < N-MWCNTs/PtNPs < N-MWCNTs/AgNPs.

The use of N-MWCNTs/MNPs (M: Rh, Pd, Ir, Pt, and Au) composite films as working electrode for simultaneous analysis of some interesting biomolecules such as ascorbic acid, dopamine, and uric acid in phosphate buffer solution PBS (pH 7.0) was also successfully applied. The results show that the detection limit of N-MWCNTs /MNPs towards oxidation of AA, DA, and UA decreases with the following order: N-MWCNTs > N-MWCNTs/RhNPs > N-MWCNTs/PdNPs > N-MWCNTs/IrNPs > N-MWCNTs/PtNPs > N-MWCNTs/AuNPs. The results exhibit once more that the AuNPs show the greatest influence on sensitivity and electrocatalytic activity in the simultaneous determination of investigated molecules. It is interesting that the prepared composite film N-MWCNTs/AuNPs was also successfully applied for simultaneous electrochemical analysis of other biomolecules such as acetaminophen (AC) and *N*-acetyl-cysteine (NAC).

It is interesting to mention that the fabricated N-MWCNTs/AuNPs films show smaller detection limit compared to other novel composite films reported in literature and exhibit a very good stability and reproducibility as electrode material.

6 References

[1] P. Levi, The periodic table, New York: Shocken Books, 1984, 227.
[2] H.W. Kroto, J.R. Heath, S.C. O'Brien, R.F. Curl, and R.E. Smalley, Nature 1985, 318,162–163.
[3] S. Iijima, Nature, 1991, 354, 56–58.
[4] S. Iijima and T. Ichihashi, Nature, 1993, vol. 363, no. 6430, 603-605.
[5] C. Ewels, http://www.ewels.info
[6] Bernholc J, Brenner D, Buongiorno Nardelli M, Meunier V, Roland C Annu, Rev Mater Res 2002, 32, 347–375.
[7] Dresselhaus, M. S.; Dresselhaus, G.; Saito, R.; Jorio, A., Physics Reports 2005, 409 (2), 47-99.
[8] K. Balasubramanian and M. Burghard, Small, 2005, 1, 180–192.
[9] Balasubramanian, K.; Burghard, M: Chem. Unserer Zeit 2005, 39, 16-25.
[10] T.Ando, H. Matsumura and T. Nakanishi, Physica B+C, 2002, 323, 44-50.
[11] Klingeler, R.; Kramberger, C.; Müller, C.; Pichler, T.; Leonhardt, A.; Büchner, B.:. Wiss. Z. TU Dresden 56 (1-2), 2007, 105-110
[12] Michael F. L. De Volder, Sameh H. Tawfick, Ray H. Baughman, A. John Hart, SCIENCE, 2013, 339, 535-539.
[13] Carbon Nanotubes Market by Type (Single Walled- And Multi-Walled), by Application (Electronics & Semiconductors, Chemical & Polymers, Batteries & Capacitors, Energy, Medical Application, Advanced Materials, Aerospace & Defense, Others) - Global Forecasts to 2020.
[14] A.C. Dupuis, Prog. Mater. Sci, 2005, 50, 929-961.
[15] Published: April 2015 | Report Code: 978-1-68038-393-5.
[16] Satishkumar, B.C., Govindaraj, A., Rao, C.N.R.: Chem. Phys. Lett. 1999, 307, 158–162.
[17] Paradise, M.; Goswami, T. Mat. Design, 2007, 28, 1477–1489.
[18] Dai H. Carbon nanotubes: opportunities and challenges. Surface Sci, 2002, 500(1–3), 218–241.
[19] Yudasaka, M., Kikuchi, R., Ohki, Y., Yoshimura, S., Carbon, 1997, 35, 195–201.
[20] Rao, C.N.R., Sen, R., Satishkumar, B.C., Govindaraj, A.: Chem. Commun, 1998, 15, 1525–1526.
[21] Muhammad Musaddique Ali Rafique, Javed Iqbal, Journal of Encapsulation and Adsorption Sciences, 2011, 1, 29-34.
[22] Dai, H., Rinzler, A.G., Nikolaev, P., Thess, A., Colbert, D.T., Smalley, R.E.: Chem. Phys. Lett, 1996, 260, 471–475.
[23] Cheng, H.M., Li, F., Sun, X., Brown, S.D.M., Pimenta, M.A., Marucci, A., Dreselhaus, G., Dresselhaus, M.S.: Chem. Phys. Lett, 1998, 289, 602–610.

[24] Satishkumar, B.C., Govindaraj, A., Sen, R., Rao, C.N.R.: Chem. Phys. Lett, 1998, 293, 47–52.
[25] Hafner, J.H., Bronikowski, M.J., Azamian, B.R., Nikolaev, P., Rinzler, A.G., Colbert, D.T.,Smith, K.A., Smalley, R.E.: Chem. Phys. Lett, 1998, 296, 195–202.
[26] Kong, J., Cassell, A.M., Dai, H.J.: Chem. Phys. Lett, 1998, 292, 567–574.
[27] Flahaut, E., Govindaraj, A., Peigney, A., Laurent, C., Rousset, A., Rao, C.N.R.: Chem. Phys. Lett, 1999, 300, 236–242.
[28] M. Endo, K. Takeuchi, S. Igarashi, K. Kobori, M. Shiraishi, and H.W. Kroto, , J. Phys. Chem. Solids , 1993, 54, 1841–1848.
[29] Y. J. Zhu, T. J. Lin, Q. X. Liu, Y. L. Chen, G. F. Zhang, H. F. Xiong and H. Y. Zhang, Mater. Sci. Eng., B 127, 2006, 198–202.
[30] Z. B. He, J. L. Maurice, C. S. Lee, C. S. Cojocaru and D. Pribat, Arabian J. Sci. Eng., Sect. B, 2010, 35, 19–28.
[31] T. Guo, P. Nikolaev, A. Thess, D. T. Colbert and R. E. Smalley, Chem. Phys. Lett, 1995, 243, 49–54.
[32] T. Ikegami, F. Nakanishi, M. Uchiyama and K. Ebihara, Thin Solid Films, 2004, 457, 7–11.
[33] Ph. Redlich, M. J. Loeffler, P. M Ajayan, J. Bill, F. Aldinger. J. Chem. Phys., 1996, 260, 465.
[34] T.W. Ebbesen, and P.M. Ajayan, Nature, 1992, 358, 220-222.
[35] Fonseca, A.; B.Nagy, J..; Biro, L.P., ernardo, C.A., bbetts, G.G, Lambin, Ph, Eds.; Kluwer Academic Publishers: Dordrecht, The Netherlands, 2001, 372, 75–84.
[36] Vito Sgobba and Dirk M. Guldi, Chem. Soc. Rev., 2009, 38, 165–184.
[37] O. Stephen, P.M. Ajayan, C. Colliex, Ph. Redlich, J. M. Lambert, P. Beirnier, P.Letin. Science, 1994, 266, 1683-1685.
[38] Koretsune T and Satio S, Phys. Rev, 2008, B 77, 165417.
[39] Lim S H, Li R, Ji W and Lin J Phys. Rev, 2007, B 76, 195406.
[40] Ayala P, Arenal R, Rummeli M, Rubio A and Pichler T, Carbon 2010, 48 575–86.
[41] Zhao M W, Xia Y Y, Lewis J P and Zhang R Q J. Appl. Phys, 2003, 94, 2398–2402.
[42] Buonocore F, Phil. Mag. 2007, 87, 1097–1105.
[43] Chen A Q, Shao Q Y and Lin Z C, Sci. China Ser, 2009. G 52 1139–45.
[44] Czerw R, Terrones M, Charlier JC, Blasé X, Foley B, Kamalakaran R, Grobert N, Terrones H, Tekleab D, Ajayan PM, Blau W, Ruhle M, Carroll DL, Nano Lett 2001, 1, 457-460.
[45] D. Golberg, Y. Bando, C. C. Tang, T. E. Zhi, Adv, Mater, 2007, 19, 2413-2432.
[46] Nevidomskyy A, Csanyi G, Payne M, Phys Rev Lett, 2003, 91:105502.
[47] Sun CL, Chen LC, Su MC, Hong LS, Chyan O, Hsu CY, Chen KH, Chang TF, Chang L, Chem Mater, 2005,17, 3749-3753.

[48] Van Dommele S, Romero-Izquirdo A, Brydson R, de Jong KP, Bitter JH, T, Carbon, 2008, 46, 138-148.
[49] Li XL, Liu YQ, Fu L, Cao LC, Wei DC, Wang Y, Carbon, 2008,46:255-260.
[50] Bulusheva LG, Okotrub AV, Kudashov AG, Shubin YuV, Shlyakhova EV, Yudanov NF, Pazhetnov EM, Boronin AI, Vyalikh DV, Carbon, 2008,46, 864-869.
[51] Koos AA, Dowling M, Jurkschat K, Crossley A, Grobert N, Carbon, 2009, 47, 30-37.
[52] J. Wiggins-Camacho and K. Stevenson, the Journal of Physical Chemistry C 113(44), 2009, 19082–19090.
[53] K.Y. Chun, H. S. Lee, and C. J. Lee, Carbon, 2009, 47(1), 169–177.
[54] S.Y. Kim, J. Lee, C.W. Na, J. Park, K. Seo, and B. Kim, Chemical Physics Letters , 2005, 413(4), 300–305.
[55] L. Panchakarla, A. Govindaraj, and C. Rao, ACS Nano, 2007, 1(5), 494–500.
[56] J. C. Li, P. X. Hou, L. Zhang, C. Liu, and H. M. Cheng, Nanoscale 2014, 6(20), 12065–12070.
[57] C. L. Pint, Z. Sun, S. Moghazy, Y. Q. Xu, J. M. Tour, and R. H. Hauge, ACS Nano, 2011, 5(9), 6925–6934.
[58] T. Thurakitseree, C. Kramberger, P. Zhao, S. Aikawa, S. Harish, S. Chiashi, E. Einarsson, and S. Maruyama, Carbon, 2012,50(7), 2635–2640.
[59] R. Sen, B.C. Satishkumar, A. Govindaraj, K.R. Harikumar, M.K. Renganathan, C.N.R. Rao, J. Mater. Chem, 1997, 7, 2335-2337.
[60] F. Villalpando-Paez, A. Zamudio, A. Elias, H. Son, E. Barros, S. Chou, Y. Kim, H. Muramatsu, T. Hayashi, J. Kong, H. Terrones, G. Dresselhaus, M. Endo, M. Terrones, and M. S. Dresselhaus, Chemical Physics Letters,2006, 424(4), 345–352.
[61] P. Ayala, A. Gr¨uneis, T. Gemming, D. Grimm, C. Kramberger, M. H. R¨ummeli, F. L. Freire, H. Kuzmany, R. Pfeiffer, A. Barreiro, B. B¨uchner, and T. Pichler, TheJournal of Physical Chemistry 2007, C 111(7), 2879–2884.
[62] P. Ayala, F. L. Freire, M. H. R¨ummeli, A. Gr¨uneis, and T. Pichler, Physica Status Solidi (b), 2007, 244(11), 4051–4055
[63] I. Maciel, J. Campos-Delgado, M. Pimenta, M. Terrones, H. Terrones, A. Rao, and A. Jorio, Physica Status Solidi (b),2009, 246(11-12), 2432–2435
[64] Jessica Campos-Delgado, Indhira O. Maciel, David A. Cullen, David J. Smith, Ado Jorio, Marcos A. Pimenta, Humberto Terrones,_ and Mauricio Terrones. ACS Nano, 2010, vol. 4. No. 3, 1696–1702.
[65] C. P. Ewels and M. Glerup, J. Nanosci. Nanotech, 2005, 5(9), 1345–1363.
[66] J.W. Jang, C. E. Lee, T. J. Lee, S. C. Lyu, and C. J. Lee. Curr. Appl. Phys., 2006, 6, 141–144.
[67] R.M.Yadav, P.S.Dobal, T.Shripathi, R.S.Katiyar, O.N.Srivastava, Nanoscale Res Lett. 2009, 4, 197-203.

[68] M. Glerup, M. Castignolles, M. Holzinger, G. Hug, A. Loiseau, and P. Bernier. Chem. Commun, 2003, 2542–2543.
[69] S. H. Lim, H. I. Elim, X. Y. Gao, A. T. S. Wee, W. Ji, J. Y. Lee, and J. Lin. Electronic and optical properties of nitrogen-doped multiwall carbon nanotubes, Phys. Rev. B. 73, 2006, 045402.
[70] R. Droppa Jr., C. T. M. Ribeiro, A. R. Zanatta, M. C. dos Santos, and F. Alvarez. Phys. Rev. B. 69, 2004, 045405.
[71] Jang, J. W.; Lee, C. E.; Lyu, S. C.; Lee, T. J.; Lee, C. J. Appl. Phys. Lett, 2004, 84, 2877–2879
[72] Bobby G. Sumpter, Vincent Meunier, José M. Romo-Herrera, Eduardo Cruz-Silva, David A. Cullen, Humberto Terrones,David J. Smith, and Mauricio Terrones, ACS NANO,2007, VOL. 1. NO. 4, 369–375
[73] Maciel, I. O.; Campos-Delgado, J.; Cruz-Silva, E.; Pimenta,M. A.; Sumpter, B. G.; Meunier, V.; Lo´ pez-Urı´as, F.; Mun˜ oz- Sandoval, E.; Terrones, H.; Terrones, M.; et al. Nano Lett, 2009, 9, 2267–2272.
[74] D. G. Larrude, M. E. H. Maia da Costa, F. H. Monteiro, A. L. Pinto, and F. L. Freire Jr. Journal of applied physics, 2012, 111, 064315.
[75] Cruz-Silva, E.; Cullen, D. A.; Gu, L.; Romo-Herrera, J. M.; Mun˜ oz-Sandoval, E.; Lo´ pez-Urı´as, F.; Sumpter, B. G.;Meunier, V.; Charlier, J.-C.; Smith, D. J.; et al, ACS Nano, 2008, 2, 441–448.
[76] Jian Liu, Hao Liu, Yong Zhang, Ruying Li, Guoxian Liang, Michel Gauthier, Xueliang Sun, Carbon, 2011, 49, 5014-5021.
[77] Eduardo Cruz-Silva, Florentino Lo´ pez-Urı´as, Emilio Mun˜ oz-Sandoval, Bobby G. Sumpter, Humberto Terrones, Jean-Christophe Charlier, Vincent Meunier, and Mauricio Terrones, ACS Nano, 2009, VOL. 3 . NO. 7, 1913–1921.
[78] Y. Homma, Y. Kobayashi, T. Ogino, D. Takagi, R. Ito, Y.J. Jung, P.M. Ajayan, J. Phys. Chem, 2003, 107, 12161-1264.
[79] C. Jin, K. Suenaga, S. Iijima, ACS. Nano, 2008, 2, 1275-1279.
[80] K. Liu, K. Jiang, C. Feng, Z. Chen, S. Fan, Carbon, 2005, 43, 2850-2856.
[81] M. Endo, T. Hayashi, Y.A. Kim, M. Terrones, M.S. Dresselhaus, Phil. Trans. Roy. Soc. Lond, 2004, 362, 2223-2238.
[82] H. Liu, D. Takagi, H. Ohno, S. Chiashi, T. Chokan, Y. Homma, J. Appl. Phys, 2008, 1, 014001.
[83] V.O. Nyamori, S.D. Mhlanga, N.J. Coville, J. Organomet. Chem, 2008, 693, 2205-2222.
[84] Charlier, J-C, and Sumio Iijima. Growth Mechanisms of Carbon Nanotubes. In M.S Dresselhaus, G Dresselhaus, Ph. Avouris (Eds.) Carbon Nanotubes: Synthesis, Structure, Properties, and Applications, New York: Springer, 2001, 55-79.
[85] Mukul Kumar,Yoshinori Ando, J. Nanosci. Nanotechnol, 2010, 10, 3739–3758.

[86] Mukul Kumar, Carbon Nanotube Synthesis and Growth Mechanism, Nanotechnology and Nanomaterials book, 2011.
[87] Lin, C.H.; Chang, H.L.; Hsu, C.M.; Lo, A.Y.; Kuo, C.T, Diamond Relat. Mater, 2003, 12, 1851–1857.
[88] Zhang, X.F.; Zhang, X.B.; Tendelloo, G.V.; Amelinckx, S.; de Beeck, M.O.; Landuyt, J.V.. J. Cryst. Growth, 1993, 130, 368–382.
[89] Suenaga, K.; Yudasaka, M.; Colliex, C.; Iijima, S. Chem. Phys. Lett, 2000, 316, 365–372.
[90] M. Reyes-Reyes, N. Grobert, R. Kamalakaran, T. Seeger, D. Golberg, M. R¨uhle, Y. Bando, H. Terrones, and M. Terrones.. Chem. Phys. Lett, 2004, 396,167–173.
[91] J. H. Yang, B. J. Kim, Y. H. Kim, Y. J. Lee, B. H. Ha, Y. S. Shin, S.-Y. Park, H. S. Kim, C.-Y. Park, C.-W. Yang, J.-B. Yoo, M. H. Kwon, K. Ihm, H.-J. Song, T.-H. Kang, H.-J. Shin, J.-Y. Park, and J.-M. Kim. J. Vac. Sci. Technol. B, 2005, 23(3), 930–933.
[92] M. Terrones, P. M. Ajayan, F. Banhardt, X. Blase, D. L. Carroll, J.-C. Charlier, R. Czerw, B. Foley, N. Grobert, R. Kamalakaran, P. K¨ohler-Redlich, T. Seeger, and H. Terrones, Appl. Phys. A, 2002, 74, 355–361.
[93] Dell'Acqua-Bellavitis, L.M.; Ballard, J.D.; Vajtai, R.; Ajayan, P.M.; Siegel R.W. J. Phys. Chem. C, 2007, 111, 2623–2630.
[94] Slawomir Boncel, Sebastian W. Pattinson, Valérie Geiser, Milo S. P. Shaffer and Krzysztof K. K. Koziol, Beilstein J. Nanotechnol, 2014, 5, 219–233.
[95] Che, G., Lakshmi, B.B., Fisher, E.R., Martin, C.R, Nature, 1998, 393, 346–349.
[96] Wang, J., Xu, D., Kawde, A.N., Polsky, R, Anal. Chem, 2001, 73, 5576–5581.
[97] Joo, S.H., Choi, S.J., Oh, I., Kwak, J., Liu, Z., Terasaki, O., Ryoo, R, Nature, 2001,412, 169–172.
[98] D. N. Muraviev, J. Macanás, M. Farre, M. Muñoz, S. Alegret Sens. Actuators B, 2006, 11, 408-417.
[99] J. Li, X. Lin Sens. Actuators B, 2007, 126, 527-535.
[100] E. Katz, I. Willner, J. Wang, Electroanalysis, 2004, 16, 19-44.
[101] X. G. Liu, N. Q. Wu, B. H. Wunsch, R. J. Barsotti, Jr. and F. Stellacci, Small, 2006, 2, 1046-1050.
[102] C. R. Raj, T. Okajima, T. Ohsaka J. Electroanal. Chem, 2003, 543, 127-133.
[103] Dursun, Z., Gelmez, B., Electroanalysis, 2010, 22, 1106–1114.
[104] C.R. Raj, T. Okajima, T. Ohsaka, , J. Electroanal. Chem, 2003, 543, 127-133.
[105] J. M. Planeix, N. Coustel, J. Coq, V. Brotons, P. S. Kumbhar, R. Dutartre, P. Geneste, P. Bernier and P. M. Ajayan, J. Am. Chem. Soc, 1994, 116, 7935-7936.

[106] W. Li, C. Liang, W. Zhou, J. Qiu, Z. Zhou, G. Sun and Q. Xin, J. Phys. Chem. B, 2003, 107, 6292-6299.
[107] V. Tzitzios, V. Georgakilas, E. Oikonomou, MA. Karakassides and D. Petridis, Carbon, 2006, 44, 848-853.
[108] R. Giordano, P. Serp, P. Kalck, Y. Kihn, J. Schreiber, C. Marhic and J.-L. Duvail, Eur. J. Inorg, Chem, 2003, 2003, 610-617.
[109] (a) T. M. Day, P. R. Unwin, N. R. Wilson and J. V. Macpherson, J. Am. Chem. Soc, 2005, 127, 10639-10647.
[110] Y. Wang, X. Xu, Z. Tian, Y. Zong, H. Cheng and C. Lin, Chem.–Eur. J., 2006, 12, 2542-2549.
[111] V. Lordi, N. Yao and J. Wei, Chem. Mater, 2001, 13, 733-737.
[112] M. S. Raghuveer, S. Agarwal, N. Bishop and G. Ramanath, Chem. Mater, 2006, 18, 1390-1393.
[113] L. Qu and L. Dai, J. Am, Chem. Soc, 2005, 127, 10806-10807.
[114] B. M. Quinn, C. Dekker and S. G. Lemay, J. Am. Chem. Soc, 2005, 127, 6146-6147.
[115] B. R. Azamian, K. S. Coleman, J. J. Davis, N. Hanson and M. L. H. Green, Chem. Commun, 2002, 366-367.
[116] R. Zanella, E. V. Basiuk, P. Santiago, V. A. Basiuk, E. Mireles, I. Puente-Lee and J. M. Saniger, J. Phys. Chem. B, 2005, 109, 16290-16295.
[117] (a) L. Liu, T. Wang, J. Li, Z.-X. Guo, L. Dai, D. Zhang andD. Zhu, Chem. Phys. Lett., 2003, 367, 747-752; (b) D. Q. Yang, B. Hennequin and E. Sacher, Chem. Mater., 2006, 18, 5033-5038.
[118] D. M. Guldi, G. M. A. Rahman, N. Jux, N. Tagmatarchis and M. Prato, Angew. Chem., Int. Ed., 2004, 43, 5526-5530.
[119] D. M. Guldi, G. M. A. Rahman, N. Jux, M. Prato, S. H. Qin and W. Ford, Angew. Chem., Int. Ed, 2005, 44, 2015-2018.
[120] L. Han, W. Wu, F. L. Kirk, J. Luo, M. M. Maye, N. N. Kariuki, Y. Lin, C. Wang and C. J. Zhong, Langmuir, 2004, 20, 6019-6025.
[121] K. Jiang, A. Eitan, L. S. Schadler, P. M. Ajayan, R. W. Siegel, N. Grobert, M. Mayne, M. Reyes-Reyes, H. Terrones and M. Terrones, Nano Lett., 2003, 3, 275-277.
[122] M. A. Correa-Duarte, J. Perez-Juste, A. Sanchez-Iglesias, M. Giersig and L. M. Liz-Marza´n, Angew. Chem., Int. Ed., 2005, 44, 4375-4378.
[123] X. Li, Y. Liu, L. Fu, L. Cao, D. Wei, G. Yu and D. Zhu, Carbon, 2006, 44, 3139-3142.
[124] L.C. Jiang, W.D. Zhang, , Biosens. Bioelectron, 2010, 25, 1402-1407.
[125] W.D. Zhang, J. Chen, L.C. Jiang, Y.X. Yu, J.Q Zhang, Microchim. Acta 2010, 168, 259-265.
[126] Tasis,D; tagmatarchis,N; Bianco,A prato,M; Chemistry of carbon nanotubes. Chem.Rev, 2006,106, 1105-1136.
[127] Sherigara BS, Kutner W, D'Souza F Electroanalysis, 2003, 15, 753–772.

[128] Campbell JK, Sun L, Crooks RM J Am Chem Soc, 1999, 121, 3779 14. Cai H, Cao X, Jiang Y, He P, Fang Y, Anal Bioanal Chem, 2003, 375, 287-293.
[129] L.C. Jiang, W.D. Zhang, Electroanalysis, 2009, 21, 1811-1815.
[130] Zeid Abdullah Alothmana, Nausheen Bukharia, Saikh Mohammad Wabaidura, Sajjad Haiderb, Sensors and Actuators B, 2010, 146, 314–320.
[131] S.A. Kumar, P.H. Lo, S.M. Chen, Biosens. Bioelectron, 2008, 24, 518-523.
[132] Bankim J. Sanghavi, Ashwini K. Srivastava, Electrochimica Acta, 2010, 55, 8638–8648.
[133] Saeed Shahrokhian, Masoumeh Ghalkhani, Mohammad Kazem Amini, Sensors and Actuators B: Chemical, 2009, 137, 669–675.
[134] Wade (Ed.), Martindale the Extra Pharmacopoeia, 27th ed., the Pharmaceutical Press, London, 1979.
[135] S.F.Wang, F. Xie, R.F. Hu, Sens Actuator B-Chem, 2007, 123, 495-500.
[136] B.D. Clayton, Y.N. Stock, Basic Pharmacology for Nurses, Mosby Inc., Harcourt Health Sciences Company, St. Louis, 2001.
[137] B.C. Lourenc ¸ ão, R.A. Medeiros, R.C. Rocha-Filho, L.H. Mazo, O. Fatibello-Filho Talanta 78 (3), 2009, 748–752.
[138] H. Beitollahi, I. Sheikhshoaie, Mater. Sci. Eng. C 32, 2012, 375.
[139] F. Ghorbani-Bidkorbeh, S. Shahrokhian, A. Mohammadi, R. Dinarvand, Electrochim. Acta 55, 2010, 2752-2759.
[140] H. Beitollahi, I. Sheikhshoaie, J. Electroanal. Chem, 2011, 661, 336-342.
[141] Z.A. Alothman, N. Bukhari, S.M. Wabaidur, S. Haider, Sens. Actuators B 146, 2010, 314-320.
[142] Houshmand M, Jabbari A, Heli H, Hajjizadeh M, Moosavi-Movahedi AA, J Solid State Electrochem, 2008,12,1117–1128.
[143] Biuck Habibi, Mojtaba Jahanbakhshi, Mohammad Hossein Pournaghi-Azar, Analytical Biochemistry, 2011, 411, 167–175.
[144] Raoof JB, Chekin F, Ojani R, Barari S, Anbia M, Mandegarzad S. J Solid State Electrochem, 2012,16, 3753–3760.
[145] W.T. Suarez, L.H. Marcolino, O. Fatibello, Microchem. J. 82, 2006, 163.
[146] R.D. Estensen, M. Levy, S.J. Klopp, A.R. Galbraith, J.S. Mandel, J.A. Blomquist, L.W. Wattenberg, Cancer Lett, 1999,147, 109-114.
[147] Masoud Fouladgar, Hassan Karimi-Maleh, Rahman Hosseinzadeh, Ionics, 2013, 19, 665–672.
[148] H. Beitollahi, J.B. Raoof, R. Hosseinzadeh, Talanta ,2011, 85, 2128-2134.
[149] J.B. Raoof, R. Ojani, M. Amiri-Aref, F. Chekin, J. Appl. Electrochem, 2010, 40, 1357-1363.
[150] H. Shayani-Jam, D. Nematollahi, Electrochim. Acta, 2011, 56, 9311-9316.
[151] A.A. Ensafi, H. Karimi-Maleh, S. Mallakpour, M. Hatami, Sens. Actuators B, 2011,155, 42.
[152] H. Karimi-Maleh, M. Keyvanfard, K. Alizad, M. Fouladgar, H. Beitollahi, A. Mokhtari, F. Gholami-Orimi, Int. J. Electrochem. Sci, 2011, 6, 6141-6150.

[153] Hadi Beitollahi, Alireza Mohadesi, Somayeh Mohammadi, Ali Akbari, Electrochimica Acta, 2012, 68, 220– 226.
[154] Hadi Beitollahi, Jahan-Bakhsh Raoof, Rahman Hosseinzadeh, Talanta, 2011, 85, 2128–2134.
[155] O. Arrigoni, M. C. De Tullio, Biochim. Biophys. Acta, 2002, 1569, 1.
[156] Lupu, S.; Mucci, A.; Pigani, L.; Seeber, R.; Zanardi, C. Polythiophene.Electroanalysis, 2002, 14, 519-525.
[157] Liu, A.H., Honma, I., Zhou, H.S., Biosens. Bioelectron, 2005, 21, 809–816.
[158] Mo, J.W., Ogorevc, B., Anal. Chem, 2001, 73, 1196–1202.
[159] R.M. Wightman, C. Amatorh, R.C. Engstrom, P.D. Hale, E.W. Kristensen, W.G. Kuhr, L.J. May, Neuroscience, 1988, 25, 513-523.
[160] V.S.E. Dutt, H.A. Mottola, Anal. Chem, 1974, 46, 1777-1781.
[161] Ullman, B., Wormsted, M.A., Cohen, M.B., Martin Jr., D.W., Proc. Natl. Acad. Sci. U.S.A, 1982, 79, 5127–5131.
[162] L.C. Jiang, W.D. Zhang, Electroanal, 2009, 21, 1811-1815.
[163] R.A.A. Munoz, R.C. Matos, L. Angnes, Talanta, 2001, 55, 855-860.
[164] J. Wang, M. Li, Z. Shi, N. Li, Z. Gu, Microchem. J, 2002, 73, 325-333.
[165] O'Neil, R.D., Analyst 1994,119, 767–779.
[166] J. Chen, J. Zhang, X. Lin, H. Wan, S. Zhang, Electroanalysis, 2007, 19, 612.
[167] B. Habibi, M.H. Pournaghi-Azar, Electrochim. Acta, 2010, 55, 5492-5498.
[168] S. Thiagarajan, T.H. Tsai, S.M. Chen, Biosens. Bioelectron, 2009, 24, 2712.
[169] R. Zhang, G.D. Jin, D. Chen, X.Y. Hu, Sens. Actuators B 138, 2009, 174.
[170] A.X. Oliveira, S.M. Silva, L. Figueiredo, R. Fernando, Electroanal, 2013, 25, 723-731.
[171] Z. Temocin, Sens.Actuat. B Chem, 2013, 176, 796-802.
[172] Aihua Liu, Itaru Honma, Haoshen Zhou, Biosensors and Bioelectronics 2007, 23, 74–80.
[173] Shuyun Zhua, Haijuan Li, Wenxin Niua, Guobao Xu, Biosensors and Bioelectronics, 2009, 25, 940–943.
[174] Ali A. Ensafi, M. Taei, Taghi Khayamian, Int. J. Electrochem. *Sc*, 2010, 5, 116 – 130.
[175] Hemández-Santos, D., González-García, M.B., García, A.C., 2002. Electroanalysis, 14, 1225–1302.
[176] Katz, E., Willner, I.,Wang, J., Electroanalysis, 2004,16, 19–44.
[177] X. Wang, M. Wu, W.J. Tang, Elec. Chem, 2013, 695, 10-16.
[178] A. Babaei, M. Aminikhah, A.R. Taheri, Sensor Lett, 2013, 11, 413-422.
[179] Ying Zhang, Wang Ren, Shulin Zhang, *Int. J. Electrochem. Sci*, 2013, 8, 6839 – 6850.
[180] Jianshe Huang, Yang Liu, Haoqing Hou, Tianyan You, Biosensors and Bioelectronics, 2008, 24, 632–637.
[181] Hayati Filik, Asiye Aslıhan Avan, Sevda Aydar, Arabian Journal of Chemistry, 2016, 9, 471–480.

[182] D. B. Williams, C. B. Carter, Transmission electron microscopy a text book for materials science second edition, Springer, New York, USA, 2009.
[183] L. KAVAN, P. RAPTA, L. DUNSCH, M. J. BRONIKOWSKI, P. WILLIS, R. E. SMALLEY, J. Phys. Chem. B, 105 (2001), 10764-10771.
[184] J.W. Niemantsverdriet, Spectroscopy in catalysis: An introduction, 3rd ed., Wiley-VCH, Weinheim, Germany, 2007.
[185] Köhler JM, Li S, Knauer A, Chem Eng Technol, 2013, 36, 887–899.
[186] Knauer A, Thete A, Li S, Romanus H, Csaki A, Fritzsche W, Köhler JM Chem Eng J, 2011,166, 1164–1169.
[187] Knauer A, Csaki A, Möller F, Hühn C, Fritzsche W, Köhler JM , J Phys Chem C, 2012, 116, 9251–9258.
[188] Knauer A, Köhler JM, Chem Ing Tech, 2013, 85, 467–475.
[189] Bard AJ, Faulkner LR, (2000) Electrochemical methods: fundamentals and applications, 2nd edn. Wiley, New York.
[190] Zoski CG, (2007) Handbook of electrochemistry. Elsevier Science, The Netherland.
[191] Wang, Joseph, 1948–Analytical electrochemistry / Joseph Wang.—3rd ed.
[192] Heinze J., Angewandte Chemie international Edition in English, 1984, 23, 831.
[193] Vadim F. Lvovich, Impedance Spectroscopy: Applications to Electrochemical and Dielectric Phenomena, Willy publisher, 2015.
[194] Paweł Szroeder, Nikos G. Tsierkezos, Peter Scharff, Uwe Ritter, Carbon 2010, 48,4489-4496.
[195] Lu Q, Hu S, Pang D, He Z, Chem Commun 2005, 20, 2584–2585.
[196] Nicholson R, Anal Chem 1965, 37, 1351–1355.
[197] Konopka SJ, McDuffie B. Anal Chem 1970, 42, 1741– 1746.
[198] Galus Z (1994) Fundamentals of electrochemical analysis, 2nd edn. Ellis Horwood, New York, p 257
[199] Pauliukaite R, Ghica ME, Fatibello-Filho O, Brett CMA. Electrochim Acta 201055, 6239–6247.
[200] Navarro I, Gonzalez-Arjona D, Roldan E, Rueda M. J Pharm Biomed Anal 1988, 6, 969–976.
[201] Mazloum-Ardakani M, Rajabi H, Bietollahi H. J Argent Chem Soc 2009, 97, 106–115.
[202] Hamann CH, Vielstich W (1998) Elektrochemie. Wiley-VCH Verlag GmbH, Weinheim.
[203] Ruiz JJ, Rodriguez-Mellado JM, Domínguez M, Aldaz A. J Chem Soc 1989, Faraday Trans 1(85), 1567–1574.
[204] Daneshegar P, Moosavi-Movahedi AA, Norouzi P, Ganjali MR, Farhadi M, Sheibani N. J Braz Chem Soc 2012, 23, 315–321.
[205] Brett CMA, Brett AMO (1998) Electroanalysis. Oxford University Press Inc., New York, p 53.

[206] Carbo AD, CRC Press/Taylor and Francis 2009.
[207] Li Y, Chen SM. Int J Electrochem Sci 2012, 7, 2175–2187.
[208] Goyal RN, Singh SP. Electrochim Acta 2006, 51, 3008–3012.
[209] Özcan L, Şahin Y, Sensors Actuators B 2007,127, 362–369.
[210] Sánchez-Obrero G, Mayén M, Mellado JMR, Rodríguez-Amaro R. Int J Electrochem Sci 2011, 6, 2001–2011.
[211] Babaei A, Khalilzadeh B, Afrasiabi M. J Appl Electrochem 2010, 40, 1537–1543.
[212] Babaei A, Dehdashti A, Afrasiabi M, Babazadeh M, Farshbaf M, Bamdad F. Sens Lett 2012, 10, 1039–1046.
[213] Bahramipur H, Jalali F (2012). Afr J Pharm Pharmacol 6, 1298–1305.
[214] Devadas B, Rajkumar M, Chen SM, Saraswathi R. Int J Electrochem Sci 2012, 7, 3339–3349.
[215] Razmi H, Habibi E.Electrochim Acta 2010, 55, 8731–8737.
[216] Zhao M, Crooks RM. Chem Mater 1999, 11, 3379–3385.
[217] Ali A. Ensafi, , Hassan Karimi-Maleh, S. Mallakpour, M. Hatami, Sensors and Actuators B: Chemical 2011, 155, 464–472.
[218] Cardoso de Sá A, Paim LL, de Oliveira Bicalho U, Ribeiro do Carmo D. Int J Electrochem Sci 2011, 6, 3754– 3767.
[219] Wang Y, Liu Q, Qi Q, Ding J, Gao X, Zhang Y, Sun Y (2013). Electrochim Acta 111, 31–40.
[220] Song YH, He ZF, Hou HQ, Wang XL, Wang L. Electrochim Acta 2012, 71, 58–65.
[221] Song Y, He Z, Zhu H, Hou H, Wang L. Electrochim Acta 2011, 58,757–763.
[222] Tabeshnia M, Rashvandavei M, Amini R, Pashaee F. J Electroanal Chem 2010, 647, 181–186.
[223] Gilmartin MAT, Hart JP. Analyst 1994, 119, 2431–2437.
[224] Sánchez-Obrero G, Mayén M, Mellado JMR, Rodríguez-Amaro R. Int J Electrochem Sci 2011, 6, 2001–2011.
[225] Li M, Jing LH. Electrochim Acta 2007, 52, 3250–3257.
[226] Wang S, Xie F, Hu R. Sens Actuators B 2007,123, 495–500.
[227] Kumar SA, Tang CF, Chen SM, Talanta 2008, 76, 997–1005.
[228] He H, Xie Q, Zhang Y, Yao S. J Biochem Biophys Methods 2005, 62, 191–205.
[229] Nikos G.Tsierkezos, Max Puschner, Uwe Ritter, Andrea Knauer, Lars Hafermann, J.Michael Köhler, Ionics 2016, 10, 1957-1965.
[230] Pandurangachar M, Swamy BEK, Chandrashekar BN, Gilbert O, Reddy S, Sherigara BS. Int J Electrochem Sci 2010, 5, 1187–1202.
[231] Niranjana E, Swamy BEK, Naik RR, Sherigara BS, Jayadevappa H. J Electroanal Chem 2009, 631, 1–9
[232] Hirano A, Kanai M, Nara T, Sugawara M. Anal Sci 2001, 17, 37–43.

[233] Perenlei G, Tee TW, Yusof NA, Kheng GJ. Int J Electrochem Sci 2011, 6, 520–531.
[234] Li Y, Chen SM. Int J Electrochem Sci 2012, 7, 2175–2187.
[235] Wang L, Wang E. Electrochem Comm 2004, 6, 49–54.
[236] Zhang J, Oyama M. Anal Chim Acta 2005, 540, 299–306.
[237] H. Yaghoubian, H. Beitollah, V. Soltani-Nejad, A. Mohadesi, D. Afzali, H. Zamani, and S. Roodsaz, Int. J. Electrochem. Sci 2011, 6, 1307-1316.
[238] B. Olsson, M. Johansson, J. Gabrielsson, P. Bolme, Eur. J. Clin. Pharmacol. 1988, 34, 77-82.
[239] H. Bahramipur and F. Jalali, Afr. J. Pharm. Pharmacol. 2012, 6, 1298-1305.
[240] A. Gmez-Caballero, M. A. Goicolea, and R. J. Barrio, Analyst 2005,130, 1012-1018.
[241] B. Devadas, M. Rajkumar, S. M. Chen, and R. Saraswathi, Int. J. Electrochem. Sci. 2012, 7, 3339-3349.
[242] K. Tungkananuruk, N. Tungkananuruk, and D. T. Burns, KMITL Sci. Tech. J 2005, 5, 547-551.
[243] M. Boopathi, M. S. Won, and Y. B. Shim, Anal. Chim. Acta 2004, 512, 191-197.
[244] O. Fatibello-Filho, K. O. Lupetti, and I. C. Vieira, Talanta 2001, 55, 685-692.
[245] I. Noviandri and R. Rakhmana, Int. J. Electrochem. Sci 2012, 7, 4479-4487.
[246] H. Karimi-Maleh, M. Keyvanfard, K. Alizad, M. Fouladgar, H. Beitollahi, A. Mokhtari, and F. Gholami-Orimi, Int. J. Electrochem. Sci. 2011, 6, 6141-6150.
[247] M. Fouladgar, H. Karimi-Maleh, and R. Hosseinzadeh, Ionics 2013, 19, 665-672.
[248] A. C. de S, L. L. Paim, U. de Oliveira Bicalho, and D. R. do Carmo, Int. J. Electrochem. Sci. 2011, 6, 3754-3767.
[249] W. T. Suarez, L. H. Marcolino Jr, and O. Fatibello-Filho, Microchem. J. 2006, 82, 163-167.
[250] P. Karabinas, D. Jannakoudakis, J. Electroanal. Chem. 1984,160, 159–167.
[251]C. Xiao, X. Chu, Y. Yang, X. Li, X. Zhang, J. Chen, Biosens. Bioelectron. 2011, 26, 2934–2939.
[252] J.L. Owens, H.A. Marsh, G. Dryhurst, J. Electroanal.Chem. 1978, 91, 231–247.
[253] R.S. Nicholson, I. Shain, Anal. Chem1964, 36, 706-723.
[254] J.L. Owens, H.A. Marsh, G. Dryhurst, J. Electroanal. Chem 1978, 91, 231-247.
[255] G. Dryhurst, J. Electrochem. Soc 1972, 119, 1659-1664.
[256] P. Karabinas, D. Jannakoudakis, J. Electroanal. Chem. 1984,160, 159-167.
[257] P. Karabinas, D. Sazou, D. Jannakoudakis, Bioelectrochem. Bioenerg. 1985, 14, 469-478.
[258] N.V. Smith, Phys. Rev. B 1974, 9, 1365-1376.

[259] R.M.C. Dawson, D.C. Elliott, W.H. Elliott, K.M. Jones, Data for Biochemical Research, third editon, Oxford Science Publications Clarendon Press, Oxford,1986.
[260] G. Karim-Nezhad, M. Hasanzadeh, L. Saghatforoush, N. Shadjou, B.Khalilzadeh, S. Ershad, , J. Serbian Chem. Soc 2009,74, 581–593.
[261] H. Wang, F. Ren, C. Wang, B. Yang, D. Bin, K. Zhang, Y. Du, RSC Adv. 2014, 4, 26895-26901.
[262] J. Ping, J. Wu, Y. Wang, Y. Ying, Biosens. Bioelectron. 2012, 34, 70-76.
[263] Z. Dursun, B. Gelmez, Electroanal. 2010, 22, 1106-1114.
[264] K. Ghanbari, N. Hajheidari, J. Polym. Res. 2015, 22, 152 (9 pages).
[265] C.L. Sun, H.H. Lee, J.M. Yang, C.C. Wu, Biosens. Bioelectron. 2011, 26, 3450-3455.
[266] J. Zhang, Z. Zhu, J. Zhu, K. Li, S. Hua, Int. J. Electrochem. Sci. 2014, 9, 1264-1272.
[267] P. Kalimuthu, S.A. John, Talanta 2010, 80, 1686-1691.
[268] R. Cui, X. Wang, G. Zhang, C. Wang, Sensor Actuat. B Chem 2012, 161, 1139-1143.
[269] D. Han, T. Han, C. Shan, A. Ivaska, Li Niu, Electroanal 2010, 22, 2001-2008.
[270] X. Liu, S. Wei, S. Chen, D. Yuan, W. Zhang, Appl. Biochem. Biotechnol. 2014, 173, 1717-1726.
[271] X. Zheng, X. Zhou, X. Ji, R. Lin, W. Lin, Sensor Actuat. B Chem. 2013,178, 359-365.
[272] S. Thiagarajan, S.M. Chen, Talanta 2007, 74, 212-222.
[273] J. Arguello, V.L. leidens, H.A. Magossa, R.R. Ramos, Y. Gushikem, Electrochim. Acta 2008, 54, 560-565.
[274] Nemanish RJ, Solin SA. Phys Rev 1979, B 20, 392-401.
[275] Choi S, Park KH, Lee S, Koh KH. J Appl Phys 2002, 92, 4007-4011.
[276] Tian ZQ, Jiang SP, Liang YM, Shen PK. J Phys Chem B 2005,110, 5343-5350.
[277] R. Zhang, G.D. Jin, D. Chen, X.Y. Hu. Sens. Actuators B 2009,138, 174-181.
[278] S. Jeyalakshmi, S. Radha Kumar, J. Senthil Mathiyarasu, K.L.N. Phani, V. Yegnaraman. Indian J. Chem. 2007 A 46, 957-961.

List of original Publications

1 N.G. Tsierkezos, Sh. Haj Othman, U. Ritter, Nitrogen-doped multi-walled carbon nanotubes for paracetamol sensing, Ionics 19 (2013) 1897-1905.

2 N.G. Tsierkezos, Sh. Haj Othman, U. Ritter, Nitrogen-doped multi-walled carbon nanotubes modified with gold nanoparticles for simultaneous analysis of *N*-acetyl-cysteine and acetaminophen, Journal of Solid State Electrochemistry 18 (2014) 629–637.

3 N.G. Tsierkezos, Sh. Haj Othman, L. Hafermann, U. Ritter, Elektrochemical sensor consisting of nitrogen-doped multi-walled carbon nanotubes decorated with platinum nanoparticles, Advanced Electrochemistry 1 (2014) 1-8.

4 N.G. Tsierkezos, Sh. Haj Othman, U. Ritter, L. Hafermann, A. Knauer, J.Michael Köhler, Nitrogen-doped multi-walled carbon nanotubes modified with platinum, palladium, rhodium and silver nanoparticles in electrochemical sensing. J Nanopart Res 16 (2014) 2660-2663.

5 N.G. Tsierkezos, Sh. Haj Othman, U. Ritter, L. Hafermann, A. Knauer, J.Michael Köhler, C. Downing, E.K. McCarthy, Nitrogen-doped multi-walled carbon nanotubes modified with rhodium, palladium, platinum, and gold nanoparticles for simultaneous electrochemical analysis of ascorbic acid, dopamine, and uric acid, Sensors and Actuators B 231 (2016) 218–229.

6 Sh. Haj Othman, U. Ritter, E.K. McCarthy, D. Fernandes, A. Kelarakis, N.G. Tsierkezos, Synthesis and electrochemical characterization of nitrogen-doped and nitrogen–phosphorus-doped multi-walled carbon nanotubes, Ionics 23 (2017) 2025–2035.